CONTENTS

The artificial microRNA mediates *GUS-GFP* gene silencing using ath-miR169d precursor as backbone☆

Chong Liu[1,2], Lan Zhang[2], Jie Sun[1,2], Yanzhong Luo[2], Mingbo Wang[3], Yunliu Fan[2], Lei Wang[2,*]

[1]*College of Agriculture*, *Key Laboratory of Oasis Ecology Agriculture of BINTUAN*, *Shihezi University*, *Shihezi* 832003, *China*; [2]*Biotechnology Research Institute/The National Key Facility for Crop Gene Resources and Genetic Improvement*, *Chinese Academy of Agricultural Sciences*, *Beijing* 100081, *China*; [3]*CSIRO Plant Industry*, *PO Box* 1600, *Canberra*, *ACT* 2601, *Australia*

Received January 13, 2009

Abstract

Artificial microRNA (amiRNA) is becoming a powerful tool for silencing genes in plants, and several amiRNA vectors have recently been developed based on the natural precursor structures of ath-miR159a, ath-miR164b, ath-miR172a, ath-miR319a and osa-miR528. In this study we generated a simple amiRNA vector (pAmiR169d) based on the structure of *Arabidopsis* miR169d precursor (pre-miR169d). Two unique restriction sites were created inside the stem region of pre-miR169d, which allows for amiRNA sequences to be cloned as either ~ 80 bp synthetic oligonucleotides or PCR products. A β-glucuronidase (GUS)/green florescent protein (GFP) fusion gene was efficiently silenced in transient assays using a pAmiR169d-derived construct targeting a *GFP* sequence. 5' RACE showed that the target *GFP* transcript was cleaved precisely at the expected position across nucleotides 10 and 11 of the amiRNA. Thus, pAmiR169d allows for both easy construction of amiRNA constructs and efficient silencing of target genes in plants. [Life Science Journal. 2009; 6(2): 1 – 7] (ISSN: 1097 – 8135).

Keywords: miRNA; hairpin RNA; artificial microRNA; silencing gene

1 Introduction

MicroRNAs (miRNAs) are 20 – 25 nt small RNAs that negatively regulate gene expression in plants and animals by base pairing with target mRNAs causing mRNA cleavage or translational repression. miRNAs are processed by RNase III-like enzyme Dicer from short hairpin-loop structures known as miRNA precursors (pre-miRNA) that are derived from longer primary miRNA transcripts (pri-miRNA). Single-stranded mature miRNAs are incorporated into RNA-induced silencing complex (RISC) containing Argonaute proteins to guide mRNA cleavage or translational repression. In animals, miRNAs are normally partially complementary to the target mRNA and cause translational arrest[1]. By contrast, in plants miRNAs typically have few (zero to five) mismatches to their targets and induce transcript cleavage and subsequent degradation[2].

Recent studies have shown that alteration of several nucleotides within a miRNA sequence does not affect its biogenesis as long as the initial base-pairing in the stem-loop structure of the precursor remain unaffected[3]. This makes it possible to modify natural miRNA sequences and generate artificial miRNA (amiRNA) targeting any gene of interest[4–6]. The amiRNA technology was first used for silencing genes in human cell lines, and recently it was successfully employed to down-regulate individual genes or groups of endogenous genes in transgenic plants[7,8]. These plant amiRNAs are expressed from vectors derived from precursors of ath-miR159a, ath-miR164b, ath-miR172a, ath-miR319a and osa-miR528. Genome-wide expression analyses in transgenic *Arabidopsis thaliana* shows that plant amiRNAs exhibit high sequence specificity similar to natural miRNAs[9], so the amiRNA sequence can be easily optimized to knock

☆Supported by the National Key Basic Research Program of China (Grant No. 2006CB101601) and National High Technology Research and Development Program of China (Grant No. 2007AA10Z147).
*Corresponding author. Email: leiwang70@163.com

down the expression of a single gene or several highly conserved genes without affecting the expression of other unrelated genes.

The miR169 family is one of the highly conserved miRNA families in plants. The ath-miR169 family consists of 4 types from 14 chromosomal locations[10]. The size of ath-miR169 precursors ranges from 154 to 411 nt, of which miR169d was the shortest, comprising only 154 nt. In this study, we modified the precursor of ath-miR169d (accession number: MI0000987) into an amiRNA vector that allows for easy cloning of amiRNA sequences. Transient assays using the green florescent protein (GFP) gene as a target indicated that miR169d-based constructs are effective at conferring gene silencing in plants.

2 Materials and Methods

2.1 Vector construction

2.1.1 AmiRNA vector pAmiR169d. The backbone of pAmiR169d was directly assembled by annealing of the following eight sense and antisense overlapping oligonucleotides: oligo1 (5'-gatccGTATCATAGAGTCTTGCATGGA-3'), oligo2 (5'-AAAATTAAAGaattcATTGAGCCAAGGATGACTTGCCGATGTT-3'), oligo3 (5'-ATCAACAAATCTTAACTGATTTTGGTGTCCGGCAAGTTGACCTT-3'), oligo4 (5'-GGCTCTGTCGACTTCTTTTCTTTTCAATGTCAAACTCTAGATATgagct-3'), oligo5 (5'-CATATCTAGAGTTTGACATTGAA-3'), oligo6 (5'-AAGAAAAGAAgtcgacAGAGCCAAGGTCAACTTGCCGGACACCA-3'), oligo7 (5'-AAATCAGTTAAGGATTTGTTGATAACATCGGCAAGTCATCCTTGGC-3') and oligo8 (5'-TCAATCGAATTCTTTAATTTTTCCATGCAAGACTCTATGATACg-3').

These oligonucleotides were phosphorylated and annealed as previously described[11], forming double-stranded DNA with 4 nt overhangs ready for ligation with *Bam*HI and *Sac*I-digested DNA.

To obtain a promoter-terminator cassette for expressing the amiRNA, the ~ 3000 bp 35S-GUS-Nos fragment was excised by *Hind*III/*Eco*RI digestion from pBI121 and gel-purified using a Qiagen agarose gel purification kit. The fragment was ligated to the binary vector pCAMBIA1303 at the *Hind*III/*Eco*RI sites, generating the plasmid pCAMBIA-35S. To remove the *Eco*RI site from pCAMBIA-35S, the plasmid was digested with *Eco*RI, the sticky ends were blunted with T4 DNA polymerase, and the linearized DNA was self-ligated to form pCAMBIA-35SE. The annealed products (~ 100 ng) described above were cloned into pCAMBIA1303-35SE at the *Bam*HI and *Sac*I sites, generating the amiRNA vector pAmiR169d.

2.1.2 AmiRNA construct targeting GFP, pAmiR-gfp. The following four oligonucleotides were synthesized and annealed as described above to form an *Eco*RI-*Sal*I fragment containing the AmiR-gfp sequenc: oligo9 (5'-aattCGATTTGTATTCCAACTTGTGGCCGATGTTAT-3'), oligo10 (5'-CAACAAATCTTAACTGATTTTGGTGTCCGGCCACAAGATGGAATACATGTCGAC-3'), oligo11 (5'-AAAATCAGTTAAGATTTGTTGATAACATCGGCCACAAGTTGGAATACAAATCG-3'), and oligo12 (5'-tcgaGTCGACATGTATTCCATCTTGTGGCCGGACACC-3').

The annealed products were ligated with pAmiR169d pre-digested with *Eco*RI and *Sal*I, generating pAmiR-gfp, in which the ath-miR169d sequence was replaced by the sequence of TTGTATTCCAACTTGTGGCCG, targeting the GFP sequence in the *GUS-GFP* fusion gene of pCAMBIA-35SE.

2.2 Transient expression analysis in *Nicotiana benthamiana* leaves using *Agrobacterium* infiltration

pAmiR-gfp was introduced into *Agrobacterium tumefaciens* strain GV3101 by electroporation. pCAMBIA1303 was also introduced into GV3101 for use as control. Growing of wild-type *Nicotiana benthamiana* and *Agrobacterium* infiltration of *N. benthamiana* leaves were carried out as previously described[12]: 0.5 ml of *Agrobacterium* containing pAmiR-gfp was infiltrated into leaves of *N. benthamiana* that had been grown to 6 – 8 leaves in pots at 24 ºC under a photoperiod of 16 h light/8 h dark. Similarly, 0.5 ml of *Agrobacterium* containing pCAMBIA1303 was infiltrated into leaves of *N. benthamiana* for use as a control. After infiltration, plants were kept under the constant conditions and grown for 48 h. The infiltrated leaves (~ 150 mg) were then excised from the plants and used for GUS expression and RNA analysis. GUS enzyme assays were measured as previously described[12].

2.3 RT-PCR analysis

Total RNA was isolated using the RNAgents Total RNA Isolation System (Promega). Portions (2 μg) of total RNAs were used for the reverse transcription using the SuperScript First-Strand Synthesis System (Invitrogen). The following primers were used to detect the GUS-GFP transcript: forward 5'-CGATGCGGTCACTCATTAC-3' and reverse 5'-TTCACACGTGGTGGTG-

GTGGT-3'. The PCR reaction was denatured at 94 ºC for 2 min, followed by 35 cycles of 20 sec at 94 ºC, 20 sec at 53 ºC and 20 sec at 72 ºC, with a final extension for 10 min at 72 ºC. The predicted size for the PCR product is ~ 2600 bp. For use as loading reference, a ~ 441 bp fragment of the tobacco Actin1 (GenBank: AB158612) RNA was amplified using the following primers: NAcfw, 5'-ATGAGCAAGAGTTGGAGACTG-3' (forward) and NAcrv, 5'-CAATGGAAGGACCAGATTCAT-3' (reverse). The reaction was denatured at 94 ºC for 2 min, followed by 25 cycles of 20 sec at 94 ºC, 20 sec at 53 ºC and 40 sec at 72 ºC, with a final extension for 10 min at 72 ºC.

2.4 5' RACE (rapid amplification of cDNA ends)

The 5' RACE assay was performed using version 2.0 of the 5' RACE System available from GIBCO BRL Life Technologies following the manufacturer's instructions. Basically, 2 μg of total RNA was reverse-transcribed using a GFP-specific primer (GFP RV: 5'-TTCACACGTGGTGGTGGTGGT). The resulting cDNA was purified to remove unincorporated dNTPs and GFP RV primer and treated with TdT (Terminal deoxynucleotidyl transferase) to add homopolymeric C tails to the 3' end. The tailed cDNA was then amplified by PCR using the anchor primer T7-G (5'-TAATACGACTCACTATAGGGGGGGGGG) and GFP RV. The reaction was denatured at 94 ºC for 2 min, followed by 30 cycles of 20 sec at 94 ºC, 20 sec at 65 ºC and 45 sec at 72 ºC, with a final extension for 10 min at 72 ºC. Nested PCR was performed using a T7 primer (5'-TAATACGACTCACTATAGGG) and GFP RV2 (5'-GTGGTGGTGGTGGCTAGCTTT). The reaction was denatured at 94 ºC for 2 min, followed by 30 cycles of 20 sec at 94 ºC, 20 sec at 55 ºC and 45 sec at 72 ºC, with a final extension for 10 min at 72 ºC. The PCR products were separated in 1% agarose gel. The ~ 300 bp DNA fragment was excised and purified using a Qiagen agarose gel purification kit. The sample was ligated to pGEM-T vector, and five individual clones were selected for sequencing.

3 Results

3.1 Construction of the amiRNA vector pAmiR169d

The construction of amiRNA vectors in the previous reports often involved cloning of relatively long DNA fragments generated by multiple PCRs. To select for a better amiRNA backbone, we screened all *Arabidopsis* miRNA precursors in the miRBase/Rfam database. We found that the ath-miR169d precursor (pre-miR169d) consists of only 154 nt and forms a simple stem-loop (Figure 1A), and the sequences can be easily modified into two restriction endonuclease sites for *Eco*RI and *Sal*I in the stem. Furthermore, ath-miR169d is expressed in several *Arabidopsis* tissues including leaves, roots and panicles, indicating that pre-miR169d can be efficiently processed by Dicer in these tissues.

The modified ath-miR169d precursor sequence was directly assembled by annealing of eight synthetic oligonucleotides, in which five nucleotides of the original pre-miR169d sequence were altered to produce the *Eco*RI and *Sal*I sites but with the secondary structure of pre-miR169d being maintained (Figure 1B). The anneal products had 4 nt overhangs in each ends, matching the *Bam*HI and *Sac*I sites, respectively. To clone this pre-miR169d sequence into an expression vector suitable for *Agrobacterium*-mediated plant transformation, the 35S-GUS-Nos cassette from pBI121 was inserted into pCAMBIA1303, generating pCAMBIA-35S (Figure 2). The *Eco*RI site of pCAMBIA-35S was subsequently removed giving rise to the intermediate plasmid pCAMBIA-35SE. The modified ath-miR169d precursor was then inserted at the *Bam*HI and *Sac*I sites downstream of the 35S promoter in pCAMBIA-35SE, forming the pAmiR169d vector (Figure 2). The *Eco*RI and *Sal*I sites are unique in pAmiR169d, and the sequence between the two restriction sites, including the miRNA and miRNA* parts, is about 80 bp. Therefore, amiRNA sequences can be conveniently cloned into the vector either as annealed synthetic oligonucleotides or as PCR fragments.

3.2 pAmiR-gfp efficiently down regulates GFP expression at mRNA and protein levels

To validate the efficacy of pAmiR169d, we chose the fusion reporter gene *GUS-GFP* from the pCAMBIA1303 vector as a target. The amiRNA targeting GFP, amiR-gfp, was designed based on the characteristics of nucleotide compositions of natural *Arabidopsis* miRNAs, 5' instability of miRNA/miRNA* duplexes, and target accessibility. The sequence, 5'-UUGUAUUCCAACUUGUGGCCG-3', contains a uridine residue at position 1 and an adenine residue at position 10, with a GC content of 48% (Figure 1C); all of these features are overrepresented in endogenous miRNAs[13]. This sequence also ensures the amiRNA/amiRNA* duplex to have 5' instability allowing preferential loading of the amiRNA strand into RISC[17]. The structural accessibility to the GFP complementary sequence by amiR-gfp was examined using Sfold[14–16], which showed that amiR-gfp has high accessibility to its complementary target sequence, with nucleotides 10 and 11 the highest having the highest accessibility (Figure 1D).

Agrobacterium infiltration-mediated transient assays have been widely used to study transgene expression and transgene-induced silencing in plants[12,17]. We therefore chose *Agrobacterium* infiltration to investigate the silencing effect of pAmiR-gfp on the target *GUS-GFP* gene that is present in the same vector. As the GUS sequence is transcriptionally fused with the GFP sequence, targeting of the GFP sequence should result in the silencing of both the *GFP* and *GUS* genes. We therefore examined the silencing effect by measuring the GUS activity. As shown in Figure 3A, *N. benthamiana* leaves infiltrated with pAmiR-gfp expressed significantly lower levels of GUS activity than those infiltrated with the control vector pCAMBA1303; GUS activity was reduced by around 50%. RT-PCR of RNA isolated from infiltrated leaves showed a dramatic reduction in *GUS-GFP* mRNA levels in pAmiR-gfp-infiltrated leaves in comparison with pCAMBIA1303-infiltrated tissues (Figure 3B). These results indicated that amiR-gfp was expressed and properly processed from pAmiR-gfp, resulting in efficient GFP silencing in *N. benthamiana* cells.

3.3 AmiR-gfp directs precise cleavage of *GUS-GFP* mRNA at the predicted position

To confirm proper processing and functioning of amiR-gfp, 5' RACE-PCR was performed to detect the cleavage site in the target GUS-GFP RNA. Cleavage of *GUS-GFP* transcript by amiR-gfp at the predicted site should generate a 317 bp RACE-PCR fragment (Figure 4B). As shown in Figure 4A, a distinct band of about

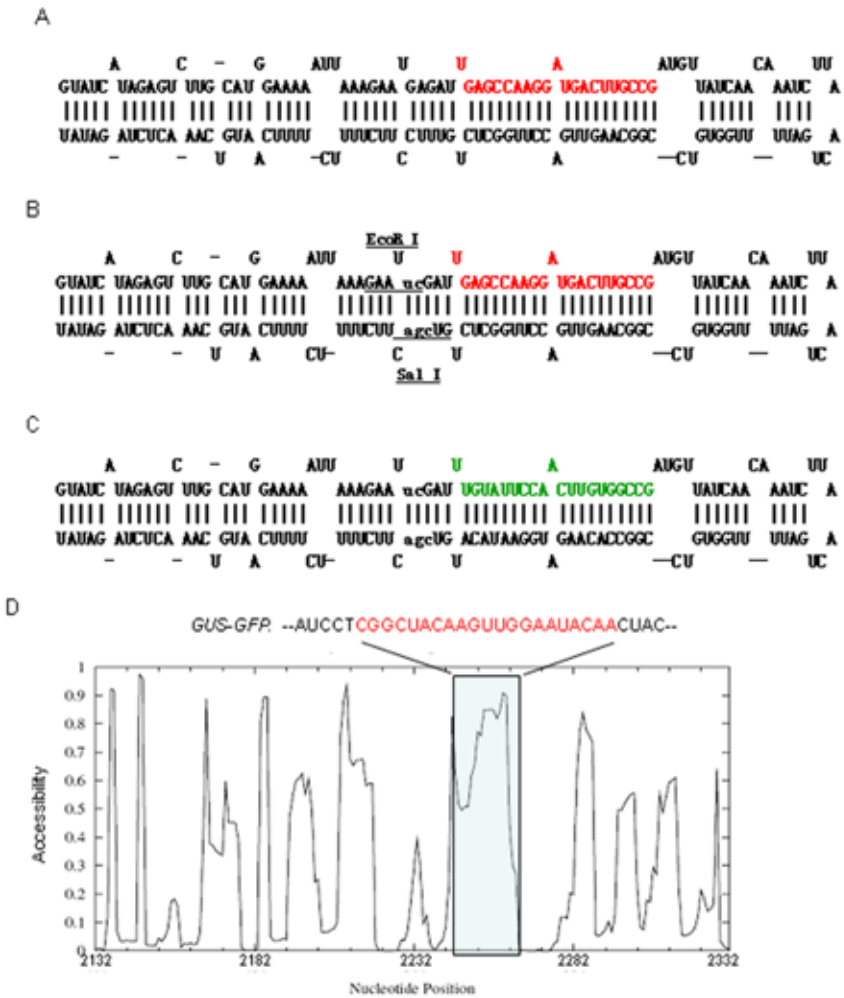

Figure 1. Predicted structure of the native ath-miR169d precursor (A), the modified amiR169d precursor (B) and the GFP amiRNA amiR-gfp (C). The ath-miR169d and amiR-gfp sequences are shown in red and green, respectively, and the modified nucleotides in the stem-loop are shown in lowercase. D. Target accessibility profiling by Sfold for part of the GUS-GFP sequence (from nt 2132 to nt 2332) containing the region targeted by amiR-gfp. Note that the amiR-gfp-binding site (shaded) is highly accessible for small RNA.

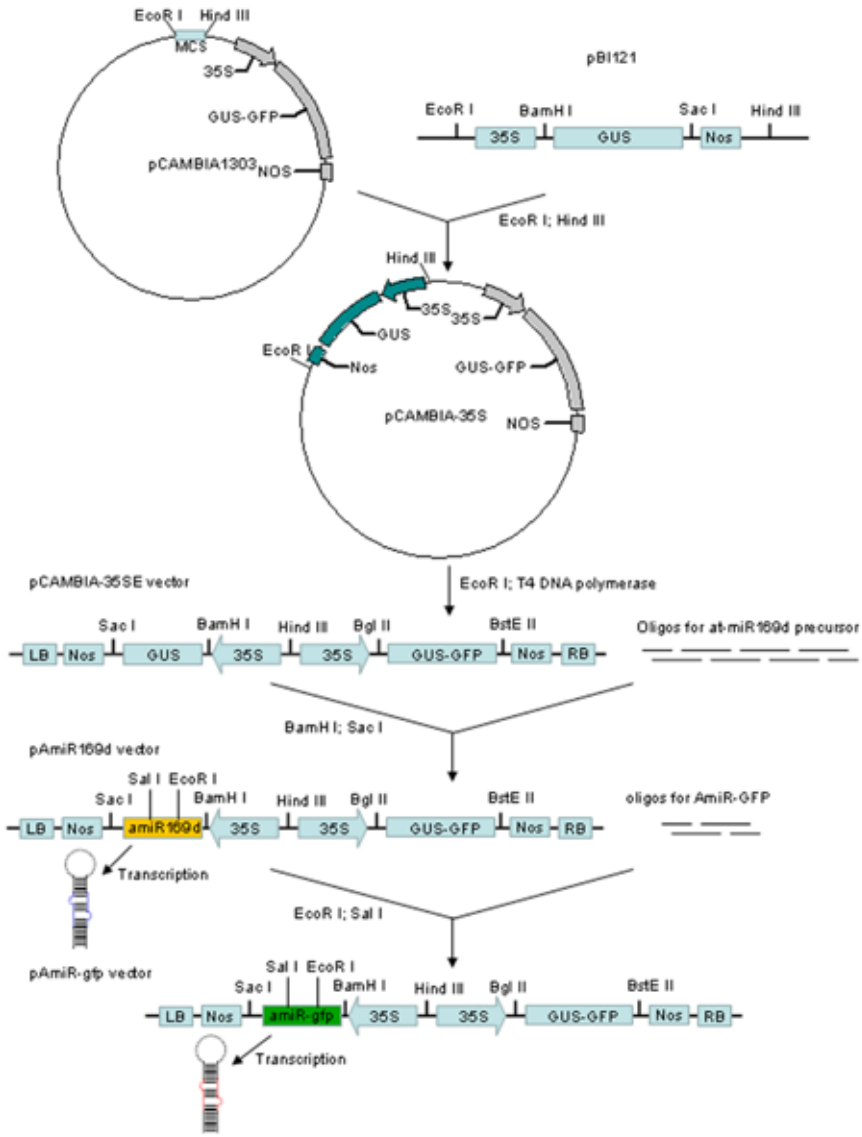

Figure 2. Flow chat for the construction of pAmiR169d and pAmiR-gfp. The 35S-GUS-Nos cassette is excised from pBI121 with *Eco*RI and *Hind*III digestion, and inserted into pCAMBIA1303, giving rise to pCAMBIA-35S. The *Eco*RI site in pCAMBIA-35S is abolished by treatment with T4 DNA polymerase to generate pCAMBIA-35SE. The Ath-miR169d precursor sequence was then assembled from 8 overlapping oligonucleotides by annealing and inserted into pCAMBIA-35SE at the *Bam*HI/*Sac*I site, forming the amiRNA vector pAmiR169d. To make the AmiR-gfp construct, 4 overlapping oligonucleotides were annealed and inserted into the *Sal*I/*Eco*RI sites in pAmiR169d.

320 bp was amplified from the sample infiltrated with pAmiR-gfp, but not from the pCAMBIA1303-infiltrated sample. This band was gel-purified and ligated into the pGEM T vector. Five clones were sequenced, and the result showed that this DNA fragment was the expected 317 bp cleavage product from the *GUS-GFP* transcript. All five clones had the same 5' terminal nucleotide corresponding to the position located between the two nucleotides complementary to nucleotides 10 and 11 of amiR-GFP (Figure 4B). This was consistent with miRNA- and siRNA-guided cleavage in plants that typically occurs across nucleotides 10 and 11 of the miRNA and siRNA sequences, and that even 24 nt siRNAs also cleave at position 10[18].

4 Discussion

In this study, the *Arabidopsis* miR169d precursor was successfully used as the backbone for the expression of

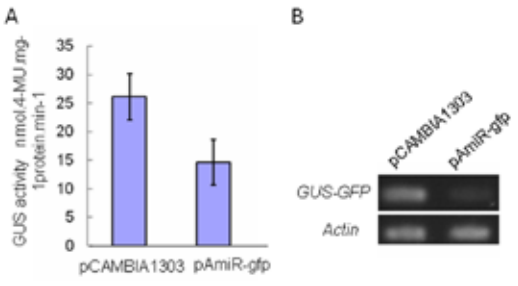

Figure 3. pAmiR-gfp induces target gene silencing in *Agrobacterium*-infiltrated *N. benthamiana* leaves. A: Analysis of GUS activity; B: Semi-quantitative RT-PCR of *GUS-GFP* transcripts.

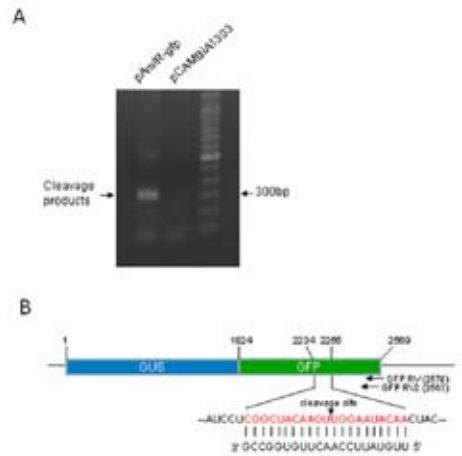

Figure 4. AmiR-gfp induces cleavage of the target GUS-GFP transcript at the predicted nucleotide position. A: 5' RACE-PCR. A distinct band of about 320 bp is present in the sample infiltrated with pAmiR-gfp but not the infiltrated with the control plasmid pCAMBIA1303. B: Target cleavage site by amiR-gfp as determined by sequencing of 5' RACE clones. The 21 nt target sequence is shown in red, and the cleavage site is indicated by an arrow head. The size of the cleavage fragment is predicted to be 317bp (from the cleavage site at nt 2245 to the 5' end of the reverse primer GFP RV2 at 2563).

of amiRNAs in plants. Preparation of amiRNA constructs in the previous reports using backbones from ath-miR159a, ath-miR164b, ath-miR172a, ath-miR319a and osa-miR528 all involves cloning of longer DNA fragments that are normally generated through multiple PCRs[4,7,8,17]. With the pre-miR169d-based vector, amiRNA sequences can be directly synthesized as ~ 80 bp oligonucleotides and cloned by a single step ligation into the unique restrictions sites *Eco*RI and *Sal*I created in the middle of the stem. This should allow for rapid and high-throughput preparation of amiRNA constructs for silencing genes in plants. The GFP-targeting amiRNA construct, amiR169d-gfp, conferred efficient silencing to the GUS-GFP fusion transgene in transient assays, and this silencing was correlated with precise cleavage of the *GUS-GFP* transcript at the predicted position across nucleotides 10 and 11 of the designed GFP amiRNA. This suggests that amiRNAs expressed from the pAmiR169d vector is accurately processed by Dicer and efficiently loaded into RISC, indicating that the introduction of the restriction sites into the pre-miR169d stem did not affect Dicer processing. Creating restriction sites into pre-miRNA stems could therefore be used for constructing amiRNA vectors from on other miRNA precursors to allow for easy cloning of amiRNA sequences.

In order to design an effective amiRNA, we examined the sequence characteristics of all known Arabidopsis miRNAs and the base-pairing feature between the miRNAs and their targets. Initially, candidate 21-mer sequences were picked from the whole length of the reverse complements of the target *GFP* transcript, which had a nucleotide A at position 10 and displayed 5' instability (higher AU content at the 5' end and higher GC content at the 3' end around position 19). These candidate sequences were further screened based on the statistic analysis of base mismatches between microRNAs and their targets, which showed that mismatches occur frequently at position 1, 2 or 21, but almost never occur at position 3, 4, 16 or 17, and G/U pairing was the most frequent mismatch. Furthermore, target accessibility by the amiRNA was analysed using the Sfold program[14]. The finally chosen amiR-gfp sequence, 5′-UUGUAUUCCAACUUGUGGCCG-3', therefore conforms with both the sequence features of microRNAs and their targeting rules. The transient assay data demonstrated that this amiR-gfp directed efficient and precise cleavage of the GUS-GFP mRNA at the predicted amiR-gfp recognition site, suggesting that this amiRNA selection pipeline is potentially applicable to the design of other amiRNAs.

References

1. Long D, Lee R, Williams P, *et al*. Principles of microRNA-target recognition. P LoS Biol 2005; 3: e85.
2. Cesar Llave, Kristin D. Kasschau, *et al*. Endogenous and silencing-associated small RNAs in plants. Plant Cell 2002; 14: 1605 – 19.
3. Vaucheret Hervé, Vazquez F, Patrice Créte, *et al*. The action of ARGONAUTE1 in the miRNA pathway and its regulation by the miRNA pathway are crucial for plant development. Genes Dev 2004; 18: 1187 – 97.
4. Niu QW, Lin SS, Reyes JL, *et al*. Expression of artificial microRNAs in transgenic Arabidopsis thaliana confers virus resistance. Nat Biotechnol 2006; 11: 1420 – 8.
5. Zeng Y, Wagner EJ, Cullen BR. Both natural and designed microRNAs can inhibit the expression of cognate mRNAs when expressed in human cells. Mol Cell 2002; 9: 1327 – 33.

6. Parizotto EA, Dunoyer P, Rahm N, *et al*. *In vivo* investigation of the transcription, processing, endonucleolytic activity, and functional relevance of the spatial distribution of a plant miRNA. Genes Dev 2004; 18: 2237 – 42.
7. Warthmann N, Chen H, Ossowski S, *et al*. Highly specific gene silencing by artificial miRNAs in rice. PLoS ONE 2008; 3: e1829.
8. Schwab R, Ossowski S, Riester M, *et al*. Highly Specific Gene Silencing by Artificial MicroRNAs in *Arabidopsis*. Plant Cell 2006; 18: 1121 – 33.
9. Schwab R, Palatnik JF, Riester M, *et al*. Specific effects of microRNAs on the plant transcriptome. Dev Cell 2005; 8: 517 – 27.
10. Wang L, Wang MB, Tu JX, Helliwell CA, *et al*. Cloning and haracterization of microRNAs from Brassica napus. FEBS Letters 2007; 581: 3848 – 56.
11. Wang L, Zhao J, Fan YL. Cloning and function analysis of ABP9 protein which specifically binds toABRE2 motif of maize Cat1 gene. Chinese Science Bulletin 2002; 47(22): 871 – 5.
12. Wang L, Luo YZ, Zhang L, *et al*. Rolling circle amplification-mediated hairpin RNA (RMHR) library construction in plants. Nucleic Acids Res 2008; 22: e149.
13. Ossowski S, Schwab R, Weigel D. Gene silencing in plants using artificial microRNAs and other small RNAs. The Plant Cell 2007; 53: 674 – 90.
14. Ding Y, Chan CY, Charles E, Lawrence. Sfold web server for statistical folding and rational design of nucleic acids. Nucleic Acids Res 2004; 32: w135 – 41.
15. Long D, Lee R, Williams P, *et al*. Potent effect of target structure on microRNA function. Nature Structural and Molecularbiology 2007; 4: 1038 – 226.
16. Kertesz M, Iovino N, Unnerstall U, *et al*. The role of site accessibility in microRNA target recognition. Nature Genetics 2007; 39: 1278 – 85.
17. Khraiwesh B, Ossowski S, Weigel D, *et al*. Specific gene silencing by artificial microRNAs in Physcomitrella patens: an alternative to targeted gene knockouts. Plant Physiology 2008; 148: 684 – 93.
18. Wang MB, Helliwell CA, Wu LM, *et al*. Hairpin RNAs derived from RNA polymerase II and polymerase III promoter-directed transgenes are processed differently in plants. RNA 2008; 14(5): 903 – 13.

Alkaline protease production by immobilized cells of *Bacillus pumilis* MTCC 2296 in various matrices

Deepika Kumari[1], Neetu Sharma[2], Gulab Pandove[3], Varenyam Achal[2,*]

[1]*Directorate of Mushroom Research*, *Solan*, *Himachal Pradesh*, *India*; [2]*Neetu Sharma*, *Department of Biotechnology*, *Thapar University*, *Patiala*, *Punjab*, *India*; [3]*Gulab Pandove*, *Department of Microbiology*, *Punjab Agricultural University*, *Ludhiana*, *Punjab*, *India*

Received January 29, 2009

Abstract

Immobilization techniques provide a special microenvironment in which cells always have different behaviors compared with free cells. In the present work, the effect of *Bacillus pumilis* MTCC 2296 cells immobilized in various matrices; such as calcium alginate, polyacrylamide and agar-agar, for the production of alkaline protease, is studied. Calcium alginate was found to be an effective and suitable matrix for higher alkaline protease productivity (491 U/ml) compared to the other matrices studied. [Life Science Journal. 2009; 6(2): 8 – 10] (ISSN: 1097 – 8135).

Keywords: *Bacillus pumilis*; immobilization; alkaline protease; calcium alginate

1 Introduction

Alkaline proteases constitute one of the most important groups of industrial enzymes. It accounts for at least a quarter of the total global enzyme production (Herbert *et al*, 1992). Proteases are essential constituents of all forms of life on earth including prokaryotes, fungi, plants and animals. Recently, the sue of alkaline protease has increased significantly in various industrial processes such as detergent and feed additives, food, dehairing, pharmaceutical, leather and silk industries. Among these, use as laundry detergent additive is one the most important industrial applications for alkaline proteases (Stevenson *et al*, 1998; Masui *et al*, 1999; Gupta *et al*, 2005). Proteases are also useful and important components in biopharmaceutical products as contact-lens enzyme cleaners and enzymatic debriders (Anwar and Saleemuddin, 2000). The enzyme also could be used in the applications of alkaline environments including aquaculture industry (Fu *et al*, 2005; Shanmughapriya *et al*, 2008). At present, the use of alkaline proteases has increased remarkably with large proportions of commercially available alkaline proteases derived from *Bacillus* strains (Adinarayana *et al*, 2005; El Enshasy *et al*, 2008; Sen and Satyanarayana, 1993).

Modification of biotechnology and processes, using immobilized biocatalysts, has recently gained the attention of many biotechnologists. Application of immobilized enzymes or whole cells is advantageous, because such biocatalysts display better operational stability (Kukubu *et al*, 1981; Fortin and Vuillemard, 1990) and higher efficiency of catalysis (Ramakrishna *et al*, 1992; Linko and Haapala, 1996) and they are reusable.

The present study was performed in order to evaluate alkaline protease production by *Bacillus pumilis* MTCC 2296 cells by using different entrapment technique under optimized as well as harsh condition and to check their efficiency with control cells.

2 Materials and Methods

Bacillus pumilis (*B. pumilis*) MTCC 2296 was used through out this study. The culture is routinely maintained on Nutrient agar in 90 mm diameter Petri plates at 37 ºC. *B. pumilis* MTCC 2296 cells were immobilized by using sodium alginate, polyacrylamide and agar-agar. The alginate entrapment of cells was performed according method of Johnsen and Flink (1986). Sodium alginate solution was prepared by dissolving sodium alginate

*Corresponding author. Tel: 0091-9216232281; Email: varenyam@gmail.com

in 100 ml boiling water and autoclaved at 121 ºC for 15 minutes.

Immobilization in polyacrylamide was done by adding cells to 2.85 g acrylamide (Sigma-Aldrich), 0.15 g bisacrylamide (Sigma-Aldrich), 10 mg ammonium persulphate (Sigma-Aldrich), and 1 ml TEMED, tetra methyl ethylene diamine (Sigma-Aldrich). The cell suspension and the above phosphate buffer mixture was mixed well and poured into sterile flat bottom 10 cm-diameter Petri plates. After polymerization (solidification), the acrylamide gel was cut into equal size cubes (4 mm^3), transferred to 0.2 M phosphate buffer (pH 7.0), and kept in the refrigerator for 1 hour for curing (Reyed, 2007).

Encapsulation in agar was done by adding cell suspension into the molten agar-agar. The solidified agar block was cut into equal size cubes (4 mm^3), added to sterile 0.1 M phosphate buffer (pH 7.0), and kept in the refrigerator (overnight) for curing (Veelken and Pape, 1982).

The immobilized beads prepared by using all the three matrices along with control *B. pumilis* MTCC 2296 were transferred into 50 ml of production medium in 250-ml flasks. The composition of production medium was 5 g/L glucose, 7.5 g/L peptone, and 5% salt solution ($MgSO_4 \cdot 7H_2O$, 5 g/L; KH_2PO_4, 5 g/L; and $FeSO_4 \cdot 7H_2O$, 0.1 g/L) with a pH of 9.0. The flasks were incubated at 37 ºC for 48 hours. Samples were withdrawn at regular intervals of 6 hours and assayed for alkaline protease activity.

Protease activity was assessed by the modified procedure based on the method of Tsuchida *et al* (1986) using 2.0% casein in 0.2 M carbonate buffer (pH 10.0) as substrate. The culture broth was centrifuged at 8,000 rpm for 10 minutes and supernatant served as the crude enzyme source. One unit of enzyme activity is defined as the amount of enzyme that released 1 µg of tyrosine/ml/minute. Protease activity was also estimated at various pH (8 to 12) using free and immobilized *B. pumilis* MTCC 2296. The buffers used were 20 mM HEPES (pH 8.0 – 9.0) and 200 mM carbonate (pH 10 – 12). All experiments were carried out in triplicate. All the data were analyzed using GraphPad Prism 4.1 software.

3 Results and Discussion

Cell immobilization is one of the common techniques for increasing the overall cell concentration and productivity. Immobilization of cells may allow continuous operation of cultivation processes at high dilution rates (Adinarayana *et al*, 2005).

The amount of cell mass entrapped in calcium alginate matrix increased gradually up to 30 hours of incubation after which there was no appreciable change (Figure 1). The enzyme production was started at 6 hours with immobilized cells and reached a maximum level (491 U/ml) by 30 hours. On further incubation, enzyme production was gradually decreased, whereas maximum enzyme titer was observed by 36 hours in the case of free cells. There was negligible change in pH profile of free cells as well as immobilized cells after 30 hours. Maximum alkaline protease production occurred at around pH 10.5 except calcium alginate matrix (pH 11.5) after 30 hours (Table 1). In case of alginate matrix, enzyme activity was continued increasing up to 36 hours at extreme pH 12 as compare to free cells and other matrices. It is evident that the alkaline protease production was higher with calcium alginate immobilized cells (491 U/ml) than that of free cells (399 U/ml). Ramakrishna *et al* (1992) reported the immobilization of *B. cereus* in calcium alginate and employed packed-bed and fluidized-bed reactors to continuously synthesize thermostable α-amylase.

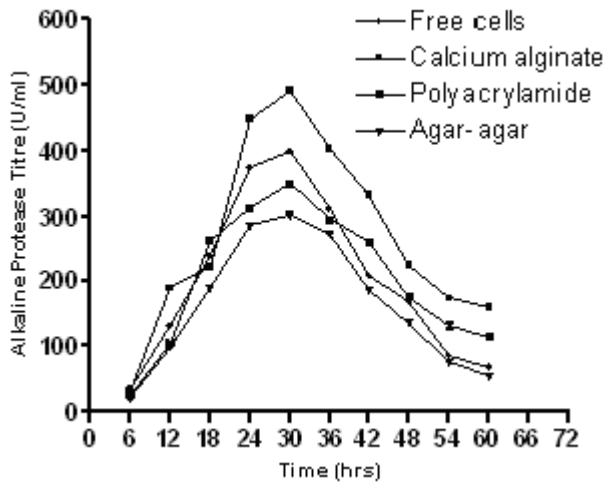

Figure 1. Time course profiles of alkaline protease production by free cell culture and immobilized culture of *B. pumilis* MTCC 2296 in calcium alginate, polyacrylamide and agar-agar.

Polyacrylamide was also found to be one of good matrices for cell immobilization. Using this matrice, gradual increase in alkaline protease production was noticed from 6 hours onwards to 30 hours; on further incubation decline in alkaline protease titer was observed. The maximum alkaline protease titer of 350 U/ml was observed at 30 hours. The alkaline protease titer obtained with this carrier was less than that of free and immobilized cells with the other carrier (calcium alginate).

Alkaline protease production pattern by immobilized

cells in agar-agar was similar to other matrices. The results are similar to Figure 1 and the data indicated that alkaline protease production was started from 6 hours onward and reached a maximum level by 30 hours (303 U/ml). The alkaline protease titer obtained with this carrier was very low compared with the titers of free cells and the immobilized cells of the above-mentioned other carriers. Anna *et al* (2003) reported that the use of agar-entrapped cells of *B. circulans* ATCC 21783 for cyclodextrin glucanotransferase production in a fluidized bed reactor led to enzyme activity (180 U/ml) after 24 hours of cultivation.

Table 1. Comparison of alkaline protease production using *B. pumilis* MTCC 2296 cells entrapped in various gel matrices after 30 hours

Support matrix	Final pH	Alkaline protease titre (U/ml)	Relative percentage of production
Calcium alginate	11.5	491.23[a]	100
Polyacrylamide	10.45	350.03[ab]	71.26
Agar-agar	10.42	302.3[b]	61.54
Free cells	10.48	399.17[a]	81.26

The alginate matrix was found to be superior to the other matrices studied in this paper. In addition, the alginate matrix is less expensive, nontoxic, and preparation of biocatalyst involves mild conditions, which is an added advantage. In contrast, free cells showed lower enzyme productivity than the calcium alginate-immobilized ones and their activity decreased markedly after 30 hours.

4 Conclusion

In conclusion, calcium alginate is a promising method of *B. pumilis* MTCC 2296 immobilization for alkaline protease production. Alkaline protease production by immobilized cells is better than that of free cells.

References

1. Adinarayana K, Jyothi B, Ellaiah P. Production of alkaline protease with immobilized cells of *Bacillus subtilis* PE-11 in various matrices by entrapment technique. AAPS Pharm Sci Tech 2005; 6(3): 391 – 7.
2. Anna V, Nigar B, Venko B. Cyclodextrin glucanotransferase production by free and agar gel immobilized cells of *B. circulans* ATCC 21783. Proc Biochem 2003; 38: 1585 – 91.
3. Anwar A, Saleemuddin M. Alkaline protease from *Spilosoma oblique*: potential applications in bio-formulations. Biotechnol Appl Biochem 2000; 31: 85 – 9.
4. El Enshasy H, Abuoul-Enein A, Helmy S, El Azaly Y. Optimization of the industrial production of alkaline protease by *Bacillus licheniformis* in different production scales. Australian J Basic Applied Sc 2008; 2(3): 583 – 93.
5. Fortin C, Vuillemard JC. Culture flourescence monitoring of immobilized cells. In: Bont JAM, Visser J, Mattiasson B, Tramper J (Eds). Physiology of Immobilized Cells. Amsterdam: Elsevier 1990; 45 – 55.
6. Fu XY, Xue CH, Miao BC, Li ZT, Gao X, Yang WG. Characterization of protease from the digestive tract of sea cucumber (*Stichopus japonicus*): high alkaline protease activity. Aquaculture 2005; 246: 321 – 9.
7. Gupta A, Roy I, Patel PK, Singh SP, Khare SK, Gupta MN. One-step purification and characterization of an alkaline protease from haloalkalophilic *Bacillus* sp. J Chromatogr 2005; 1075: 103 – 8.
8. Herbert RA, Sharp RJ, Fewson CA. Molecular biology and biotechnology of extremophiles. Trends Biotechnol 1992; 10: 330.
9. Johnsen A, Flink JM. Influence of alginate properties and gel reinforcement on fermentation characteristics of immobilized yeast cells. Enz Microb Technol 1986; 8: 737 – 48.
10. Kukubu T, Karube I, Suzuki S. Protease production by immobilized mycelia of *Streptomyces fradiae*. Biotechnol Bioeng 1981; 23: 29 – 37.
11. Linko S, Haapala R. Progress in biotechnology. In: Wijffels RH, Buitellar RM, Bucke C, Tramper J (Eds). Immobilized Cells: Basics and Applications. Amsterdam, The Netherlands: Elsevier 1996; 140 – 53.
12. Masui A, Fujiwara N, Takagi M, Imanaka T. Feasibility study for decomposition of gelatin layers on X-ray films by thermostable alkaline protease from alkaliphilic *Bacillus* sp. Biotechnol Lett 1999; 13: 813 – 5.
13. Ramakrishna SV, Jamuna R, Emery AN. Production of ethanol by immobilized yeast cells. Appl Biochem Biotechnol 1992; 37: 275 – 82.
14. Reyed RM. Biosynthesis and properties of extracellular amylase by encapsulation bifidobatrium bifidum in batch culture. Australian J Basic Applied Sciences 2007; 1(1): 7 – 14.
15. Sen S, Satyanarayana T. Optimization of alkaline protease production by thermophilic *Bacillus licheniformis* S-40. Indian J Microbiol 1993; 33: 43 – 7.
16. Shanmughapriya S, Krishnaveni J, Selvin J, Gandhimathi R, Arunkumar M, Thangavelu T, Kiran GS, Natarajaseenivasan K. Optimization of extracellular thermotolerant alkaline protease produced by marine *Roseobacter* sp. (MMD040). Bioprocess Biosyst Eng 2008; 31: 427 – 33.
17. Stevenson DE, Ofman DJ, Fenton GA. Protease-catalyzed condensation-oligomerization of hydrophobic peptides as a means of flavor modification. J Mol Catal Enzymatic 1998; 5: 39 – 44.
18. Tsuchida O, Yamagota Y, Ishizuka J. An alkaline proteinase of an alkalophilic *Bacillus* sp. Curr Microbiol 1986; 14: 7 – 12.
19. Veelken M, Pape H. Production of tylosin and nikkomycin by immobilized Streptomyces cells. Eur J Appl Microbiol Biotechnol 1982; 15: 206 – 10.

AFLP analysis of genetic relationships and diversity of some Chinese *Osmanthus fragrans* cultivars[☆]

Xueyan Yan[1,#], Baolin Xiao[1,#], Yuanji Han[1], Wangjun Yuan[1,2], Fude Shang[1,*]

[1]*College of Life Sciences & Institute of Agricultural Biotechnology*, *Henan University*, *Kaifeng*, *Henan* 475001, *China*;
[2]*College of Pharmaceutical Sciences*, *Henan University*, *Kaifeng*, *Henan* 475001, *China*

Received December 14, 2008

Abstract

The genetic diversity and genetic relationships of 46 *Osmanthus fragrans* cultivars, collected from Hubei, Zhejiang, and Guangxi provinces in China, were analyzed by the technique of amplified fragment length polymorphism (AFLP). Ten primer combinations were used and generated 436 scorable bands including 269 polymorphic. It indicated that each primer combination generated 26.9 polymorphic bands. Genetic similarities were obtained using simple matching (SM) coefficients, and a dendrogram of the 46 cultivars was established by UPGMA clustering method. The high level genetic variations in 46 *O. fragrans* cultivars were proved by the SM coefficient value from 0.69 to 0.87. The cluster analysis suggested that the 46 *O. fragrans* cultivars could be divided into five groups, and this result was not absolutely consistent with the morphology-based traditional classification. The cluster analysis showed that there were close genetic relationships among cultivars of the same flower color, and the geographic origin of *O. fragrans* was correlated with the analysis cluster results at a certain level. Cluster analysis also indicated that Guangxi cultivars were distinct from those of Hubei and Zhejiang. [Life Science Journal. 2009; 6(2): 11 – 16] (ISSN: 1097 – 8135).

Keywords: AFLP; *Osmanthus fragrans*; cultivar; genetic diversity; UPGMA

1 Introduction

Osmanthus fragrans (*O. fragrans*), belongs to the Oleaceae family, is cultivated extensively as one of the most valuable of fragrance and ornamental plants in China. A long history of domestication was confirmed by the descriptions of this plant in 2500 years old documents. As *O. fragrans* has been cultivated for a long time, a large number of intraspecific varieties occurred under the influence of both natural and artificial selections. At present, there are about 157 cultivars which could be categorized into 4 cultivar groups (Asiaticus Group, Albus Group, Luteus Group, and Aurantiacus Group) according to morphological and physiological characteristics[1,2].

Gene diversity research is significant to illuminate the evolutionary and classification in cultivars of *O. fragrans* not only in theory but also in cultivar breeding and arrangement in garden. However, no reasonable and accepted taxonomic principles and system are established up to now, and there is still much confusion in cultivar nomenclature. There is still a need for a better genetic diversity assessment and varietal identification by using high throughput marker technologies.

The identification of *O. fragrans* cultivars has been traditionally carried out by morphological and physiological traits[2]. Although these methods are efficient, they present practical drawbacks because of the effect of environmental fluctuations on the expression of most morphological traits.

Several researchers sought to rectify the weakness of the traditional approach by using biochemical markers[3,4]. Although such studies provided some useful insights, they posed their own problems. Biochemical markers are not necessarily genotype-specific, and may be influenced by environmental and developmental fac-

[☆]Supported by NSFC (Grant No. 30670137) and Innovation Scientists and Technicians Troop Construction Projects of Henan Province (Grant No.094100510018).
[*]Corresponding author. Tel. & Fax.: 86-378-3886199; Email: fudeshang@henu.edu.cn
[#]Both are equal contribution to this work.

tors[5]. Unaffected by environmental variables, genetic markers can be used to reliably and accurately identify *O. fragrans* cultivars. The randomly amplified polymorphic DNA (RAPD) technique was employed in initial studies of *O. fragrans* genetic markers[6–9]. Recently, the amplified fragment length polymorphism (AFLP)[10] technique was used in *O. fragrans*[11] and showed many advantages over the technique of RAPD, restriction fragment-length polymorphism (RFLP) and SSR (microsatellites)[12–14].

The objectives of this study were to analyze the genetic relationships and diversity among 46 *O. fragrans* cultivars, and then to use this genetic diversity information to suggest strategies for the germplasm identification, breeding, protection and conservation.

2 Materials and Methods

2.1 Plant materials

We collected mature leaves of 46 *O. fragrans* cultivars from Hubei, Zhejiang, and Guangxi provinces (Table 1) in September 2007. These were dried in Silica gel and stored at – 70 ºC.

2.2 Genomic DNA extraction

DNA was extracted from 0.5 g – 0.6 g of leaf tissue using a modified CTAB method[15,16], then purified with 5 mol/L NaCl, water-saturated ether, and RNase.

2.3 AFLP analysis

We followed the protocol used by Han *et al*[11]. Genomic DNA (250 ng) was digested with *Eco*RI and *Mse*I at 37 ºC for 3 h, and then at 65 ºC for 2.5 h. The digested DNA fragments were ligated to *Mse*I and *Eco*RI adaptors (Table 2) with T4 DNA ligase for 2 h at 25 ºC. The ligated fragments were diluted 10-fold in TE buffer (10 mM Tris-HCl, 0.1 mM EDTA) and used as templates in the 20-cycle[10] preamplification PCR. Ten primer combinations were used for the selective amplification (Table 2). The PCR amplifications were carried out in a PTC-100 Thermal Cycler (MJ Research Inc.).

Amplified products were separated by electrophoresis with 6% denaturing polyacrylamide gels in 1 × TBE buffer. The gels were then stained with 0.1% silver nitrate[17] and air dried overnight before being photographed. Only unambiguous bands were scored. The presence of a band was scored as 1 and the absence of a band was scored as 0.

2.4 Data analysis

Polymorphic AFLP markers were manually scored as binary data with presence as “1” and absence as “0”, and

Table 1. *O. frangrans* cultivars analyzed in this study

Group	Code	Cultivar	Origin
Luteus	HT1	Zaojingui-1	Hubei
	HT2	Zijingui	Hubei
	HT3	Yuanban Jingui-1	Hubei
	HT4	Huangchuan Jingui	Hubei
	HT5	Jinhuataige	Hubei
	HT6	Qiugui-1	Hubei
	ZT1	Qiugui-2	Zhejiang
	ZT2	Jinqiugui‘Jinqiu’	Zhejiang
	ZT3	Wandian Jin	Zhejiang
	ZT4	Congzhong Xiao	Zhejiang
	GT1	Juye Zijingui	Guangxi
	GT2	Yuanye Zijingui	Guangxi
	GT3	Taoye Jingui	Guangxi
	GT4	Zaojingui-2	Guangxi
	GT5	Yuanban Jingui-2	Guangxi
	GT6	Hanxiao	Guangxi
	GT7	Yuanye Jingui	Guangxi
	GT8	Heishan Jingui	Guangxi
	GT9	Heishanzhizhu	Guangxi
	HT7	Zuiyun	Hubei
Albus	HL1	Zigeng Zigui	Hubei
	HL2	Changgengbai	Hubei
	HL3	Yinxing	Hubei
	HL4	Jiangnan Liren	Hubei
	ZL1	Wanyingui	Zhejiang
	ZL2	Yulinglong	Zhejiang
	GL1	Yuanye Ziyingui	Guangxi
	GL2	Chiye Ziyingui	Guangxi
	GL3	Qinyun	Guangxi
	GL4	Yaotiaoshunv	Guangxi
	GL5	Cuizhu	Guangxi
	GL6	Ruichi Yingui	Guangxi
	GL7	Ziyun	Guangxi
Aurantiacus	HA1	Chiye Dangui	Hubei
	HA2	Gecheng Dangui	Hubei
	HA3	Dangui	Hubei
	HA4	Mantiaohong	Hubei
	ZA1	Zhuangyuanhong	Zhejiang
	ZA2	Yingye Dangui	Zhejiang
	ZA3	Hongyan Ningxiang	Zhejiang
	ZA4	Zuijihong	Zhejiang
Asiaticus	HF1	Sijigui-1	Hubei
	ZF1	Sijigui-2	Zhejiang
	ZF2	Tianxiang Taige	Zhejiang
	ZF3	Danzhuang	Zhejiang
	ZF4	Tiannv Sanhua	Zhejiang

only bands showing unambiguous polymorphism were entered into a data matrix. Genetic similarities between pairs of cultivars were determined by calculating simple matching (SM) coefficients[18,19]. Then the similarity matrices were followed by unweighted pair group method with arithmetic mean algorithm (UPGMA) method[20] by using SAHN clustering analysis of NTSYS-pc version 2.1[19].

3 Results

3.1 Results of DNA amplification

The 10 AFLP primer combinations used amplified 436 scorable bands ranging from 0.1 kb to 1.5 kb, of which 269 were polymorphic (Table 2). The primer combination E-AAC/M-CAC yielded the largest number of scorable bands (55). Bands generated by E-AAG/M-CTC had the highest polymorphism ratio (70%). Each *O. fragrans* cultivar had its unique fingerprinting and could be easily distinguished from each other. It fully indicated abundant polymorphism existed between *O. fragrans* cultivars genomes. Part of AFLP bands amplified by primer combination E-AAC/M-CAG was presented in Figure 1.

3.2 Genetic relationship and cluster analysis

The result of cluster analysis is shown on the dendrogram (Figure 2) depicting the pattern of relationships among the studied cultivars. There was obvious difference among different cultivars.

Pair-wise genetic similarity ranged from 0.69 to 0.87. The UPGMA dendrogram revealed two distinct clusters that could be further divided into five groups at GS value of 0.72: (1). The first group consisted of 4 cultivars from Hubei province, including 1 cultivar of Aurantiacus

Table 2. Performance of 10 AFLP primer combinations (primers sequence were also lined out)

Primer combination *Eco*RI/*Mse*I	No. of amplified bands	No. of polymorphic bands	Polymorphism ratio (%)	Primer sequence
AAC/CAG	39	27	69.23	Adaptors
AAC/CAC	55	30	54.55	*Eco*RI 5′ctc gta gac tgc gta cc
AAC/CTC	53	32	60.38	cat ctg acg cat ggt taa 5′
AAG/CTC	40	28	70.00	*Mse*I 5′gac gat gag tcc tga g
AAC/CTG	31	20	64.52	ta ctc agg act cat 5′
ACT/CTC	44	30	68.18	Pre-selective primer
AGC/CTC	43	24	55.81	*Eco*RI (a) 5′gac tgc gta cca att c-a
AGC/CTG	34	18	52.94	*Mse*I (c) 5′gat gag tcc tga gta a-c
AGC/CTA	44	29	65.91	Primers
ACT/CTG	53	31	58.49	*Eco*RI (a) 5′gac tgc gta cca att c-axx*
Total	436	269		*Mse*I (c) 5′gat gag tcc tga gta a–cYY*
Mean	43.6	26.9	61.70	

* XX is null for plus 1 primers; CC, CT, GG, AG, CG for plus 3 primers; YY are null for plus 1 primers; AG, GC, AC, TG for plus 3 primers.

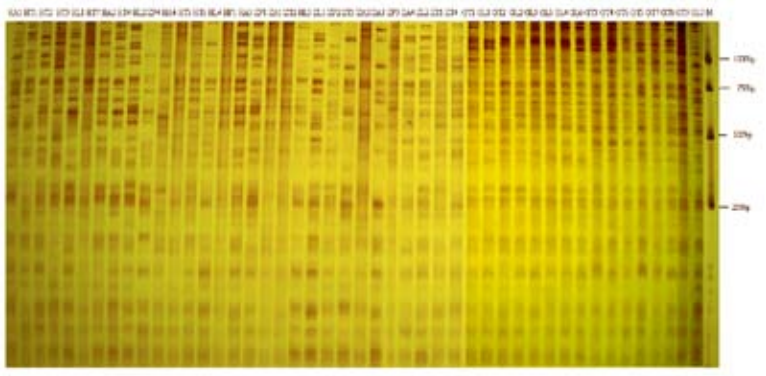

Figure 1. AFLPs generated from genomic DNA of 46 materials using primer combination E-AAC/M-CAG.

Group (HA1) and 3 cultivars of Luteus Group (HT1, HT2, HT4); (2). The second group could be examined more precisely by cutting the dendrogram at GS value of 0.735, the group thus was split to four major sub-groups, leaving HT3 as the first one sub-group and HL1 as the second. There formed 3 minor rami within the third sub-group: the first minor ramus was composed of 3 cultivars (HL2, HL4, HL3) from Hubei province, which belong to Albus Group; the second minor ramus was composed of 2 cultivars (ZF4, ZF3) from Zhejiang province, which belong to Asiaticus Group; the third minor ramus was composed of 5 cultivars from Zhejiang province, including 3 cultivars of Aurantiacus Group (ZA1, ZA2, ZA3) and 2 cultivars of Luteus Group (ZT2, ZT3).The fourth sub-group included 2 cultivars of Aurantiacus Group (HA2, HA4), 2 cultivars of Luteus Group (HT5, ZT1) and 1 cultivar of Albus Group (ZL1); (3).The third group was composed of 2 cultivars of Luteus Group (HT7, HT6) and 3 cultivars of Asiaticus Group (HF1, ZF2, ZF1). (4).The fourth group could be divided into two sub-groups at GS value of 0.72: the first included 2 cultivars of Aurantiacus Group (HA3, ZA4), 1 cultivar of Albus Group (ZL2) and 1 cultivar of Luteus Group (ZT4). They all were collected from Zhejiang province except for HA3, which from Hubei province; the second was exclusively composed of 15 cultivars from Guangxi province, and the 15 cultivars were classified into two sub-groups: one included 5 cultivars of Luteus Group (GT3, GT5, GT4, GT6, GT8); the other included 7 cultivars of Albus Group (GL1, GL2, GL3,GL5,GL4, GL6, GL7) and 3 cultivars of Luteus Group (GT1,GT2,GT9). GL1 and GT2, which were all collected from Guangxi province but belong to different cultivars groups, exhibited the highest genetic similarity of 0.87. (5) The fifth group included only one cultivar (GT7) from Guangxi province, which belongs to Luteus Group.

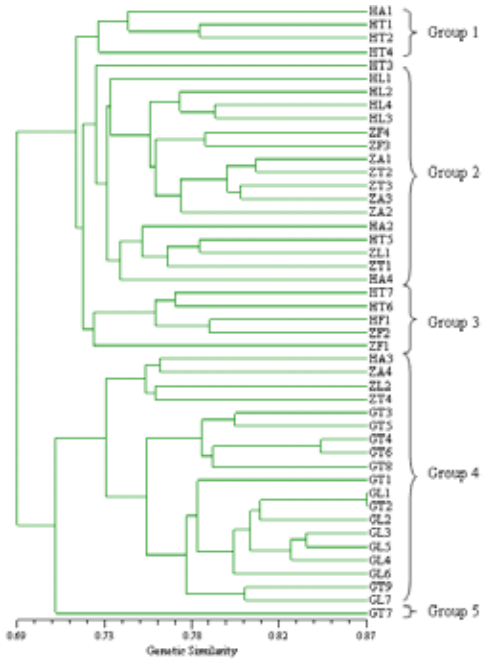

Figure 2. Dendrogram based on simple matching coefficient for 46 materials using ten primer combinations.

4 Discussion

Traditionally, *O. fragrans* cultivars were grouped in either Fragrans Division or Autumn Division according to flowering time. Autumn Fragrans cultivars were further divided into Albus Group, Luteus Group and Aurantiacus Group based on flower color[21–24]. Cluster analysis in present study was not completely in accordance with the traditional classification. The cultivars of the same color could be clustered together at the early stage showed that there were close genetic relationships among cultivars of the same flower color. RAPD and AFLP were used to obtained the similar results from different *O. fragrans* cultivars[6,25]. Zhao *et al* and Liu *et al*, in their analysis of *O. fragrans* cultivars by RAPD[6,25], and Han *et al*, in their AFLP study, obtained the similar results from analysis of different *O. fragrans* cultivars. These similar results suggested that flower color was an advanced criteria of classification which could be used to discriminate efficiently *O. fragrans* germplasm. Cultivars with the same flowering time on the other hand clustered in different groups[25], indicating that flowering time was not a reliable classification criterion. The high natural and artificial selections of this ornamental plant probably has resulted in significant morphological and physiological variations among closely related cultivars, contributing to the discrepancies between the morphology/physiology-based classification and the genetic marker-based groupings. However, these discrepancies may have been exaggerated because the genetic markers used to date possibly do not sufficiently cover regions coding for morphological and physiological traits.

Among the four *O. fragrans* cultivars groups evaluation, the genenic relationship between Luteus Group and Aurantiacus Group was closer than either of them to Albus Group and Asiaticus Group demonstrated by cluster analysis. These data supported the conclusion that Aurantiacus Group cultivars probably originated from bud sports of some Luteus Group cultivars[1,25]. In the light of the laws of evolution and research data, Asiaticus Group

was more primitive than other cultivar groups, while the evolutionary sequence from primitive to advanced in Autumn Division was Albus Group, Luteus Group and Aurantiacus Group[22,27]. Although our conclusion held out this view, there was some difference about the relationship of Asiaticus Group and other cultivar groups. Some researchers obtained the similar conclusion that Asiaticus Group had remote relationship comparing with other three cultivar groups[4,9,11,21,22,25.26]. But, in the dendrogram, the cultivars of Asiaticus Group were clustered with those of other three cultivar groups, which was not in accordance with their conclusion. This difference was probably not typical as a whole because of the limited number of cultivars of Asiaticus Group included in this experiment. So, for further understand the relationship and the evolutive relation of the four cultivar groups, more *O. fragrans* cultivars especially some cultivars of Asiaticus Group were needed.

The geographic origin of *O. fragrans* was correlated with the analysis cluster results at a certain level. Cultivars originating from the same place could be clustered together in the AFLP dendrogram. As was shown in the dendrogram, some cultivars of Hubei were clustered into one group (HA1,HT1, HT2, HT4), some met in one minor group (HL2, HL4, HL3); some cultivars of Zhejiang cultivars were put into one minor group (ZA1, ZA2, ZA3, ZT2, ZT3); all cultivars from Guangxi were clustered into one subgroup with close relationship except GT07. The results confirmed that the *O. fragrans* cultivars from the same place had closer genetic relationships. Cluster analysis indicated that the relationship between Hubei and Zhejiang *O. fragrans* cultivars was nearer and gathered together first, then clustered with Guangxi cultivars, indicating that Guangxi cultivars were distinct from those of Hubei and Zhejiang. Such geographically distinct groups of *O. fragrans* cultivars have been observed in a recent study by Han *et al*[28], and their analysis of the AFLP data also revealed that *O. fragrans* cultivars of the Guilin region formed a distinct subgroup. More studies employing genetic markers are required to map out the geographic distribution of *O. fragrans* cultivar genotypes in China.

This work also established the existence of homonym problems in *O. fragrans* cultivars,the most obvious example is that cultivars with the same name but from different places were clustered into different groups (such as HT1 and GT4, HT3 and GT5, HT6 and ZT1), which suggested that they maybe not the same cultivars. So, we should reexamine the criteria of *O. fragrans* cultivar's classification and establish a rational cultivar classification system.

5 Conclusion

Our study provided valuable information for the identification of *O. fragrans* cultivars and for detecting genetic diversity of the 46 cultivars as well as determining genetic relationships among them. A thorough understanding of the genetic diversity of *O. fragrans* cultivars is critical to future *O. fragrans* cultivars germplasm identification, breeding, protection and conservation. So, further studies may obtain more refined phylogenetic trees of *O. fragrans* cultivars from different geographical areas by combining genetic marker techniques and morphology/physiology-based classification methods.

Acknowledgments

We thank the following individuals for their assistance in collecting the cultivars used: Wang Caiyun, Lu Ling, Zhou Yun, Meng Hongxiang, Bao Zhixian, and Huang Ying.

References

1. Zang DK , Xiang QB. Studies on the cultivar classification of Chinese Sweet Osmanthus. Landscape Plants 2004; 11: 40 – 9 (in chinese).
2. Huang YY, Huang DL. Theories of flowers. Shanghai : New Century Press . 1949 (in chinese).
3. Chen JY, Ning YX, Zhao CH, *et al*. Studies on the isoperoxidase of *Osmanthus fragrans* Varieties in Henan. Acta Horticulturae Sinica 1995; 24(5): 310 – 1 (in Chinese).
4. Zhao XL,Yao CH. Studies on the isozyme of sweet osmanthus varieties. Journal of Huazhong Agricultural University 2000; 19(6): 595 – 9 (in Chinese).
5. Zhang L, Hakins PO, Kochert G, *et al*. Differentiation of bermudagrass (*Cynodon* spp.) genotypes by AFLP analyses. Theor Appl Genet 1999; 98: 895 – 902.
6. Zhao XL,Yao CH. Preliminary RAPD analysis of *Osmanthus fragrans* cultivars. Journal of Huazhong Agricultural University 1999; 18(5): 484 – 7 (in Chinese).
7. Zhu C, Liu FY. To apply RAPD in classification and differention of cultivar of *Osmanthus fragrans* Lour. Guilin 1999; 19(2): 190 – 2 (in Chinese).
8. Shang FD, Yi YJ, Zhang T. The RAPD Analysis of 17 *Osmanthus fragrans* cultivars in Henan Province. Acta Horticulturae Sinica 2004; 31(5): 685 – 7 (in chinese).
9. Yi YJ, Huang Y, Shang FD. Identifying *Osmanthus fragrans* cultivars in Guilin City and evaluating their genetic relationships by RAPD markers. Guihaia 2005; 25(20): 129 – 33 (in chinese).
10. Vos P, Hogers R, Bleeker M, *et al*. AFLP: a new technique for DNA fingerprinting. Nucleic Acids Res 1995; 23: 4407 – 14.
11. Han YJ, Dong MF, Yuan WJ, *et al*. Study on the genetic diversity of some *Osmanthus fragrans* cultivars based on AFLP markers. Acta Horticulturae Sinica 2008; 35(1):137 – 42 (in chinese).
12. Powell W, Morgante M, Andre C, *et al*. The comparison of RFLP, RAPD, AFLP and SSR (microsatellite) markers for germplasm analysis. Molecular Breeding 1996; 2: 225 – 38.
13. Russell JR, Fuller JD, Macaula YM, *et al*. Direct comparison of lev-

els of genetic variation among barely accessions detected by RFLPs, SSRs and RAPDs. Theor Appl Genet 1997; 95: 714 – 2.
14. Pejic I, Ajmone-Marsan P, Morgante M, *et al*. Comparative analysis of genetic similarity among maize inbred lines detected by RFLPs, RAPDs, SSRs and AFLPs. Theor Appl Genet 1998; 97: 1248 – 55.
15. Ude G, Pillay M, Nwakanma D, *et al*. Analysis of genetic diversity and sectional relationships in Musa using AFLP markers. Theor Appl Genet 2002; 104: 1239 – 45.
16. Cheng YJ, Yi HL, Pang XM, *et al*. An efficient method for genomic DNA extraction from woody fruit plants. Journal of Huazhong Agricultural University 2001; 20(5): 481 – 3 (in chinese).
17. Bassam BJ, Caetano-Anollés G, Gresshoff PM. Fast and sensitive silver staining DNA in polyacrylamide gels. Anal Biochem 1991; 196: 80 – 3.
18. Sokal RR, Michener CD. A statistical method for evaluating systematic relationships. Univ Kansas Sci Bull 1958; 38: 1409 – 38.
19. Rohlf FJ. NTSYS-PC numerical taxonomy and multivariate analysis system. Version 2.1. Exeter Software, Setauket, NY. 1999.
20. Sneath PHA, Sokal RR. Numerical taxonomy. Freeman, San Francisco, USA, 1973.
21. Liu YL, Xiang QB. Studies on the classification of *Osmanthus fragrans* cultivars. 20 years of science and technology development of Chinese flowers. S cience Press. 2002; 1: 631 – 42 (in chinese).
22. Zang DK, Xiang QB, Liu YL. A study on the origin and evolution of sweet Osmanthus cultivars. Sweet Osmanthus (Collection on the Application to International Cultivar Registration Authority (ICRA) of *Osmanthus fragrans* Cultivars (II)). Jilin Science and Technology Press. 2002; 1 – 12 (in chinese).
23. Liu YL. Study on the classification of *Osmanthus fragrans* cultivars and utilize of species resources of Osmanthus. Journal of Plant Resources and Environment 1993; 2(2): 44 – 8 (in chinese).
24. Zhu CS, Li RF,Yuan JD, et al. Investigation on the classification of *Osmanthus fragrans* lour. curtivars in Henan. Acta Agriculturae University. Henanensis 1992; 26(2): 192 – 201 (in chinese).
25. Liu LC, Xiang QB, Liu YL. The application of RAPD marker in diversity detection and cultivar identification of *Osmanthus fagrans*. Journal of Nanjing Foresry University (Natural Science Edition) 2004; 28: 76 – 82 (in Chinese).
26. Hu SQ, Zhang HY, Wu GH, *et al*. Studies on resource and taxon of *Osmanthus fragrans* cultivars. Journal of Zhejiang University (Agric1 & Life Sci) 2005; 31(4): 445 – 8 (in chinese).
27. Liu YL, Xiang QB. An Illustrated Monograph of the Sweet *Osmanthus Cultivars* in China. Zhejiang: Zhejiang Science and Technology Press. 2008; 88 – 9 (in chinese and english).
28. Han YJ, Dong MF, Yuan WJ, *et al*. Study on the Genetic Diversity of Osmanthus fragrans Cultivars CHINESE BULLETIN OF BOTANY 2008; 25(5): 559 – 64.

Development of core collection using morphological descriptors in Sweet osmanthus (*Osmanthus fragrans* Lour.) germplasm☆

Wangjun Yuan, Jinsheng Lei, Yuanji Han, Xueyan Yan, Fude Shang*

College of Life Sciences & Institute of Agricultural Biotechnology, *Henan University*, *Kaifeng*, *Henan* 475001, *China*

Received December 19, 2008

Abstract

Sweet osmanthus (*Osmanthus fragrans* Lour.) is one of the most valuable and ornamental plants of China. *O. fragrans* in medicinal uses with an anti-tussive of its flowers and its essential oil used as a flavouring. The development of a core collection could facilitate easier access to sweet osmanthus genetic resources for their use and simplify the genebank management. The present study was initiated to develop a core subset of sweet osmanthus based on 12 qualitative traits and 5 quantitative traits on 122 sweet osmanhus accessions. The accessions were stratified by group, and data on 12 qualitative traits and 5 quantitative traits were used for clustering following Ward's method. About 30 % of the accessions were randomly selected from each cluster to constitute a core subset of 38 accessions. Mean comparisons using *t*-test, frequency distribution using χ^2-test, and Shannon-Weaver diversity index of 17 descriptors indicated that the genetic variation available for these traits in the entire collection has been preserved in the core subset. There was a fair degree of similarity in phenotypic correlation coefficients among traits in the entire collection and core subset, suggesting that this core subset has preserved most of the co-adapted gene complexes controlling these associations. [Life Science Journal. 2009; 6(2): 17 – 22] (ISSN: 1097 – 8135).

Keywords: sweet osmanthus; core collection; genetic resources; Shannon-Weaver diversity index

1 Introduction

Sweet osmanthus belongs to the genus *Osmanthus* in the Oleaceae family. Descriptions of this plant appear in 2500 years old documents, suggesting a long history of domestication[1]. It is certain that sweet osmanthus is a plant originated from a China-Himalayan region, in the southwest China, from the eastern Himalayan Mountains extending to northern Thailand[2]. Sweet osmanthus is one of the most valuable and ornamental plants of China. Appreciating osmanthus flowers in golden autumn is a traditional habitude in China. In order to develop and expand osmanthus culture, Osmanthus festivals are solemnly and grandly held every year in China to promote their local tourism[1]. It is especially valued as an additive for tea and other beverages and is native to Asia which extends from the Himalayas east through China to Japan. *Osmanthus fragrans* Lour. (*O. fragrans*) is used in cosmetics for the hair and skin, but is mostly used for aromatic therapy. In addition, *O. fragrans* in medicinal uses with an anti-tussive of its flowers and its essential oil used as a flavouring[3].

Long-standing cultivation and the process of history has enabled us to boast of rich cultivars of sweet osmanthus, but due to the limitations of history, there had never been any detailed sweet osmanthus investigation, or theoretical and systematical classification research on sweet osmanthus and its cultivars had never been conducted until the 1980s. At that time a group of scientists devoted themselves to research into sweet osmanthus and its cultivars, and into its classification system (Chen, 1983; Liu, 1985; Lu, 1986; Zhu, 1992)[1]. At present, there are about 166 cultivars which could be categorized into 4 cultivars groups (Asiaticus Group, Albus Group, Luteus Group, and Aurantiacus Group) according to morphological and physiological characteristics[4]. The detailed characters of 122 cultivars of sweet osmantus were described in Xiang's an

☆Supported by the NSFC (Grant No. 30670137) and Innovation Scientists and Technicians Troop Construction Projects of Henan Province (Grant No. 094100510018).

*Corresponding author. Tel and Fax: 86-378-3886199; Email: fudeshang@henu.edu.cn

Illustrated Monograph of the sweet Osmanthus Cultivars in China (2008). Accordintg to the flowing time and corolla color all the cultivars also are divided into 4 groups: Asiaticus Group, Albus Group, Luteus Group, and Aurantiacus Group.

Frankel (1984) proposed ''core collection'' which would represent, with a minimum of repetitiveness, the genetic diversity of a crop species and its relatives[5]. Frankel and Brown (1984)[6] and Brown (1989)[7] outlined the procedure for the development of core collection by using information on the origin and characteristics of the accessions. The issues that should be taken into consideration while developing a core are the size, the sampling strategy, the grouping within the collection, and the number of accessions to be included in the core from each group. The core collection should be about 10% of the total collection that will retain over 70% of the alleles in the whole collection[7]. Using the stratified sampling, the collection is first divided into non-overlapping groups or strata, and then a simple random sampleis drawn from within each group. Passport and characterization data may be used to determine the groups within the germplasm collection. The hierarchy of groupings begins with the groupings suggested by taxonomy followed by assigning accessions to major geographic groups or agro-ecological regions. Clustering within the broad geographic group could be done based on information from available genetic diversity, cytological variation, marker loci or quantitative traits, and data on stress tolerances. Collection with abundant discriminating data of this type will require a multivariate clustering to discern groups of similar accessions[8]. The number of accessions selected from each cluster will depend on the strategy used. A good core collection should have maximum genetic diversity and no genotypically redundant entries, should represent the whole collection, and should be small enough to manage easily[9].

Core collection has been developed in many crops[10–14]. Core collection has also been developed in some horticultral plants. Johnson *et al* developed a core subset (CS) of 210 safflower accessions based on branching pattern, flower color, flowering time, growth habit, head diameter, plant height, iodine number, lysine content, oil content, and spineless on 2000 accessions from 50 countries[15]. The present study was therefore aimed to develop a CS of sweet osmanthus based on four groups, 12 qualitative traits and 5 quantitative traits.

2 Materials and Methods

We used 122 accessions of four groups described by Xiang (2008) to develop the CS for sweet osmanthus (Table 1). The accessions were first stratified by group. The data on 12 qualitative traits in each group was standardized using the range of each variable to eliminate scale differences[16]. The standardized data was subjected to the hierarchical cluster algorithm of Ward[17], using SPSS13.0. This method optimizes an objective functionbecause itminimizes the sum of the square within groups and maximizes the sum of squares among groups. The agglomerative procedure starts with n groups (i.e., one observation in one group; maximum among group sum of squares), and proceeds by merging observations in groups so that the between-groups sum of squares decreases and within-groups sum of squares increases. In certain cases the within-groups sum of square will remain the same, but it will never decrease[18]. From each cluster, 30% of the accessions were randomly selected for inclusion into the CS. At least one accession was included from those clusters that had less than 3 accessions.

Means of the entire collection (EC) and CS for the 12 morphological descriptors were compared using Newman-Keuls procedure[19]. The homogeneity of variances of the EC and CS was tested with the Levene's test[20]. The distribution homogeneity for each descriptor among the EC and the CS was analyzed by the χ^2-test. The phenotypic correlation among different traits in the EC and CS was estimated to know whether these associations, which may be under genetic control, were conserved in the CS.

3 Results

A CS of 38 accessions was established from 122 sweet osmantus accessions. These 38 accessions were arrayed into 4 distinct clusters (Table 2). Albus Group and Luteus Group accounted for 66.4% (81 accessions) of the accessions in the EC, and this predominance was also reflected in the CS that contain, 65.8% (25 accessions) of the accessions from the two groups. About 13.1% (5) of the accessions in the CS were from Asiaticus Group, 21.1% (8) from Aurantiacus Group.

The ranges, means, and variances of the 12 qualitative traits and 5 quantitative traits are given in Table 3. Differences among means of the EC and CS for the 12 qualitative traits used in developing the CS were not significant, and the variances of the EC and CS were homogeneous for all the traits. The CS captured 100% range variation for 10 qualitative traits and 90% for leaf margin and shape of spring leaf. The differences between means and variances of the EC and CS for the 5 quantita-

Table 1. List of morphological descriptors recorded on 122 sweet osmanthus accessions

Morphological descriptor	Abbreviation	Classes and stage of evalution
Qualitative traits		
Growth habit	GH	shrub-1, tree-2, shrub or tree-3
Growth status	GS	vigorous-1, medium vigorous-2, slight vigorous-3
Shape of tree crown	STC	ellipsoidal-1, spheroidal-2, spheroidal or broad spheroidal-3, ovoid-4, ellipsoidal or spheroidal-5, ovoid or spheroidal-6, oblate spheroidal-7, long spheroidal-8, obovoid-9, irregular spheroidal-10
Leaf margin	LM	entire or nearly-1, entire-2, thin serrate-3, serrate-4, entire or sprase serrate-5, entire or serrate-6, always serrate-7, dense serrate-8, sprase serrate-9
Base of leaf	BL	cuneate-1, narrow cuneate-2, cuneate or narrow-3, broad cuneate-4, rounded-5
Shape of spring leaf	SPL	elliptic-1, obovate-elliptic-2, obovate-ellipticto broad elliptic-3, broad elliptic to rounded-4, elliptic to broad elliptic-5, obovate or obovate-ellipticto-6, elliptic to elliptic-lanceolate-7, elliptic-lanceolate-8, linear-lanceolate-9, oblanceolate-10, elliptic to ovate-elliptic-11, linear-12, oblong-lanceolate-13, lanceolate-14
No. buds per node	NBN	1 pair-1, 2 pairs-2, 1-2 pairs-3, 1-3 pairs-4, 2-3pairs-5, 3-4pairs-6
Corolla color	CC	Yellow white-1, milky white-2, silvery white-3, milky yellow-4, white-5, light orange-6, orange yellow-7, light yellow-8, golden-yellow-9, yellow-10, deep yellow-11, deep orange yellow-12, orange red-13
Expand mode of corolla	EMC	spreading-1, inclined-2, spreading or inclined-3, reflexed-4, unexpanding-5
Shape of corolla lobe	SCL	elliptic-1, ovate-2, obovate-3, oblong-4, linear-5, elliptic orrounded-6, obovate or elliptic-7
No. flowering of every year	NFE	1 time-1, 2 times-2, 1-2 times-3, 2-3 times-4, 3-4 times-5, time after time-6
Pistil	PI	fruit-1, sterile-2, abortive-3
Leaf length (cm)	LL	Average length
Length of petiole (mm)	LP	Average length
No.of leaf side venation (pair)	NLV	Average pair
Corolla diameter (mm)	CD	Average diameter
Length of pedicel (mm)	LPE	Average length

tive traits were also not significantly different. The CS captured over 90% range variation for three quantitative traits (Leaf length, Corolla diameter and Length of pedicel).

Table 2. Group representation of accessions in EC and CS in sweet osmanthus

Group	No. of accessions in EC	No. of accessions in CS
Asiaticus	14	5
Albus	46	15
Luteus	35	10
Aurantiacus	27	8

The analysis of frequency distribution of 12 morphological descriptors indicated the homogeneity of distribution among the EC and CS inferred from probability (> 0.05) (Table 4).

Ortiz *et al* emphasized the importance of proper and adequate sampling for the conservation of phenotypic associations arising from coadapted gene complexes in core collection[21]. There is a fair degree of similarity in phenotypic correlation coefficients among qualitative and quantitative traits, suggesting that this CS has preserved most of the co-adapted gene complexes controlling these associations. The correlation (*r*) values were low but significant (48 and 42 correlation coefficients in EC and CS, respectively in Table 5 and 7 and 6 correlation coefficients in EC and CS, respectively in Table 6), indicating that these correlation's did not explain a large fraction of the total variation.

The Shannon-Weaver diversity index (H′) was used to measure allelic richness and evenness in the EC and CS. A low H′ indicates an extremely unbalanced frequency of classes for an individual trait and a lack of genetic diversity. In the present study, H′ values for all the 12 qualitative traits and quantitative traits were similar in the EC and CS (Table 7), indicating that the diversity of the EC was represented in the CS.

Table 3. Range, mean, and variance of 12 qualitative traits and 5 quantitative traits recorded in the EC and CS of sweet osmanthus

Qualitative traits	Range		Mean*		Significance	Variance**			
	EC	CS	EC	CS		EC	CS	*F*-value	*P*-value
GH	1 – 3	1 – 3	2.2	2.3	NS	0.57	0.49	0.325	0.570
GS	1 – 3	1 – 3	1.5	1.4	NS	0.38	0.41	0.027	0.871
STC	1 – 10	1 – 10	3.4	3.5	NS	6.54	7.18	0.012	0.914
LM	1 – 9	1 – 8	4.0	4.1	NS	4.76	4.48	0.071	0.791
BL	1 – 5	1 – 5	2.9	2.9	NS	2.53	2.69	0.087	0.769
SPL	1 – 14	1 – 13	6.4	6.1	NS	14.53	14.75	0.019	0.891
NBN	1 – 6	1 – 6	3.7	3.4	NS	2.05	2.07	0.191	0.663
CC	1 – 13	1 – 13	6.1	6.2	NS	16.42	17.74	0.160	0.690
EMC	1 – 5	1 – 5	2.0	2.2	NS	0.62	0.86	1.513	0.220
SCL	1 – 7	1 – 7	3.5	3.4	NS	3.66	3.44	0.153	0.696
NFE	1 – 6	1 – 6	2.6	2.7	NS	2.84	3.22	0.703	0.403
PI	1 – 3	1 – 3	1.8	1.8	NS	0.22	0.19	2.434	0.121
LL (cm)	6 – 14.5	7 – 13	9.8	10.0	NS	2.93	2.27	0.342	0.559
LP (mm)	5 – 15	6 – 15	9.8	9.8	NS	4.68	5.67	0.474	0.492
NLV (pair)	6 – 12	6 – 12	8.5	8.5	NS	1.63	1.92	0.236	0.628
CD (mm)	4.5 – 12	6 – 11	7.7	7.6	NS	2.56	2.85	0.517	0.473
LPE (mm)	4 – 14.5	5 – 14.5	8.5	8.4	NS	5.31	5.18	0.135	0.714

*: NS (Non significant) at 0.05; **: Differences between mean of EC and CS were tested by Newman-Keuls test, and variance homogeniety was tested by Levene's test.

Table 4. Chi-square test and probability for comparison of frequency distribution of 12 qualitative traits between the CS and entire sweet osmanthus collection

Descriptor	No. of classes	χ^2	Probability
GH	3	0.831	0.660
GS	3	0.239	0.887
STC	8	3.057	0.962
LM	8	5.015	0.756
BL	5	1.015	0.908
SPL	13	4.494	0.985
NBN	6	2.701	0.746
CC	14	6.490	0.927
EMC	4	2.661	0.616
SCL	7	1.203	0.977
MFE	6	1.014	0.908
PI	3	0.888	0.641

4 Discussion

Based on the conception and the significance of the core collection, and the characteristics and the status of germplasmand core collection of horticultural plants, we should quickly set up some core collections of traditional famous and important horticultural plants aimed at making full use of the germplasm resources, promoting innovation ability of germplasm resources and propelling horticultural industry[22]. Sweet osmanthus, as a traditionally popular flower in china, should set up core collection and possess the condition by the efforts of the scientists of International Cultivars Regitration Center For Osmanthus. In the present study we developed core cellection of sweet osmanthus base on 12 qualitative traits and 5 quantitative traits described in Xiang's an Illustrated Monograph of the sweet Osmanthus Cultivars in China. We expect to provide some help for protecting of germplasm resources and breeding of sweet osmanthus.

Suresh and Balakrishnan compared the diversity of the core sample with that of the whole collection using six different sampling strategies. The pool diversity index based on 28 descriptors was close to the diversity of the whole collection. However, when accessions from different diversity groups were allocated with equal frequency or in proportion to the logarithm of the number of accessions in each group or in the proportion to the square root-proportion of the number of accessions in each group, the resultant core sampleshad higher levels of diversity than the whole collection[23]. Liu *et al* also reported that a core of 719 mungbean accessions, roughly

Table 5. Correlation coefficients between 12 morphological descriptors in the EC (above diagonal) and CS (below diagonal) of sweet osmanthus

	GH	GS	STC	LM	BL	SPL	NBN	CC	EMC	SCL	NFE	PI
GH	–	0.093	– 0.111	– 0.111	0.171*	0.027	– 0.030	– 0.224*	0.241*	– 0.161*	0.196*	– 0.274*
GS	– 0.095*	–	– 0.282*	– 0.077*	– 0.056	– 0.314*	– 0.082	0.124*	0.039	0.120*	– 0.082*	– 0.030
STC	0.032	– 0.110*	–	0.043	0.073	0.163*	0.090*	0.017	0.127*	0.103*	– 0.086	0.135*
LM	0.211**	– 0.170*	0.153*	–	0.142*	– 0.080*	0.065	– 0.022	– 0.074	0.057	– 0.131*	– 0.342*
BL	0.173*	– 0.022	0.005	0.134*	–	0.131*	0.279*	– 0.169*	0.209*	0.272*	0.376*	0.014
SPL	0.099*	– 0.188*	0.109*	0.153*	0.084*	–	0.233*	0.101*	0.382*	– 0.325*	– 0.078*	0.010
NBN	0.041	– 0.063*	0.112*	0.049	0.171*	0.153*	–	– 0.164*	0.256*	– 0.052	– 0.308*	0.002
CC	– 0.051*	– 0.110*	0.128*	0.075*	– 0.120*	0.057*	– 0.020	–	0.011	0.020	– 0.339*	0.092
EMC	0.088*	0.062*	– 0.001	0.116*	0.075*	0.066*	0.052*	– 0.151*	–	0.114*	0.079*	0.074*
SCL	– 0.050*	0.114*	– 0.063*	0.000	– 0.023	– 0.006	0.021	0.044	0.117*	–	0.097	0.213*
NFE	– 0.133*	0.181*	– 0.128*	– 0.115	0.117*	– 0.102*	0.113*	– 0.245*	0.120*	– 0.011	–	0.118*
PI	– 0.061*	– 0.049	– 0.072*	0.024	0.008	0.090*	0.237*	0.155*	– 0.029	0.074*	0.070*	–

* and **: Significant at 0.05 and 0.01 probability level, respectively.

Table 6. Correlation coefficients between 5 quantitative traits in the EC (above diagonal) and CS (below diagonal) of sweet osmanthus

	LL	LP	NLV	CD	LPE
LL	–	0.350*	0.342*	0.172	– 0.021
LP	0.320**	–	0.281*	0.068	0.222*
NLV	0.460**	0.223**	–	0.071	– 0.217*
CD	0.249**	0.086	0.198*	–	0.439**
LPE	0.102	0.203*	0.009	0.437**	–

* and **: Significant at 0.05 and 0.01 probability level, respectively.

Table 7. Shannon-Weaver diversity index for 12 morphological and 5 quantitative traits in the ES and CS of sweet osmanthus

Qualitative traits	EC	CS
GH	1.05	0.99
GS	0.85	0.85
STC	1.84	1.77
LM	1.46	1.43
BL	1.51	1.44
SPL	2.08	2.03
NBN	1.50	1.60
CC	2.32	2.28
EMC	1.10	1.12
SCL	1.57	1.66
NFE	1.41	1.49
PI	0.64	0.59
LL (cm)	2.54	2.35
LP (mm)	2.77	2.61
NLV (pair)	2.20	2.14
CD (mm)	2.49	2.43
LPE (mm)	2.75	2.51

14.2% of the 5072 accessions, represented the whole collection[24]. The accessions were stratified by group, and data on 12 qualitative traits and 5 quantitative traits were used for clustering following Ward's method. About 30% of the accessions were randomly selected from each cluster to constitute a CS of 38 accessions. Mean comparisons using t-test, frequency distribution using χ^2-test, and Shannon-Weaver diversity index of 17 descriptors indicated that the genetic variation available for these traits in the EC has been preserved in the CS. There was a fair degree of similarity in phenotypic correlation coefficients among traits in the EC and CS, suggesting that this CS has preserved most of the co-adapted gene complexes controlling these associations.

References

1. Xiang QB, Liu YL. An illustrated monograph of the sweet osmanthus cultivars in China. Zhejiang Science & Technology Press, 2008 (in chinese).
2. Green PS. A monographic revision of Osmanthus in eaet Asia and north America. Notes from the Royal Botanic Garden Edingurg 1958; 22: 435 – 542.
3. Deng C, Song G, Hu Y. Application of HS-SPME and GC-MS to characterization of volatile compounds emitted from Osmanthus flowers. Annali di chimica 2004; 94: 921 – 27.
4. Zang DK , Xiang QB. Studies on the cultivar classification of Chinese Sweet Osmanthus. Landscape Plants 2004; 11: 40 – 9 (in chinese).
5. Frankel OH. Genetic perspective of germplasm conservation. In: Arber W, Llimensee K, Peacock WJ, Starlinger P (Eds). Genetic Manipulations: Impact on Man and Society. Cambridge University Press, Cambridge, England, 1984; 161 – 70.
6. Frankel OH, Brown AHD. Current plant genetic resources – a critical appraisal. In: Chopra VL, Joshi BC, Sharma RP, Bansal HC (Eds). Genetics: New Frontiers, Vol IV. Oxford and IBH Publishing Company, New Delhi, India, 1984; 1 – 63
7. Brown AHD. Core collections: a practical approach to genetic re-

sources management. Genome 1989; 31: 818 – 24.
8. Spagnoletti Zeuli PL, Qualset CO. Geographical diversity for quantitative spike characters in a world collection of durum wheat. Crop Science 1987; 27: 235 – 41.
9. Brown AHD. The case for core collections: a practical approach to genetic resources management. In: Brown AHD, Frankel OH, Marshall DR, Williams JT (Eds). The Use of Plant Genetic Resources. Cambridge University Press, Cambridge, England, 1989; 136 – 55.
10. Erskine W, Muehlbauer FJ. Allozyme and morphological variability, outcrossing rate and core collection formation in lentil germplasm. Theoretical and Applied Genetics 1991; 83: 119 – 25.
11. Cordeiro CMT, Morales EAV, Ferreira P, Rocha DMS, Costa IRS, Valois ACC, Silva S. Towards a Brazilian core collection of cassava. In: Hodkin T, Brown AHD, van Hintum ThJL, Morales BAV (Eds). Core Collection of Plant Genetic Resources, International Plant Genetic Resources Institute (IPGRI). John Wiley and Sons, New York, USA, 1995; 155 – 68.
12. Upadhyaya HD, Bramel PJ, Singh S. Development of a chickpea core subset using geographic distribution and quantitative traits. Crop Science 2001; 41: 206 – 10.
13. Upadhyaya HD, Bramel PJ, Ortiz R, Singh S. Developing a mini core of peanut for utilization of genetic resources. Crop Science 2002; 42: 2150 – 6.
14. Upadhyaya HD, Bramel PJ, Ortiz R, Singh S. Development of a groundnut core collection using taxonomical, geographical and morphological descriptors. Genetic Resources and Crop Evolution 2003; 50: 139 – 48.
15. Johnson RC, Stout DM, Bradley VL. The US Collection: a rich source for safflower germplasm. In: Dajue L, Yuanzhou H (Eds). Proceedings of the Third International Safflower Conference, Beijing Botanical Garden, Institute of Botany. Chinese Academy of Sciences, 1993; 202 – 8.
16. Milligan GW, Cooper MC. An examination of procedures for determining the number of clusters in a data set. Psychometrika 1985; 50: 159 – 79.
17. Ward J. Hierarchical grouping to optimize an objective function. Journal of the American Statistical Association 1963; 38: 236 – 44.
18. Dwivedi SL, Upadhyaya HD, Hegde DM. Development of core collection using geographic information and morphological descriptors in safflower (*Carthamus tinctorius* L.) germplasm. Genetic Resources and Crop Evolution 2005; 52: 821 – 30.
19. Newman D. The distribution of range in samples from a normal population expressed in terms of an independent estimate of standard deviation. Biometrika 1939; 31: 20 – 30.
20. Levene H. Robust tests for equality of variances. In: Olkin I (Ed). in Honour of Harold Hotelling. Stanford University Press, Stanford, 1960; 278 – 92.
21. Ortiz R, Ruiz-Tapia EN, Mujica-Sanchez A. Sampling strategy for a core collection of Peruvian quinoa germplasm. Theoretical and Applied Genetics 1998; 96: 475 – 83.
22. Li BY, Zhang QX. Reviewof the studieson core collection for horticultural plants. Journal of Fruit Science 2007; 24(2): 204 – 9 (in chinese).
23. Suresh KK, Balakrishnan R. Strategies for developing core collection of safflower (*Carthamus tinctorius* L.) germplasm – Part 1. Sampling from diversity groups of quantitative morphological descriptors. Indian J Plant Genet Resour 2001; 14: 22 – 31.
24. Liu CY, Wang SH, Wang LX, Sun L, Mei L, Xu N, Cheng XZ. Establishment of candidate core collection in Chinese Mungbean germplasm resources. Acta Agromomica Sinica 2008; 34(4): 700 – 5 (in chinese).

Enhancement of enzyme cytotoxicity mediated by HIV-1 TAT protein with Gly_4 linker *in vitro*: a study with TAT-TK fusion construct☆

Zhe Wang[1], Zujiang Yu[2], Quancheng Kan[1,*], Jie Zhao[1], Heqing Jiang[2], Xiaofei Li[1]

[1]*Department of Pharmacology*, *The First Affiliated Hospital of Zhengzhou University*, *Zhengzhou*, *Henan* 450052, *China*; [2]*Department of Infectious Disease*, *The First Affiliated Hospital of Zhengzhou University*, *Zhengzhou*, *Henan* 450052, *China*

Received March 19, 2009

Abstract

Background. Suicide gene therapy using herpes simplex virus type-1 (HSV-1) thymidine kinase (TK) is a widely exploited approach for gene therapy of cancer and other hyperproliferative disorders. Despite its popularity, clinical success has been so far hampered mostly by the relative inefficiency of TK gene transfer and its limited bystander effect. *Materials and Methods*. Here we report that fusion of TK to HIV-1 Tat protein with different Gly linker imparts cell membrane translocating ability to the enzyme and significantly increases its cytotoxic efficacy, and Gly4 linker between fusion protein show a major impact to enhancement of TK tumor cells killing compared to Gly_0, Gly_2 and Gly_6. Experiments were performed by incubated HepG2 cells with Dulbecco's modified Eagle's medium (DMEM) containing 10 μg/ml different Gly linker fusion proteins. *Results*. The clearance of TK-expressing cells is confirmed by Immunofluorescence assay and results show that transcellular transfer of active HSV-1 thymidine kinase could be mediated by HIV-1 Tat. Meanwhile, the proportion of apoptosis cells detected by cell flow cytometry and survival cell populations by trypan blue suggested that the remarkable enhancement of fusion protein with Gly_4 linker cytotoxicity can be detected in different group *in vitro*. *Conclusions*. This modification of TK might constitute an important step in the optimization of TK suicide gene strategy for gene therapy of cellular proliferation. [Life Science Journal. 2009; 6(2): 23 – 28] (ISSN: 1097 – 8135).

Keywords: thymidine kinase; Tat; glycine; internalization effects

1 Introduction

Thymidine kinase (TK) from human herpes simplex virus type 1 (HSV-1) is the most extensively exploited gene for the control of cellular proliferation in gene therapy[1]. Cells expressing TK convert the nucleoside analogues acyclovir (ACV) and ganciclovir (GCV) into their phosphorylated forms, which are in turn incorporated into replicating DNA where they block further chain elongation and consequently induce cell death[2]. Prodrug gene therapy using TK has found application in several instances. However, the results so far obtained have shown only marginal clinical benefit, mainly due to the poor rate of delivery of the HSV-TK gene to tumor cells[3,4]. In the last few years, some proteins, which present the unusual characteristic of crossing the cell membranes through noncanonical processes of secretion or internalization, have been described. In particular, chemical cross linking of Tat peptides with heterologous proteins[5] or more efficiently, production of recombinant proteins facilitates the intracellular delivery of these proteins. Monica and her colleagues have recently observed that recombinant proteins fused to full-length Tat (86 amino acids) efficiently enter the cells when present in the extracellular medium and are readily transported to the nucleus in an active form[6–8].

Given this peculiar characteristic of fusion protein, the

☆Supported by the National Key Technologies R & D Program of China during the 10th Five-Year Plan Period (Grant No. 2004BA719A13).
*Corresponding author. Tel: 86-371-65027108; Email: johnyu@zzu.edu.cn

success of this approach depends on the possibility either of expressing the suicide gene in the majority of cancer cells (a still unrealistic possibility) or of extending its effect to a proportion of cells sufficiently large to achieve complete cell killing after prodrug treatment. As far as the latter possibility is concerned, further improvements in the TK gene approach might also benefit from prolonged persistence of the K-producing cells in the context of the tumor mass for the whole duration of GCV treatment. Meanwhile, how to construct the fusion protein that confers TK a remarkably therapeutic efficacy is not still defined. To address this question well, we constructed a series of HIV-1-Tat-TK fusion protein that contained Gly_0, Gly_2, Gly_4 or Gly_6 different linker between them. Our results show that fusion of Tat to TK permits transcellullar transfer of the enzyme in HepG2 cells, and the remarkable enhancement of fusion protein with Gly_4 linker cytotoxicity can be detected in different group *in vitro*.

2 Materials and Methods

2.1 Materials

Plasmid pcDNA3-TK containing TK gene, pcDNA3-Tat carrying truncated HIV-Tat (1 – 200 nt) gene and *E. coli* DH5α were maintained in our laboratory. Eukaryotic expression vectors pcDNA3 and prokaryotic expression vector-PBK were from Invitrogen Co., Netherlands. Purification kit for PCR product was obtained from QIAGEN Company (Germany). Restriction endonucleases such as *Eco*RI, *Bam*HI, and T4 DNA ligase were from Huamei Bioengineering Company (Luoyang, China). All the PCR primers used in the study were designed by Genebank and synthesized by Takara Ltd. (Dalian, China). Sephadex G-100 and Sepharose CL-4B were from Pharmacia Ltd. Monoclonal antibodies of HIV-Tat and TK proteins were gently gift from MD. Zqi Han, Medical College North-western University, USA.

2.2 Chimer genes preparation

Primers for polymerase chain reaction (PCR): Recombinant protein of HIV Tat and TK gene containing 2 glycines. HIV Tat left primer: 5'-GTGGATCCATGGAGCCAGTAGATCCTA-3', HIV Tat: 5'-ATCGAAGCATACCTCCCTTTTCCTTCGGGCCAG-3'; TK left primer: 5'-GGAGGTATGCTTCGTAC CCCTGCCATC-3', TK right primer: 5'-CAGGATCCAGTTAGCCTCCCCCATCTC-3'.

Recombinant protein of HIV Tat and TK gene containing 4 glycines HIV Tat left primer: 5'-GTGGATCCATGGAGCCAGTAGATCCTA-3', HIV Tat right primer: 5'-GCATACCTCCACCTCCCTTTTCCTTCGGGCCAG-3'; TK left primer: 5'-GGAGGTGGAGGTATGCTTCGTACCCCTGCC-3', TK right primer: 5'-CAGGATCCAGTTAGCCTCCCCCATCTC-3'.

Recombinant protein of HIV Tat and TK gene containing 6 glycines HIV Tat left primer: 5'-GTGGATCCATGGAGCCAGTAGATCCTA-3', HIV Tat right primer: 5'-ACCTCCACCTCCACCTCCCTTTTCCTTCGGGC-3'; TK left primer: 5'-GGAGGTGGAGGTGGAGGTATGCTTCGTAC-3', TK right primer: 5'-CAGGATCCAGTTAGCCTCCCCCA TCTC-3'.

2.3 Ligation of objected genes and clone

2.3.1 The 1st ligation of Tat and TK (Recombinant protein containing 0 or 2 glycines). Extracted the pcDNA3-Tat and pcDNA3-TK plasmid as routine methods, HIV Tat left primer: 5'-GTGAATTCATGGAGCCAGTAGATCCTA-3' (containing *Eco*RI site, underline showed), HIV Tat right primer: 5'-ATCGAAGCATACCTCCCTTTTCCTTCGGGCCAG-3', TK left primer: 5'-GGAGGTATGCTTCGTACCCCTGCCATC-3', TK right primer: 5'-CAGGATCCAGTTAGCCTCCCCCATCTC-3' (containing *Bam*HI site, underline showed), amplified Tat and TK gene, the PCR profiles were denaturation at 92 ºC for 30 s, annealing at 55 ºC for 30 s, and extension at 72 ºC for 60 s for 30 cycles, at last extension at 72 ºC for 10 min. Amplification products were resolved by agarose gel electrophoresis, stained with ethidium bromide, and quantified until use.

The ligation of antisense fragment of TK gene with HIV Tat gene segment was performed by gene SOEing PCR[11] with Puf enzyme. Briefly, there were a sense and antisene sequence between the primers of Tat and TK gene (underline showed): HIV Tat right primer: 5'-ATCGAAGCATACCTCCCTTTTCCTTCGGGCCAG-3', TK left primer: 5'-*GGAGGT*ATGCTTCGTACCCCTGCCATC-3' (Slanting base pairs are codon of glycine). The above products of Tat and TK were mixed as a certain proportion. The fragment of HIV Tat-$(Gly)_2$-TK was further amplified by PCR with the major round to be 92 ºC for 30 s, 50 ºC for 45 s and 72 ºC for 60 s for 30 cycles, and the final extension step being 10 min at 72 ºC, in which the HIV Tat left primer: 5'-GTGAATTCATGGAGCCAGTAGATCCTA-3', and the TK right primer: 5'-CAGGATCCAGTTAGCCTCCCCCATCTC-3', were employed as primers. Amplification products were resolved by agarose gel electrophoresis, stained with ethidium bromide, and quantified for the next PCR ligations or cloned.

2.3.2 The 2nd ligation of Tat and TK (Recombinant protein containing 4 glycines). The above prod-

ucts of HIV Tat-$(Gly)_2$-TK were amplified, HIV Tat left primer: 5'-GTGAATTCATGGAGCCAGTAGATCCTA-3', HIV Tat right primer: 5'-GCATACCTCCACCTCCCTTTTCCTTCGGGCCAG-3' and TK left primer: 5'-GGAGGTGGAGGTATGCTTCGTACCCCTGCC-3', TK right primer: 5'-CAGGATCCAGTTAGCCTCCCCCATCTC-3' was employed as two pair primers to amplify respectively for the first step PCR. The two products of the first step PCR were mixed as a certain proportion, HIV Tat left primer: 5'-GTGAATTCATGGAGCCAGTAGATCCTA-3' and TK right primer: 5'-CAGGATCCAGTTAGCCTCCCCCATCTC-3' were employed for the 2nd step PCR. Amplification products were resolved by agarose gel electrophoresis, stained with ethidium bromide, and quantified for the next PCR ligations or cloned.

2.3.3 The 3rd ligation of Tat and TK (Recombinant protein containing 6 glycines). The above products of HIV Tat-$(Gly)_4$-TK were amplified, HIV Tat left primer: 5'-GTGAATTCATGGAGCCAGTAGATCCTA-3', HIV Tat right primer: 5'-ACCTCCACCTCCACCTCCCTTTTCCTTCGGGC-3' and TK left primer: 5'-GGAGGTGGAGGTGGAGGTATGCTTCGTAC-3', TK right primer: 5'-CAGGATCCAGTTAGCCTCCCCCATCTC-3' were employed as two pair primers to amplify respectively for the first step PCR. The two products of the first step PCR were mixed as a certain proportion, HIV Tat left primer: 5'-GTGAATTCATGGAGCCAGTAGATCCTA-3' and TK right primer: 5'-CAGGATCCAGTTAGCCTCCCCCATCTC-3' were employed for the 2nd step PCR. Amplification products were resolved by agarose gel electrophoresis, stained with ethidium bromide, and quantified for clone.

2.4 Clone and determination of ligation products

2.4.1 Determination of chimer Tat-Gly-TK gene. The above 3 kinds of PCR ligation products, pcDNA3-TK and PBK vector were digested by *Eco*RI and *Bam*HI, purified, ligated by T4 ligase. Ligation products were transferred into DH5α with routine principle, sifted and maintained at 37 ºC, poke out single clone of DH5α and cultured. Both of the newly-constructed vectors were confirmed by restriction endonuclease digestion, PCR with specific primers and finally by DNA sequencing (Baosheng Co., Dalian, China).

2.4.2 Expressed and extracted of the recombinant Tat-Gly-TK protein. The positive *E. coli* after determination was planted in LB medium with gentamicin, culture at 37 ºC. While OD value (A_{600}) of *E. coli* was coming to 0.4 – 0.6, isopropyl-1-thio-β-D-galactoside (IPTG, destined titer, 0.4 mM) was added and induced expressed, collected the *E. coli* after 6 h, destroyed the *E. coli* by ultrasonic in ice-cold and washed by 4 M urea buffer[12–14].

2.4.3 Recovery and purified of the recombinant Tat-Gly-TK protein. *E. coli* were resolved into the buffer containing 8 M urea, passed Sephadex G-100 and acquired the crude protein. The crude protein were incubated in pH 8.0 buffer (containing 10 mM PBS, 5 mM reduction-glutathione, 2 mM oxidation-glutathione) at 16 ºC for 12 h, after purifying through Sepharose CL-4B which was incubated with HIV Tat monoclonal antibody[9] or TK protein monoclonal antibody, and recombinant proteins were loaded on a 10% SDS-polyacrylamide gel and visualized by Coomassie Blue staining[12–14].

2.4.4 Determination on the biological property of Tat-Gly-TK. Cells: To study the biological property of recombinant Tat internalization, HepG2 cells were divided into 6 groups (HIV Tat protein group, Tat-TK protein group, Tat-$(Gly)_2$-TK protein group, Tat-$(Gly)_4$-TK protein group, Tat-$(Gly)_6$-TK protein group and the positive control TK protein) and seeded in 8-well dishes at the density of $(1 – 2) \times 10^4$ cells/cm^2 in DMEM containing 10% fetal calf serum. After 24 h, cell cultures were washed twice and incubated for an additional 24 h in fresh medium containing 10% fetal calf serum, 100 μM chloroquine, and recombinant Tat protein. Incubation in the presence of chloroquine favors Tat uptake by modifying the pH of endolysosomal vesicles and preventing protein degradation[10,11]. After 24 h, the medium was changed to DMEM, 10% fetal calf serum, and cells were incubated for an additional 24 h. At the end of incubation, cells were fixed and determined by immunostaining. Alternatively, cells were cultured for 3 days continued with DMEM containing 10 μg/ml gencilorvir, at last cells collected, stained by trypan blue and analyzed by FACS[12].

Immunofluorescence assay and trypan blue exclusion test: Fixed cells were washed twice with 0.1% Triton X-100 in PBS for 10 min and incubated with monoclonal antibodies of HIV Tat in PBS supplemented with 0.15% glycine and 0.5% bovine serum albumin. Images obtained by microscopy using an Olympus FV300 microscope. Green-fluorescence in cells showed recombinant Tat internalization. Meanwhile, the photograph recorded cell shapes and the survival cell ratio was assessed by the 0.1% trypan blue exclusion test on the 3rd day of post-transfection and the data determined were analyzed by statistics (*t*-test).

Flow cytometry: To analyze HIV Tat internalization by cell cytometry, cells were washed four times with PBS, stained by ethidium iodide, washed with PBS again

and analyzed with a FACScan flow cytometer (Becton Dickinson). A total of 10000 events per sample were considered.

3 Results

According to the length of glys in the HIV Tat-$(Gly)_n$-TK, the diffreent primers were employed for the first PCR or the second PCR. We acquired a series of chimer genes of HIV Tat-$(Gly)_n$-TK inserted different numbers of glycines, and fragments were about 1200 bp as expected (Figure 1).

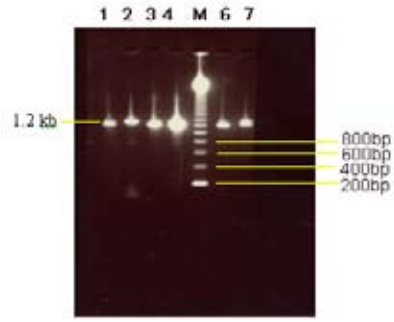

Figure 1. PCR of four fragments which contained 0, 2, 4 or 6 Glycines. M: Marker; Lane 1: HIV Tat-TK; Lane 2: HIV Tat-$(Gly)_2$-TK; Lane 3: HIV Tat-$(Gly)_4$-TK; Lane 4: HIV Tat-$(Gly)_6$-TK.

3.1 SDS-PAGE of recombinant protein

The chimer genes of HIV Tat-$(Gly)_n$-TK were expressed in *E. coli* and purified by Sepharose CL-4B decorated by Tat monoclonal antibody, SDS-PAGE (Figure 2). Recombinant proteins were loaded on a 10% SDS-polyacrylamide gel and visualized by Coomassie Blue staining. The weight was about 53 KD as expected (the protein of HIV Tat-$(Gly)_6$-TK gene expressed is the same as HIV Tat-$(Gly)_4$-TK, the data isn't shown).

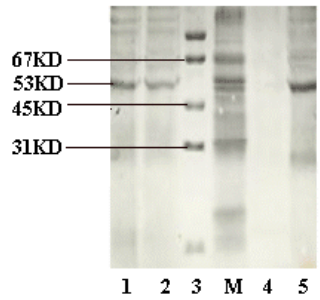

Figure 2. SDS-PAGE of recombined protein after purify. M: Marker; Lane 1: HIV Tat-TK; Lane 2: HIV Tat-$(Gly)_2$-TK; Lane 3: mixture protein of *E. coli* after ultrasonic destroy; Lane 4: HIV Tat-$(Gly)_4$-TK; Lane 5: HIV Tat-$(Gly)_6$-TK.

3.2 Immunofluorescence assay

HepG2were incubated with the fusion protein of HIV Tat-$(Gly)_n$-Tk for 3 days, and the cells were determined by immunofluorescence assay. Excepted for TK group, the green-fluorescence was showed in the Cells of the other 5 groups and the ratios of translocation to the nucleus in 5 groups were the same extend. But in the TK group, there was no green-fluorescence in the cells. Images were obtained by microscopy (Figure 3).

3.3 Assessment by trypan blue exclusion test

The lethiferous effect of HIV-Tat-$(Gly)_n$-TK on the HepG2 cells was continued to be aggravated on the 3rd day post-transfection, in which the majority of the transfected HepG2 cells were observed shrunken, rounded in shape and even dead. With the assessment by trypan blue exclusion test, the dead cell ratios of recombinant pro-

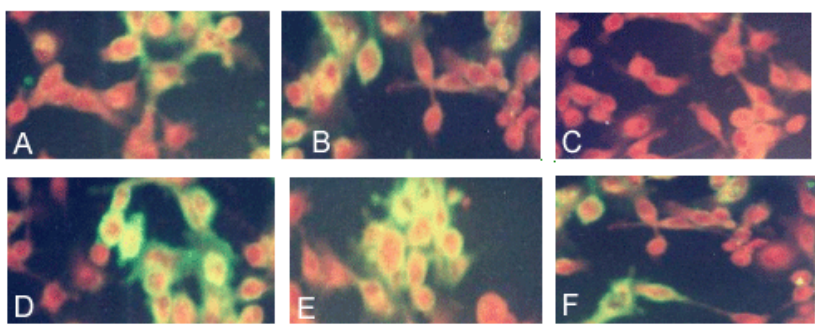

Figure 3. Immunofluorescence assay. A: HIV Tat; B: HIV Tat-$(Gly)_2$-TK; C: PBK-TK; D: HIV Tat-$(Gly)_4$-TK; E: HIV Tat-$(Gly)_6$-TK; F: HIV Tat-TK.

teins containing 0, 2, 4, 6 glycines or pcDNA3-TK (the positive on the 3rd day post-transfection) were 58.4%, 65.4%, 80.2% and 56.7% in order, in the negative control (HIV Tat or TK protein group) only 9.1%. There were obvious difference in the above groups(*t*-test, $P < 0.05$)

3.4 Flow cytometry

Cells were cultured for 3 days continued with DMEM containing 10 μg/ml gencilorvir. After scan of FACScan flow cytometer, the apoptosis cell ratios of recombinant proteins containing 0, 2, 4, or 6 glycines on the 3rd day post-transfection were 8.31%, 12.69%, 14.77% or 4.36% in order and in the control (HIV Tat or TK protein group) was only 1.00%. There were obvious difference in the above groups (*t*-test, $P < 0.05$).

4 Conclusion

The efficacy of HSV-1 TK-GCV suicide gene therapy of cancer, as well as of other hyperproliferative conditions including arterial restenosis, has been widely attributed to the bystander effect[13,14]. This phenomenon is credited with providing complete tumor regression when only a small percentage of tumor cells express the enzyme. However, the marginal clinical benefit so far observed in patients clearly indicates that the natural bystander effect of TK does not sufficiently compensate a poor rate of delivery of the HSV-TK gene to tumor cells[15,16]. Thus, clinical effectiveness of suicide gene therapy is entirely dependent, on the one hand, on the development of novel strategies to increase bystander cell killing and, on the other and, on the improvement of the efficacy of gene transfer.

In this work, we show that tagging TK with HIV-1 Tat confers trafficking capacity to the enzyme and a major impact to enhancement of TK tumor cells killing was observed in the Gly_4 linker between fusion protein compared to Gly_0, Gly_2 and Gly_6. Different chimer genes were obtained by DNA recombinant technique and then clone into prokaryotic expression vector – PBK, fusion protein purified by monoclonal antibody of HIV Tat, containing 0, 2, 4, or 6 glycines linker, cultured with HepG2 cells, proportion of apoptosis cell 8.31%, 12.69%, 14.77% or 4.36%, respectively, suggested that fusion protein inserted Gly_4 between them contributed a remarkable enhancement of TK activity to HepG2 killing, these results are agreement with trypan blue stain experiment.

Taken together, these results indicate that Tat may serve as a protein delivery tool by which candidate proteins can be administered in a functional form to HepG2 cells. It must be appreciated that a 1-fold to 2-fold amplification in TK efficacy might not be sufficient in itself to render this suicide gene therapy approach of cancer immediately effective in a clinical setting. However, such amplification in protein delivery might be additive to the other ameliorations to TK gene therapy that are currently being considered, including amino acid modification to increase enzymatic efficacy[17,18], increased canonical bystander effect[19,20], and, clearly, improved gene delivery. It is conceivable that clinical success might eventually be attained through a combination of improvements in all these different aspects of suicide gene therapy.

References

1. Kieback DG. Adenovirus-mediated thymidine kinase gene therapy induces apoptosis in human epithelial ovarian cancer cells and damages PARP-1. *In Vivo* 2009; 23: 77 – 80.
2. Jaffrelo L, Chabas S, Reigadas S, Pflieger A, Wychowski C, Rumi J, Ventura M, Toulme JJ, Staedel C. A functional selection of viral genetic elements in cultured cells to identify hepatitis C virus RNA translation inhibitors. Nucleic Acids Res 2008; 36: e95.
3. Rautsi O, Lehmusvaara S, Ketola A, Maatta AM, Wahlfors J, Pellinen R. Characterization of HIV-1 TAT peptide as an enhancer of HSV-TK/GCV cancer gene therapy. Cancer Gene Ther 2008; 15: 303 – 14.
4. Maitani Y, Yano S, Hattori Y, Furuhata M, Hayashi K. Liposome vector containing biosurfactant-complexed DNA as herpes simplex virus thymidine kinase gene delivery system. J Liposome Res 2006; 16: 359 – 72.
5. Dietz GP, Bahr M. Delivery of bioactive molecules into the cell: the Trojan horse approach. Mol Cell Neurosci 2004; 27: 85 – 131.
6. Passiatore G, Rom S, Eletto D, Peruzzi F. HIV-1 Tat C-terminus is cleaved by calpain 1: implication for Tat-mediated neurotoxicity. Biochim Biophys Acta 2009; 1793: 378 – 87.
7. Hidalgo-Estevez AM, Punzon C, Sanchez-Duffhues G, Munoz E, Fresno M. HIV-1-Tat potentiates CXCL12/stromal cell-derived factor 1-induced downregulation of membrane CXCR4 in T lymphocytes through protein kinase C zeta. Mol Immunol 2008; 46: 106 – 15.
8. Tunnemann G, Martin RM, Haupt S, Patsch C, Edenhofer F, Cardoso MC. Cargo-dependent mode of uptake and bioavailability of TAT-containing proteins and peptides in living cells. FASEB J 2006; 20: 1775 – 84.
9. Jaschke B, Milz S, Vogeser M, Michaelis C, Vorpahl M, Schomig A, Kastrati A, Wessely R. Local cyclin-dependent kinase inhibition by flavopiridol inhibits coronary artery smooth muscle cell proliferation and migration: Implications for the applicability on drug-eluting stents to prevent neointima formation following vascular injury. FASEB J 2004; 18: 1285 – 7.
10. Ribault S, Neuville P, Mechine-Neuville A, Auge F, Parlakian A, Gabbiani G, Paulin D, Calenda V. Chimeric smooth muscle-specific enhancer/promoters: valuable tools for adenovirus-mediated cardiovascular gene therapy. Circ Res 2001; 88: 468 – 75.
11. Roelants V, Labar D, de Meester C, Havaux X, Tabilio A, Gambhir SS, Di Ianni M, Bol A, Bertrand L, Vanoverschelde JL. Comparison between adenoviral and retroviral vectors for the transduction of the thymidine kinase PET reporter gene in rat mesenchymal stem cells. J Nucl Med 2008; 49: 1836 – 44.
12. Saijo M, Suzutani T, Mizuta K, Kurane I, Morikawa S. Characterization and susceptibility to antiviral agents of herpes simplex virus type 1 containing a unique thymidine kinase gene with an amber codon between the first and the second initiation codons. Arch Virol 2008; 153: 303 – 14.

13. Su Z, Emdad L, Sauane M, Lebedeva IV, Sarkar D, Gupta P, James CD, Randolph A, Valerie K, Walter MR, Dent P, Fisher PB. Unique aspects of mda-7/IL-24 antitumor bystander activity: establishing a role for secretion of MDA-7/IL-24 protein by normal cells. Oncogene 2005; 24: 7552 – 66.
14. Ahn M, Lee SJ, Li X, Jimenez JA, Zhang YP, Bae KH, Mohammadi Y, Kao C, Gardner TA. Enhanced combined tumor-specific oncolysis and suicide gene therapy for prostate cancer using M6 promoter. Cancer Gene Ther 2009; 16: 73 – 82.
15. Shand N, Weber F, Mariani L, Bernstein M, Gianella-Borradori A, Long Z, Sorensen AG, Barbier N. A phase 1-2 clinical trial of gene therapy for recurrent glioblastoma multiforme by tumor transduction with the herpes simplex thymidine kinase gene followed by ganciclovir. GLI328 European-Canadian Study Group. Hum Gene Ther 1999; 10: 2325 – 35.
16. Rainov NG. A phase III clinical evaluation of herpes simplex virus type 1 thymidine kinase and ganciclovir gene therapy as an adjuvant to surgical resection and radiation in adults with previously untreated glioblastoma multiforme. Hum Gene Ther 2000; 11: 2389 – 401.
17. Kokoris MS, Sabo P, Adman ET, Black ME. Enhancement of tumor ablation by a selected HSV-1 thymidine kinase mutant. Gene Ther 1999; 6: 1415 – 26.
18. Qiao J, Black ME, Caruso M. Enhanced ganciclovir killing and bystander effect of human tumor cells transduced with a retroviral vector carrying a herpes simplex virus thymidine kinase gene mutant. Hum Gene Ther 2000; 11: 1569 – 76.
19. Marconi P, Tamura M, Moriuchi S, Krisky DM, Niranjan A, Goins WF, Cohen JB, Glorioso JC. Connexin 43-enhanced suicide gene therapy using herpesviral vectors. Mol Ther 2000; 1: 71 – 81.
20. Tanaka M, Fraizer GC, De La Cerda J, Cristiano RJ, Liebert M, Grossman HB. Connexin 26 enhances the bystander effect in HSVtk/GCV gene therapy for human bladder cancer by adenovirus/PLL/DNA gene delivery. Gene Ther 2001; 8: 139 – 48.

Randomness-induced evolution of the first-order to the second-order phase transition in two-dimensional six-state potts model[☆]

Chiachi Shih[1], Shingmin Hu[1], Muhsin Chen[2], Shuanyu Huang[3,*]

[1]*Department of Electronics Engineering and Computer Science*, *Tung-Fan Institute Technology*, *No*. 110, *Tungfang Rd*., *Hunei Township*, *Kaohsiung County* 82941, *Taiwan*, *China*; [2]*Department of Optometry*, *Chung Hwa University of Medical Technology*, *No*. 89, *Wunhua 1st St*., *Rende Township*, *Tainan County* 717, *Taiwan*, *China*; [3]*School of Optometry*, *Chung Shan Medical University No*. 110, *Sec.* 1, *Jianguo N.Rd.*, *Taichung City* 402, *Taiwan*, *China*

Received December 10, 2008

Abstract

Employing Monte Carlo simulation method, we have studied randomness-induced evolution of the first-order to the second-order phase transition in two-dimensional six-state Potts model system. Biological applications of the Potts model are developed very much recently. We change the transition from first-order to second-order through tuning the bonds strength or the concentration of void bonds. The evolution of phase transition in two-dimensional six-state Potts system is examined with energy histogram and the Binder cumulant analysis. [Life Science Journal. 2009; 6(2): 29 – 32] (ISSN: 1097 – 8135).

Keywords: Monte Carlo; randomness; Potts model; phase transition

1 Introduction

It has attracted much interest that randomness influences cellular phase transition behavior both in theoretical and experimental studies. The disorder produced by porous media reveals experimental evidence of randomness affecting phase transition of a system. For a system exhibiting continuous phase transition in pure case, the quenched bond randomness or field randomness can change the value of critical exponent and may even eliminate the phase transition[1–3]. The phenomenological renormalization-group arguments[4–5] suggest that addition of bond randomness can smoothen the first order phase transition and induce a continuous phase transition. This conjecture arises recent research interest to explore randomness effect upon the nature of phase transition with second-order system, which originally carried on the first-order phase transition in the pure case[4–8]. As for experimental work, extensive studies of the isotropic to nematic phase transition of nCB liquid crystals in aerogel shows that the transition temperature is lowered compared with the pure situation[9–12].

It is well known that the Potts model possesses fruitfully critical behavior. The q-state Potts model on two-dimensional cellular lattices exhibits temperature-driven phase transition both in first-order and second-order[14]. The phase transition is first-order for $q > 4$ and is continuous for $q \leq 4$. So it could be a good candidate for testing the emergence of randomness-induced evolution of the first-order to second-order phase transition. Chen S *et al*[6–7] and Janke W[15] have performed Monte Carlo simulation study for the random bond Potts model in two-dimensional system with strong first-order region ($q = 8$). Yet some debated contradiction appears between the works of Chen S *et al* and Janke W demonstrates that quenched random-bond induces the second-order phase transition in two-dimensional eight-state Potts model. On the contrary, Janke W *et al* ascertain that the phase transition remains the first-order on random lattices in the same model. Paredesv R *et al*[13] study the five-state-Potts model with weak first-order region, and Yang CS *et al*[8] study the three-state Potts anti-ferromagnetic model

[☆]Supported by the National Science Council of China, Taiwan (Grant No. NSC95-2112-M-272-002-MY2).

[*]Corresponding author. Email: syhuang@csmu.edu.tw

on triangular lattice. Both models appear variation of the nature in phase transition induced by randomness.

In order to illustrate the randomness-induced change of the nature in phase transition, we investigate the six-state Potts model with various random by means of Monte Carlo simulation. Because the system has first-order phase transition in pure case, we may alter the nature of phase transition to the second-order through diluting the system, randomly introducing certain concentration of blank bonds or weakening strength of partial bonds. Applying field on the system, random effect also induce the change of nature in phase transition. We examine the evolution of phase transition in two-dimensional six-state Potts system with energy histogram and the Binder cumulant analysis in this study.

2 Model

The Hamiltonian of a six-state Potts model with quenched random interaction can be written as follows:

$H = \sum_{<i,j>} K_{ij}\delta\sigma_i\sigma_j$

Where δ is a Kronecker delta function; the spin σ_i can take on the values 1, 2, 3 ... 6; < i, j > indicates summation over all nearest-neighbor pairs of sites. The coefficient K_{ij} is the nearest-neighbor (< i, j >) random bond coupling constant, which can be randomly selected according to the following distribution.

$P(K_{ij}) = f\delta(K_{ij} - K_\alpha) + (1 - f)\delta(K_{ij} - K_\beta)$

Where f is a positive real number smaller than or equal to 1. Two differently prescribed random cases are studied. (1) The self-dual system (SD system): we randomly assign half of the total bonds to be the coupling K_1, and the rest bonds are the coupling K_2. The strength ratio is $r = K_a/K_b$. (2) The random dilution system (RD system): partial bonds is void, i.e. $r \rightarrow 0$. In order to investigate the evolution of phase transition, we tune the strength and the concentration of blank bonds systematically. In SD system we set the normal bond coupling (K_b) to be one, and then decrease the strength ratio to make the pure system uneven. In RD system we gradually increase the concentration of blank bonds from zero.

3 Simulation and Analysis

Consider a two-dimensional square lattice with fraction f as quenched bonds and fraction $(1 - f)$ as normal bonds. We perform extensive simulation on 90 × 90 lattices with periodic boundary conditions. The Monte Carlo steps are up to 10^6 typically. The first 20% of the steps are discarded, and we accumulate the remaining data at equilibrium states in our simulation. The temperature of the heat capacity peak corresponds to the transition temperature. We explore transition properties by analyzing energy histogram near the transition temperature. Usually the energy distribution displays a Gaussian type around some central energy due to fluctuation at thermal equilibrium states in a finite size system. As the first-order phase transition occurs, there may co-exist two states at the transition temperature. The energy histogram would display two distinct humps. By analyzing the histogram, one may be able to identify the presence of the first-order phase transition[15–17].

We study the phase transition of pure system first. The behavior of specific heat indicates that the transition temperature is $T = 0.808$. Thus, we explore the energy distribution around this temperature extensively. Figure 1 shows the energy histograms of pure case. The diagram displaying energy histogram near the transition temperature is sensitively dependent on temperature. At $T = 0.807$, the system start to melt, and the energy histogram displays a double-hump structure – a large right hump and a small left one. Then at $T = 0.808$, the energy histogram demonstrates a distinct double-hump structure, which has two humps of almost equal size. Just beyond the transition temperature, at $T = 0.809$, the energy histogram shows an inverse double-hump structure comparing to $T = 0.807$, with large left hump and a small right one. At a slight temperature difference away from the transition, $T = 0.812$, the energy histogram falls back Gaussian structure. Our simulation result reveals that the six-state pure Potts model proceeds a first-order phase transition at $T = 0.808$.

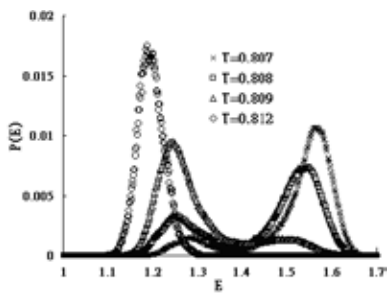

Figure 1. The energy histograms of pure case.

We then conduct the systematic study for the effect of randomness. The RD system is studied with randomly putting blank bonds. Figure 2 displays energy histograms of various blank bond fraction $f = 0.1$, 0.15, and 0.2, respectively. The transition temperature decreases with increasing the blank bond concentration, $T = 0.715$, 0.664, and 0.614, respectively. They display different

types of state distribution at transition temperature. The distribution of $f = 0.1$ still demonstrates a distinct two-hump structure. The histogram of $f = 0.15$ smears out to be a broad single hump. Yet, it is hard to find distinct dip. The distribution of $f = 0.2$ changes into nearly Gaussian type. In this case, the nature of phase transition may evolve into second-order behavior.

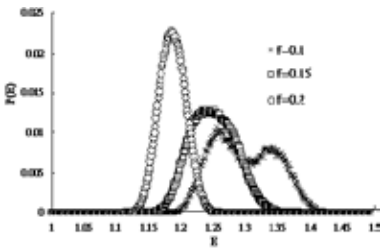

Figure 2. The energy histograms of various empty bond fraction $f = 0.1$, 0.15, and 0.2 in RD system, at transition temperature, $T = 0.715$, 0.664, and 0.614, respectively.

In the SD system with randomly selected half of the total bonds quenched, we vary the coupling strength ratio. Figure 3 displays energy histogram of various strength ration $r = 0.5$, 0.4, and 0.3. The phase transition temperature decreases with decreasing strength ratio, $T = 0.588$, 0.540 and 0.484, respectively. The evolution of the diagram is similar to that in Figure 2. The energy histogram of $r = 0.5$ and 0.4 displays an unsymmetrical broad hump. The distribution of $r = 0.3$ changes into nearly Gaussian type, which shows second-order phase transition behavior due to larger bond strength variation.

As for applying field on the system, we see systematic variation of the energy histogram with increasing the randomness. Simulation reveals that the nature of first-order phase transition will change into the second-order induced by randomness.

Furthermore we inspect the quantity of the Binder's fourth cumulant of energy defined as $V_L = 1 - (E^4)_L/3(E^2)^2$, which is used to distinguish numerically between first-order and continuous transitions. The concept is as the following: The energy distribution $P_L(E)$ for lattice $L \times L$ is described by a single Gaussian. It will reduce to δ-function singularity in thermally dynamical limit, while the system is away from the transition. The fourth-order being reduced cumulant of energy yields the value of $V_L = 2/3$, while $L \to \infty$, at $T \neq T_c$. And the quantity holds at T_c for second-order transition due to Gaussian energy distribution. On the other hand, the energy distribution $P_L(E)$ in finite lattice is considered to be a double Gaussian over a small range around T_c. The corresponding order and disorder states will yield a nontrivial value of V_L. There will be a minimum value of V_L at T_c.

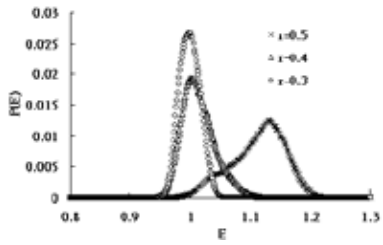

Figure 3. The energy histograms of various strength ratio $r = 0.5$, 0.4, and 0.3 in SD system, at transition temperature, $T = 0.588$, 0.540 and 0.484, respectively.

Figure 4 displays the Binder's cumulant V_L near the transition temperature in RD system. We can find the minimum dip of V_L at T_c in the pure system and in the case of empty bond fraction $f = 0.15$. Comparatively for the case of empty bond fraction $f = 0.2$, we find the V_L is very close to 2/3.

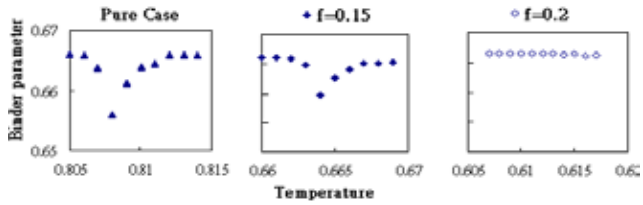

Figure 4. The Binder's cumulant V_L near the transition temperature in RD system.

Figure 5 displays the Binder's cumulant V_L near the transition temperature in SD system. We can also find that in the case of strength ratio $r = 0.3$, V_L is very close to 2/3. Therefore, we can ascertain the phase transition is changed by randomness from first-order to second-order.

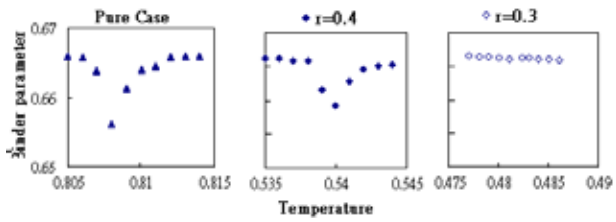

Figure 5. The Binder's cumulant V_L near the transition temperature in SD system.

4 Conclusion

We have conducted Monte Carlo simulation of two-di-

mensional six-state Potts model with constant couplings and random couplings. With thorough analysis, we have found that strength ratio $r = 0.3$ in SD system and blank bond ratio $f = 0.2$ in RD system will induce the variation of phase transition from the first-order to the second-order.

References

1. Harris AB. Effect of random defects on the critical behaviour of Ising models. J Phys C: Solid State Phys 1974; 7: 1671 – 92.
2. Imry Y, Ma SK. Random-field instability of the ordered state of continuous symmetry. Phys Rev Lett 1975; 35: 1399 – 401.
3. Berker AN. Harris criterion for direct and orthogonal quenched randomness. Phys Rev B 1990; 42(13): 8640 – 2.
4. Aizenman M, Wehr J. Rounding of first-order phase transitions in systems with quenched disorder. Phys Rev Lett 1989; 62(21): 2503 – 6.
5. Hui K, Berker AN. Random-field mechanism in random-bond multicritical systems. Phys Rev Lett 1989; 62(21): 2507 – 10.
6. Chen S, Ferrenberg AM, Landau DP. Randomness-induced second-order transition in the two-dimensional eight-state Potts model: a Monte Carlo study. Phys Rev Lett 1992; 69(8): 1213 – 5.
7. Chen S, Ferrenberg AM, Landau DP. Monte Carlo simulation of phase transitions in a two-dimensional random-bond Potts model. Phys Rev E 1995; 52(2): 1377 – 86.
8. Yang CS, Jiang IM. Randomness-induced evolution of first-order to second-order phase transition in the three-state Potts antiferromagnetic model on a triangular lattice. Physica A 2000; 281: 282 – 6.
9. Bellini T, Clark NA, Muzny CD, Wu L, Garland CW, Schaefer DW, Olivier BJ. Phase behavior of the liquid crystal 8CB in a silica aerogel. Phys Rev Lett 1992; 69(5): 788 – 91.
10. Clark NA, Bellini T, Malzbender RM, Thomas BN, Rappaport AG, Muzny CD, Schaefer DW, Hrubesh L. X-ray scattering study of smectic ordering in a silica aerogel. Phys Rev Lett 1993; 71(21): 3505 – 8.
11. Wu XI, Goldburg WI, Liu MX, Xue JZ. Slow dynamics of isotropic-nematic phase transition in silica gels. Phys Rev Lett 1992; 69(3): 470 – 3.
12. Iannacchione GS, Finotello D. Calorimetric study of phase transitions in confined liquid crystals. Phys Rev Lett 1992; 69(14): 2094 – 7.
13. Paredesv R, Valbuena J. Effects of quenched disorder in the two-dimensional Potts model: A Monte Carlo study. Phys Rev E 1999; 59(6): 6275 – 80.
14. Wu FY. The Potts model. Rev Mod Phys 1982; 54(1): 235 – 68.
15. Janke W, Villanova R. Two-dimensional eight-state Potts model on random lattices: A Monte Carlo study. Phys Lett A 1995; 209(3 – 4): 179 – 83.
16. Lee J, Kosterlitz JM. New numerical method to study phase transitions. Phys Rev Lett 1990; 65(2): 137 – 40.
17. Lee J, Kosterlitz JM. Finite-size scaling and Monte Carlo simulations of first-order phase transitions. Phys Rev B 1991; 43(4): 3265 – 77.
18. Challa MSS, Landau DP, Binder K. Finite-size effects at temperature-driven first-order transitions. Phys Rev B 1986; 34(3): 1841 – 52.

Pulmonary functions and blood biochemical markers for workers with and without coal worker pneumoconiosis☆

Qinghan Jin[1,2], Ailin Liu[1], Qinghai Li[3], Shaohua Xie[1], Enguang Wan[3], Shaohui Zhang[1], Yinfeng Tan[1], Xiaofeng Li[1], Hong Xie[1], Wenqing Lu[1,*]

[1]*Department of Occupational and Environmental Health and the MOE Key Laboratory of Environment and Health*, *School of Public Health*, *Tongji Medical College*, *Huazhong University of Science and Technology*, *Wuhan* 430030, *Hubei*, *China*; [2]*Health Bureau of Jining*, *Jining* 272000, *Shandong*, *China*; [3]*Institute for Labor Hygiene and Occupational Disease*, *Yanzhou Coal Mining Group*, *Yanzhou* 273500, *Shandong*, *China*

Received March 8, 2009

Abstract

Objective. This study aimed to evaluate the feasibility of using pulmonary functions and blood biochemical markers in monitoring coal dust-induced early lung damages and the status of coal worker's pneumoconiosis (CWP). *Methods.* Sixty-four coal workers including tunneling workers, coal hewers, ancillary workers and 45 patients with CWP at different stages were investigated for their pulmonary functions, routine blood biochemical panel and CC16, SOD, CAT and MDA. *Results.* Among coal workers globulin levels were higher in both tunneling workers (27.67 ± 2.45) and hewers (26.71 ± 2.26) than in ancillary workers (25.97 ± 3.39). Compared with coal workers, CWP patients showed decreases in VC, FVC, and FEV1 ($P < 0.01$ for all); those with the stage I and II disease showed lower CAT and higher globulin levels ($P < 0.01$ for both). The decreases of CAT and CC16 levels were associated with the increases of working ages ($P < 0.05$ for both). *Conclusions.* Pulmonary functions and globulin levels may be used as biomarkers to monitor coal dust-induced early lung damages and the CWP progression, respectively. The usefulness of CC16 and CAT levels for these purposes is not determined. [Life Science Journal. 2009; 6(2): 33 – 39] (ISSN: 1097 – 8135).

Keywords: coal worker's pneumoconiosis; pulmonary function; blood biochemical parameters; Clara protein; anti-oxidative response

1 Introduction

Frequent exposure to coal dusts causes serious diseases, mainly the characteristic coal worker pneumoconiosis (CWP); therefore, the effective prevention from the hazardous coal dusts has become a major occupational and public health issue. However, up to date, coal dusts still pose a great threat to the health of coal workers due to the lack of effective monitoring and diagnostic tools for coal dust-induced early lung damages.

The current practice for the CWP prevention is mainly through the routine monitoring of the pulmonary functions[1–3]. Some studies revealed that damages of pulmonary functions existed not only in the patients of CWP but also in many coal workers without an active disease[4–7]. Interestingly, at diagnosis, many CWP patients showed abnormalities of the routine blood biochemical panel[8,9], suggesting that the blood biochemical biomarkers may be used as markers to monitor the coal dust-induced early lung damages and to determine CWP disease progression.

Loss of the oxidation and anti-oxidation balance has been proposed to be a leading cause of the damages to the alveolar macrophages[10,11]. Superoxide dismutase (SOD) and catalase (CAT) are two important enzymes to salvage free radicals and their levels are correlated with the anti-oxidative capacity of the body[12]. On the other hand, malondialdehyde (MDA) is the product of the lipid peroxidation, and its levels are correlated with the

*Supported by the National Natural Science Foundation of China (NNSFC) (Grant No. 30800901).

*Corresponding author. Tel.: 86-27-83610149; Fax: 86-27-83657765; Email: luwq@mails.tjmu.edu.cn

degree of oxidative stress. Therefore, the levels of these molecules may be useful to evaluate the status of oxidation and anti-oxidation, as well as the degree of oxidative damages. Although there have been evidences that CWP patients and coal miners lost the balance of oxidation and anti-oxidation[13–15], whether these molecules are effective markers for the detection of coal dust-induced early lung damages and CWP disease status is still largely unknown.

Clara cell protein (CC16) is a protein secreted by the Clara cells. This protein has strong immuno-suppressive and anti-inflammatory activities and participates in many pathological and physiological processes. It has been shown that the level of CC16 in the bronchial epithelial lining fluid was associated with the cytotoxicity of silicon dioxide to the epithelium of the airway[16,17]; changes in CC16 levels can lead to the accumulation of fibroblasts and promote pulmonary fibrosis[18,19]. CC16 in the bronchial epithelial lining fluid can enter the blood stream by passive diffusion against the concentration gradient, so serum CC16 level can be used as a sensitive marker for the detection of early changes in the integrity of the Clara cells and the pulmonary capillaries[16,20]. Since the protein is correlated to the degree of pulmonary fibrosis, the decrease in serum CC16 level may also reflex the conditions of early lung damages and pulmonary fibrosis.

In this study, we analyzed the pulmonary functions and a panel of blood biochemical biomarkers for coal workers exposed to different levels of coal dusts, and CWP patients with different disease status. The blood biochemical biomarkers included CC16, SOD, CAT and MDA, in addition to other routine blood biochemical parameters. We hope such study will offer the theoretical basis and a practical method for the monitoring of the coal dust-induced early lung damages and the determination of CWP disease status.

2 Materials and Methods

2.1 Subjects

All subjects were workers in a coal mining factory of Shandong province in China. There were 64 normal coal workers without active CWP, including a high exposure group of 34 tunneling workers, a moderate exposure group of 13 coal hewers, and a control group of 17 ancillary workers who worked on the ground level with very little exposure to concentrated coal dusts. All these workers had been worked in the environments of mixed coal dusts, with the average dust density of 7.04 mg/m^3 for the tunneling working environment, 5.21 mg/m^3 for the hewers' environment, and 0.98 mg/m^3 for the ground level environment of the ancillary workers. In addition, there were 45 workers with CWP including 23 stage 1, 19 stage II and 3 stage III patients, whose diagnosis was made by a group decision from doctors licensed in the nation's first level hospital in the second class with specialty in the pulmonary system according to the "Diagnostic Criteria of Pneumoconiosis" (GBZ 70-2002) (Ministry of Health of the People's Republic of China, 2002). The diagnosis of pneumoconiosis depended fundamentally on evidence of occupational exposure history and radiographic findings; pulmonary function testing results were also considered. All subjects were males without other diseases in the heart, the liver and the kidney by routine physical examinations; they were all asked to complete a questionnaire for weight, height, living habit, professional history, family history and other related information. Blood samples were collected from veins and serum samples were prepared for the study.

2.2 Pulmonary functional tests

AS-PAL Pulmonary Function Testing System (Minato, Japan) was used to analyze all parameters of pulmonary functions including vital capacity (VC), forced vital capacity (FVC), forced expiratory volume in one second (FEV1), and the ratio of forced expiratory volume in one second to forced vital capacity (FEV1/FCV).

2.3 Blood biochemical analysis

Serum samples were collected from blood samples by centrifugation, and all measurements were carried out under the preset conditions. Olympus AU400 Automatic Biochemistry Analyzer was used to measure the routine blood biochemical parameters. Serum CC16 levels were measured by the human CC-16 assay kit from Wuhan USCN Sciences Co., LTD according to the manufactory manual. Serum SOD, CAT and MDA levels were measured by a SOD assay kit, a CAT assay kit, and a MDA assay kit, respectively, all from Nanjing Jiancheng Bioengineering Research Institute according to the manufactory manuals.

2.4 Data analysis and statistics

A database was established by Epidata 3.1 software, and all data were subjected to statistical analysis with SPSS12.0 program. Differences in the routine blood biochemical parameters were analyzed by multivariate analysis of variance; differences in the pulmonary functions and the levels of SOD, CAT and MDA were analyzed by analysis of variance; multi-level comparisons were made by dunnett's t-test and SNK test. Differences

in the serum CC16 levels among groups were analyzed by Kruskal-Wallis nonparametric test. The general linear regression or the nonconditional logistic regression analysis was applied for the multivariate analysis for the influencing factors of the pulmonary functional and the biochemical biomarkers. The correlations of SOD, CAT and MDA with pulmonary functional parameters were analyzed by Spearman rank correlation analysis. The confidence coefficient was set at the level of 0.05.

3 Results

3.1 Subject statistics

The 64 study subjects had an average age of 36.2 ± 8.2 years, specifically an average of 38.3 ± 7.3 years for the tunneling workers, 34.5 ± 9.0 years for the coal hewers, and 33.3 ± 8.4 years for the ancillary workers. The averaged age of the tunneling workers was significantly higher than those of the other two groups ($P < 0.05$). In this study, there were no significant differences in the average working age (14.7 ± 8.8 years), the body weight, and cigarette and alcohol consumptions among different groups of workers. The average ages of the CWP patients were 64.2 ± 6.3 years for patients with stage I disease, 68.7 ± 8.6 years for the stage II patients and 67.0 ± 9.0 years for the stage III patients, which were all significantly older than those of coal workers without the disease ($P < 0.01$). The average working ages of the CWP patients were 22.3 ± 9.0 years for the stage I patients, 24.8 ± 10.4 years for the stage II patients, and 16.7 ± 10.0 years for the stage III patients, which were also significantly older than the average working age of the general coal workers ($P < 0.01$). The percentages of smokers and alcohol consumers for the CWP patients were actually significantly lower than those of the general coal workers ($P < 0.01$ and $P < 0.05$, respectively, for the smokers and the alcohol consumers).

3.2 Pulmonary functions and the associated factors

Table 1 shows that there was no significantly differences in all the pulmonary functional parameters among different groups of coal workers without CWP. However, the CWP patients of all stages displayed significantly lower values of VC, FVC and FEV1 than the non-CWP coal workers ($P < 0.01$). The stage I CWP patients had significant lower values of FEV1/FVC than all other coal workers ($P < 0.05$) but these values were not significantly different between the stage II and III patients and all other coal workers ($P > 0.05$).

From Table 1, for the general linear regression analysis to determine the factors associated with or affecting the pulmonary functions, each of the pulmonary functional parameters was used as the dependent variable, and surveyed factors such as age, working age, weight, smoking status, alcohol consumption, job type, CWP disease stage were used as the independent variables. All variables belonging to multiple classifications were transformed to the dummy variables.

As shown in Table 2, compared with the coal workers without the disease, patients with stage I CWP had lower values of VC, FEV1 and FEV1/FVC, the stage II patients had lower values of VC and FEV1, and the stage III patients had lower values of FEV1. Values of VC and FCV decreased with increase of age, and FEV1 decreased with increase of the working age.

3.3 Routine blood biochemical parameters and associated factors

Table 3 shows that both the tunneling workers and the hewers had higher alanine aminotransferase-aspartate transaminase ratio (ALT/AST ratio) and blood glucose levels, the tunneling workers had the lower blood sodium level and the hewers had the higher urea nitrogen than the ancillary workers. Compared with the coal workers without CWP, the CWP patients of all stages showed higher total bilirubin and indirect bilirubin levels, lower albumin levels, higher globulin levels, lower Albumin/Globulin ratios, higher ALT/AST ratios and glucose levels, as well as lower urea nitrogen and blood sodium

Table 1. Pulmonary functional status of coal workers and CWP patients

Biomarkers	Without CWP				CWP patients			
	Tunneling workers	Hewers	Ancillary workers	All groups	Stage I	Stage II	Stage III	All groups
VC (L)	3.22 ± 0.12	3.70 ± 0.15	3.46 ± 0.19	3.38 ± 0.71	1.90 ± 0.65**	1.60 ± 0.64**	1.76 ± 0.29**	1.76 ± 0.64
FVC (L)	3.05 ± 0.10	3.46 ± 0.23	3.42 ± 022	3.23 ± 0.74	1.74 ± 0.67**	1.49 ± 0.86**	1.70 ± 0.30**	1.63 ± 0.74
FEV1 (L)	2.53 ± 0.98	2.61 ± 0.18	2.66 ± 0.17	2.58 ± 0.62	1.15 ± 0.59**	1.09 ± 0.56**	1.28 ± 0.25**	1.13 ± 0.55
FEV1/FVC (%)	83.19 ± 1.83	76.54 ± 3.70	78.01 ± 3.22	80.46 ± 12.13	65.58 ± 20.96*	74.87 ± 20.14	74.90 ± 2.26	70.12 ± 20.19

Data were presented as χ^2 ± SD. *P* values were calculated in comparison with the coal workers; *: $P < 0.05$, **: $P < 0.01$.

levels.

Table 2. General linear regression analysis for the affecting factors on pulmonary functions

Pulmonary functional biomarkers	Factors	Estimated regression coefficient	t	P	95% CI	
					Upper limit	Lower limit
VC (L)	CWP stage I	– 0.75	– 2.37	< 0.05	– 1.37	0.12
	CWP stage II	– 0.86	– 2.51	< 0.05	– 1.54	– 0.18
	Age (year)	– 0.03	– 1.42	< 0.05	– 0.05	– 0.01
FVC (L)	Age (year)	– 0.03	– 2.60	< 0.05	– 0.06	– 0.01
FEV1 (L)	CWP stage I	– 1.15	– 3.88	< 0.01	– 1.74	– 0.56
	CWP stage II	– 1.09	– 3.38	< 0.01	– 1.73	– 0.45
	CWP stage III	– 1.00	– 2.04	< 0.05	– 1.96	– 0.03
	Work age (year)	– 0.02	– 2.00	< 0.05	– 0.03	– 0.00
FEV1/ FVC (%)	CWP stage I	– 30.78	– 2.43	< 0.05	– 46.66	– 14.89

To determine the factors associated with or affecting the blood biochemical parameters, a general linear regression analysis was performed with each of the parameter as a dependent variable, and factors such as age, working age, body weight, smoking status, alcohol consumption, job type, and CWP stage as the independent variables. Results showed that the ratios of AST/ALT decreased with the increase of body weights ($P < 0.05$), total bilirubin and indirect bilirubin levels increased with the increase of age and amount of alcohol consumption (both had $P < 0.05$). Levels of blood albumin decreased with the increase of age. Smokers showed lower globulin levels ($P < 0.05$). The tunneling workers and the hewers had higher globulin levels than the ancillary workers ($P < 0.05$). The CWP patients also showed higher globulin levels than the non-CWP workers ($P < 0.05$). All the analyzed factors showed no significant associations with the levels of blood glucose, sodium, and urea nitrogen.

3.4 Serum CC16 levels and associated factors

As shown in Table 4, Kruskal-Wallis nonparametric test revealed that there was no statistically significant difference in serum CC16 levels between the CWP patients and the non-CWP coal workers ($x^2 = 2.94$, $v = 3$, $P = 0.40$), nor among the coal workers from different groups ($P = 0.20$, $v = 2$, $P = 0.90$).

Based on the mean value of serum CC16 levels, the subjects were divided into two groups: a high CC16 group with at least 100 pg/ml serum CC16 and a low CC16 group with CC16 levels below 100 pg/ml. CC16 was used as the dependent variable and the factors listed in the subject questionnaire were used as the independent variables for a non-conditional logistic regression analysis. After a series of selections and medical considerations, the independent variables were determined to be the smoking status, alcohol consumption, job type, age, working age and the CWP stage. Results showed that increase of the working age was significantly associated with the decrease in the serum CC16 levels ($P < 0.05$, OR = 0.900, 95%CI = 0.823 – 0.985). Other factors were not significantly correlated with the serum CC16 levels.

3.5 Serum SOD, CAT MDA levels associated factors and correlations with pulmonary functions

As shown in Table 5, there were no significant differences in the levels of SOD, CAT and MDA among different groups of coal workers without CWP. However, patients with stage I CWP had significantly lower serum CAT levels than coal workers without CWP ($P < 0.01$); patients with the stage II CWP showed lower levels of both serum SOD and CAT than the workers without the disease (both with $P < 0.01$). The levels of MDA were not significantly different among all study groups.

With each of the oxidative response biomarker as the dependent variable, and using age, working age, body weight, smoking status, alcohol consumption, job type, and CWP stage as the independent variables, general linear regression analysis was used to determine the factors associated with the oxidative response capacity. CWP patients of stages I and II had CAT levels lower than the non-CWP workers. The serum CAT levels decreased with the increase of working ages ($P < 0.05$), and SOD levels decreased along with increase of ages ($P < 0.05$). All other factors showed no significant associations with serum MDA levels. Spearman rank correlation analysis showed positive correlations of VC, FVC, and FEV1 with serum SOD and CAT levels. The correlation coefficients of VC with SOD and CAT were 0.225 and 0.195, respectively ($P < 0.05$ for both); the correlation coefficients of FVC with SOD and CAT were 0.216 and 0.207, respectively ($P < 0.05$ for both); the correlation coefficients for FEV1 with SOD and CAT were 0.210 and 0.298, respectively ($P < 0.05$, $P < 0.01$).

4 Discussion

Table 3. Biochemical biomarkers in coal workers without CWP and CWP patients

Biomarkers	Without CWP				CWP patients			
	Tunneling workers	Hewers	Ancillary workers	All groups	Stage I	Stage II	Stage III	All groups
Total bilirubin (μmol/L)	14.45 ± 5.88	11.94 ± 4.18	15.21 ± 8.37	14.14 ± 6.37	18.03 ± 7.50	18.59 ± 8.64$^{\#}$	20.40 ± 3.25	18.40 ± 7.71
Direct bilirubin (μmol/L)	4.28 ± 1.60	3.75 ± 1.03	4.46 ± 2.04	4.22 ± 1.64	5.04 ± 1.83	5.03 ± 2.21	4.60 ± 1.23	5.00 ± 1.93
Indirect bilirubin (μmol/L)	10.17 ± 4.43	8.19 ± 3.23	10.75 ± 6.38	9.92 ± 4.84	12.99 ± 5.74	13.56 ± 6.49$^{\#}$	15.80 ± 2.34	13.40 ± 5.87
Total protein (g/L)	74.84 ± 3.08	73.98 ± 3.88	72.61 ± 5.47	74.08 ± 4.04	72.87 ± 4.46	74.01 ± 4.12	79.77 ± 0.72	73.80 ± 4.45
Albumin (g/L)	44.18 ± 1.81	47.27 ± 2.28	46.65 ± 2.92	47.06 ± 2.22	44.32 ± 1.92$^{\#\#}$	44.28 ± 2.03$^{\#\#}$	46.40 ± 2.08	44.40 ± 2.00
Globulin (g/L)	27.67 ± 2.45	26.71 ± 2.26	25.97 ± 3.39	27.02 ± 2.75	28.57 ± 3.43	29.73 ± 3.15$^{\#\#}$	33.37 ± 1.36$^{\#\#}$	29.40 ± 3.39
Albumin/globulin ratio	1.72 ± 0.16	1.79 ± 0.13	1.83 ± 0.19	1.76 ± 0.17	1.56 ± 0.18$^{\#\#}$	1.51 ± 0.17$^{\#\#}$	1.37 ± 0.12$^{\#\#}$	1.50 ± 0.18
ALT (U/L)	26.46 ± 11.62	23.78 ± 15.23	33.80 ± 18.40	28.50 ± 15.90	22.52 ± 7.82	18.78 ± 6.56	18.23 ± 6.19	20.70 ± 7.33
AST (U/L)	28.77 ± 8.95	25.00 ± 5.97	29.71 ± 14.75	28.25 ± 10.34	26.14 ± 5.68	26.00 ± 5.47	30.33 ± 7.64	26.40 ± 5.67
AST/ALT	1.21 ± 0.39*	1.31 ± 0.61**	0.90 ± 0.40	1.20 ± 0.50	1.25 ± 0.36	1.52 ± 0.52$^{\#\#}$	1.73 ± 0.32$^{\#}$	1.40 ± 0.45
Alkaline phosphatase (U/L)	99.50 ± 22.9	99.00 ± 23.53	97.29 ± 26.87	98.80 ± 23.70	105.26 ± 29.23	98.53 ± 18.13	108.67 ± 33.32	102.60 ± 25.01
γ-glutamyl transpeptidase (U/L)	30.60 ± 14.20	31.20 ± 22.22	35.42 ± 14.94	32.00 ± 16.10	32.60 ± 18.90	22.64 ± 7.02	17.77 ± 4.48	27.40 ± 4.48
Urea nitrogen (mmol/L)	5.97 ± 1.20	6.79 ± 1.19*	5.27 ± 1.23	5.95 ± 1.30	5.19 ± 1.12$^{\#}$	5.06 ± 0.97$^{\#}$	5.37 ± 0.95	5.10 ± 1.03
Creatinine (μmo/L)	68.74 ± 9.36	68.88 ± 7.18	70.09 ± 8.53	69.13 ± 8.63	69.29 ± 7.93	70.00 ± 8.28	75.10 ± 4.61	70.00 ± 7.90
Glucose (mmol/L)	5.19 ± 0.43*	5.33 ± 0.62*	4.80 ± 0.54	5.12 ± 0.53	5.81 ± 1.07$^{\#\#}$	5.87 ± 1.51$^{\#\#}$	5.00 ± 0.83	5.80 ± 1.26
Potassium (mmol/L)	4.37 ± 0.33	4.28 ± 0.33	4.31 ± 0.42	4.33 ± 0.35	4.40 ± 0.35	4.22 ± 0.35	4.45 ± 0.46	4.30 ± 0.36
Sodium (mmol/L)	143.85 ± 1.57**	145.02 ± 1.75	145.29 ± 1.23	144.47 ± 1.65	142.00 ± 3.40$^{\#\#}$	140.52 ± 4.48$^{\#\#}$	143.53 ± 1.10	141.5 ± 3.85
Chloride (mmol/L)	101.90 ± 1.83	103.05 ± 2.61	102.56 ± 1.83	102.31 ± 2.03	102.87 ± 2.13	102.10 ± 2.23	102.32 ± 2.10	102.30 ± 2.22
Calcium (mmol/L)	2.42 ± 0.07	2.41 ± 0.05	2.36 ± 0.20	2.41 ± 0.12	2.35 ± 0.06	2.35 ± 0.08	2.44 ± 0.05	2.40 ± 0.07
CO2 combining power (mmol/L)	23.40 ± 1.91	23.50 ± 1.79	23.18 ± 1.76	23.36 ± 1.82	23.97 ± 1.75	24.03 ± 2.26	22.93 ± 0.31	23.90 ± 1.93

*: $P < 0.05$, and **: $P < 0.01$ for the ancillary workers in comparison with the tunneling workers and the hewers. $^{\#}$: $P < 0.05$, and $^{\#\#}$: $P < 0.01$ for workers without CWP in comparison with the CWP patients.

Coal worker's pneumoconiosis is one of the most serious occupational diseases, which can be pathologically characterized by the silicotic nodule formation and the wide-spread diffuse interstitial pulmonary fibrosis. Although great progress has been made from many studies in recent years, our knowledge on its pathogenesis is still limited, and there is still no effective cure for the disease. Therefore, seeking sensitive biomarkers to monitor the coal dust-induced early lung damages and to determine the CWP progression is critical to the prevention and treatment of this disease. In this study we explored the possibility of using pulmonary functional and the blood

Table 4. Serum CC16 (pg/ml) levels in coal workers without CWP and CWP patients

Group		No. (*n*)	Mean ± SD	Median values (range)
CWP stages	None	64	110.18 ± 142.14	20.73 (9.45 – 399.26)
	Stage I	23	62.57 ± 114.92	17.19 (8.76 – 412.47)
	Stage II	19	76.89 ± 104.55	37.76 (11.58 – 386.62)
	Stage III	3	84.67 ± 122.24	15.46 (12.73 – 255.81)
Work types	Tunneling workers	34	108.11 ± 147.84	20.73 (9.45 – 399.26)
	Hewers	13	99.84 ± 137.67	22.80 (11.06 – 388.57)
	Ancillary workers	17	122.23 ± 141.45	20.25 (10.79 – 343.96)

Table 5. Serum SOD, CAT and MDA levels of coal workers and CWP patients

Biomarkers	Without CWP				CWP Patients			
	Tunneling workers	Hewers	Ancillary corkers	All groups	Stage I	Stage II	Stage III	All groups
SOD (U/ml)	36.94 ± 21.91	36.16 ± 24.40	42.64 ± 11.42	41.35 ± 18.33	38.94 ± 29.64	20.11±16.74**	24.72 ± 15.02	29.66 ± 22.12
CAT (U/ml)	4.24 ± 4.96	3.48 ± 4.46	7.13 ± 10.89	4.87 ± 7.01	2.09 ± 2.76**	1.29 ± 0.97**	1.89 ± 0.83	1.77 ± 2.03
MDA (U/ml)	8.56 ± 12.74	9.42 ± 9.17	6.60 ± 4.49	8.19 ± 10.31	6.83 ± 5.95	6.89 ± 6.37	4.06 ± 1.58	6.89 ± 5.73

Data were presented as χ^2 ± s. *P* values were calculated in comparison with the coal workers; **: $P < 0.01$.

biochemical biomarkers as such markers.

The lung damage caused by coal dusts is a leading cause of the labor force decrease in the coal mining industry. Our study showed that all CWP patients had significantly damages of the pulmonary functions, which was worsened in the stage II patients. General linear regression analysis revealed that the pulmonary functions were correlated with the stages of CWP, suggesting that the pulmonary functional parameters may be used as the markers for CWP staging.

Our results did not show any significant differences in these markers among coal workers with different levels of coal dust exposure. This may be due to the strong functional compensation of the lung, which does not display signs of abnormality unless the damages are accumulated to certain high levels. Therefore, the pulmonary functional parameters may not be sensitive enough for the detection of early lung damages before the disease onset.

The damages in the bronchioles and other pulmonary tissues may affect the exchange of air between the body and the outside, ultimately resulting in a chronic hypoxic state of the body. This condition may in turn lead to the degeneration and necrosis of cardiac myocytes, hepatic cells, renal glomerular and tubular cells, and then further change the blood biochemical parameters. In this study, general linear regression analysis showed that levels of globulin varied among all groups of coal workers with or without CWP, and it increased with the increase of exposure level to coal dusts and the stage of CWP in the CWP patients; therefore, globulin may offer a sensitive marker for the detection of the coal dust-induced early lung damages and the CWP disease progression.

Recent studies have shown that CC16 is a sensitive marker for the early detection of the acute or chronic changes in Clara cells and the alveolar membrane structures[21,22]. In this study, levels of serum CC16 decreased with the longer exposure to coal dusts; it may be because that Clara cells are the stem cells for the renewal of the epithelial cells in the bronchioles, the cell number and CC16 secretion may decrease as the result of the damages in the pulmonary epithelial cells by coal dusts[23]. On the other hand, CC16 is passively transported to the blood stream across the lung-blood barrier[10,22]. The lung damages may decrease the permeability of the barrier then decrease the CC16 levels in the peripheral blood. However, we did not observe any significant differences of serum CC16 levels among all study groups with different exposure levels to coal dusts or with different CWP stages; therefore, the use of serum CC16 as marker for the detection of the coal dust-induced early lung damages and CWP disease progression still needs to be further studied.

The generation of reactive oxygen species (ROS) and the response to such oxidative stress play important roles in the pathogenesis of lung damages induced by external toxic particulate matters[24,25], which are also the key factors causing pulmonary fibrosis and decrease in the pulmonary functions. Our results showed that although there were no significant differences in the anti-oxidative capacity among non-CWP coal workers from three groups of different job types, there was a significant difference in the CAT values between the non-CWP workers and the CWP patients. In addition, CAT and SOD levels were shown to be positively correlated with the pulmonary functional parameters, and CAT values decreased with the increase of the working ages. Therefore, levels of CAT and SOD may offer complementary or reference values for the detection of coal dust-induced early lung damages and CWP disease progression. Whether they can be also used as true markers for the detection of coal dust-induced early lung damages is still a question.

We also observed that serum CAT levels decreased along with the disease progression in CWP patients. This may be the result of the enzyme consumption by the large amount of free radicals released from the alveolar macrophages while uptaking the coal dusts in the lung[26]. This process may activate the reactions of free radicals to cause the oxidation of the alveolar macrophage membrane and increase the fatty acid perioxidation, therefore ultimately leading to the release of a large amount of free radicals.

References

1. Wang X, Yu IT, Wong TW, *et al*. Respiratory symptoms and pulmonary function in coal miners: looking into the effects of simple pneumoconiosis. Am J Ind Med 1999; 35: 124 – 31.
2. Yeoh CI, Yang SC. Pulmonary function impairment in pneumoconiotic patients with progressive massive fibrosis. Chang Gung Med J 2002; 25: 72 – 80.
3. Akkoca Yildiz O, Eris Gulbay B, Saryal S, *et al*. Evaluation of the relationship between radiological abnormalities and both pulmonary function and pulmonary hypertension in coal workers' pneumoconiosis. Respirology 2007; 12: 420 – 6.
4. Mamuya SH, Bratveit M, Mashalla YJ, *et al*. Airflow limitation among workers in a labour-intensive coal mine in Tanzania. Int Arch Occup Environ Health 2007; 80: 567 – 75.
5. Naidoo RN, Robins TG, Seixas N, *et al*. Differential respirable dust related lung function effects between current and former South African coal miners. Int Arch Occup Environ Health 2005; 78: 293 – 302.
6. Wang ML, Wu ZE, Du QG, *et al*. Rapid decline in forced expiratory volume in 1 second (FEV1) and the development of bronchitic symptoms among new Chinese coal miners. J Occup Environ Med 2007; 49: 1143 – 8.
7. Mamuya SH, Bratveit M, Mashalla Y, *et al*. High prevalence of respiratory symptoms among workers in the development section of a manually operated coal mine in a developing country: a cross sectional study. BMC Public Health 2007; 7: 17.
8. Liu B, Qin X. Application and analysis of biochemical indices for the evaluation of antisilicosis treatment. Study on anti-silicosis therapy and its evaluation research group. Wei Sheng Yan Jiu 1998; 27: 222 – 4.
9. Perrin-Nadif R, Auburtin G, Dusch M, *et al*. Blood antioxidant enzymes as markers of exposure or effect in coal miners. Occup Environ Med 1996; 53: 41 – 5.
10. Castranova V, Vallyathan V. Silicosis and coal workers' pneumoconiosis. Environ Health Perspect 2000; 108(4) (suppl): 675 – 84.
11. Morrow DM, Entezari-Zaher T, Romashko J, *et al*. Antioxidants preserve macrophage phagocytosis of Pseudomonas aeruginosa during hyperoxia. Free Radic Biol Med 2007; 42: 1338 – 49.
12. Greenwald RA. Superoxide dismutase and catalase as therapeutic agents for human diseases. A critical review. Free Radic Biol Med 1990; 8: 201 – 9.
13. Altin R, Armutcu F, Kart L, *et al*. Antioxidant response at early stages and low grades of simple coal worker's pneumoconiosis diagnosed by high resolution computed tomography. Int J Hyg Environ Health 2004; 207: 455 – 62.
14. Dalal NS, Newman J, Pack D, *et al*. Hydroxyl radical generation by coal mine dust: possible implication to coal workers' pneumoconiosis (CWP). Free Radic Biol Med 1995; 18: 11 – 20.
15. Nadif R, Bourgkard E, Dusch M, *et al*. Relations between occupational exposure to coal mine dusts, erythrocyte catalase and Cu^{++}/Zn^{++} superoxide dismutase activities, and the severity of coal workers' pneumoconiosis. Occup Environ Med 1998; 55: 533 – 40.
16. Broeckaert F, Clippe A, Knoops B, *et al*. Clara cell secretory protein (CC16): features as a peripheral lung biomarker. Ann N Y Acad Sci 2000; 923: 68 – 77.
17. Bernard AM, Gonzalez-Lorenzo JM, Siles E, *et al*. Early decrease of serum Clara cell protein in silica-exposed workers. Eur Respir J 1994; 7: 1932 – 7.
18. Lesur O, Bernard A, Arsalane K, *et al*. Clara cell protein (CC-16) induces a phospholipase A2-mediated inhibition of fibroblast migration in vitro. Am J Respir Crit Care Med 1995; 152: 290 – 7.
19. Lesur O, Bernard AM, Begin RO. Clara cell protein (CC-16) and surfactant-associated protein A (SP-A) in asbestos-exposed workers. Chest 1996; 109: 467 – 74.
20. Wang SX, Liu P, Wei MT, *et al*. Roles of serum clara cell protein 16 and surfactant protein-D in the early diagnosis and progression of silicosis. J Occup Environ Med 2007; 49: 834 – 9.
21. Hermans C, Bernard A. Pneumoproteinaemia: a new perspective in the assessment of lung disorders. Eur Respir J 1998; 11: 801 – 3.
22. Hermans C, Bernard A. Lung epithelium-specific proteins: characteristics and potential applications as markers. Am J Respir Crit Care Med 1999; 159: 646 – 78.
23. Evans MJ, Cabral-Anderson LJ, Freeman G. Role of the Clara cell in renewal of the bronchiolar epithelium. Lab Invest 1978; 38: 648 – 53.
24. Vallyathan V, Shi X. The role of oxygen free radicals in occupational and environmental lung diseases. Environ Health Perspect 1997; 105(1) (suppl): 165 – 77.
25. MacNee W. Oxidants/antioxidants and COPD. Chest 2000; 117: S303 – 7.
26. Yao W, Wang ZM, Wang MZ, *et al*. Oxidative injury and serum cytokines in coal workers with pneumoconiosis. Sichuan Da Xue Xue Bao Yi Xue Bao 2005; 36: 510 – 2.

Study of the influence of environmental tobacco smoke to trachea and lung of the animal model

Shuling Wang[1], Tianqi Wang[1], Shen Cherng[2]

[1]*College of Basic Medical Science*, *Zhengzhou University*, *Zhengzhou*, *Henan*, *China*; [2]*Department of Computer Science and Information Engineering*, *Chengshiu University*, *Niaosong*, *Kaohsiung*, *Taiwan*, *China*

Received January 20, 2009

Abstract

The environmental tobacco smoke (ETS) can influence the expression of androgen acceptor (AR) in organs of trachea and lung of animals of Wistar Rats. The rising of AR expression could be one of the mechanisms of smoking pathogenesis. Moreover, discontinuing ETS can not make the ascension of the AR back to normal level for the animals. [Life Science Journal. 2009; 6(2): 40 – 42] (ISSN: 1097 – 8135).

Keywords: environmental tobacco smoke (ETS); androgen acceptor (AR); pathogenesis

1 Introduction

World Health Organization's (WHO) indicated the population of smoker being approximately 13 hundred million in the world. The investigation demonstrated[1] male smoker is about 66%[2]. The environmental tobacco smoke (ETS) can produce 6000 different kinds of chemical substance[1–3]. Major parts of the substances can be harmful and being as carcinogen. ETS is acting direct or the indirect role at many kinds of disease as well as the developing process, such as respiratory disorders, lung cancer, chronic bronchitis and asthma. Recently, multi-aspects research seeing from the immunity function, cell apoptosis, and oxidized damage and so forth, have carried on the discussion to the smoking pathogenesis mechanism. It is well known that ETS can affect the shape and function of testis[4]. However, a pathogenesis mechanism proposed that androgen acceptor (AR) consists of eight exons with coding nucleoprotein being composed of 918 amino acids[5] is related to ETS. Androgen can diffuse into both target and non-target organs. But, it only functions in target organs. Similar like steroid hormone, AR is also a transcriptional factor. AR, if excited by Androgen, can recognize the target factor in a specific segment in DNA and combine with it to adjust the gene transcription expressing a new protein as well as changing the function of the cell[5]. In this article, we use RT-PCR and immunostaining LAB-SA to exam the AR expressing in tracheal sac and lung of the mice.

*Corresponding author. Email:

2 Material and Method

36 Wistar healthy male mice with body weight 180 g – 220 g provided by the Henan Province experimental animal center were randomly divided into three groups, group A was for ETS exposure, group B for being as control group, and group C as natural ETS exposure group. Each group has two cages. Each cage was raised six mice. An ETS room, 1740 mm × 1100 mm × 1500 mm was constructed by acrylic plate with a 2 mm × 3 mm air hole on top for exposing tobacco smoke and air. Group A was in ETS exposed 60 minutes, twice a day for the first 38 days and changed to being in exposure for once a day 60 minutes for another 38 days. In group A, the ETS was provided by burning "Hongxi Cigarette" in a bundle of five pieces of 84mm cigarettes in every fifteen minutes for four times. Basic components of a cigarette consist of 17 mg tar, 1.1 mg smoke alkali. The antibody of AR is taken anti-AR carboxyl group end multi-peptide fragment to affine purified multi-clone immune body from the rabbit which is the product of Santa Cruz Corporation. The SP series driving fluid reagent box and DAB reagent box were the products from Beijing Zhongshan

Biological Technology Limited Company. In control group B, no ETS was provided. In natural group C, same ETS exposure was provided but the animals being sacrificed one month later after quitting ETS exposure. The animals in group A should be in surgical treatment on the day of 76th at abdominal cavity ketamine (3 mg/kg) injection for taking organs of trachea and lung being fixed in 4% formaldehyde solution for 24 hours. For group C, similar sample collection procedures with group A were performed 30 days later after 76 days ETS exposure. Tissue sample in preparation: Using ethyl alcohol gradient for dehydration of tissue sample embedded with paraffin wax (low melting point) in 3 – 4 μm slice, and then, processed with the chrome alum gelatin on glass slide being ready for staining.

Method of immunohistochemistry staining (immunostaining) of AR: Taking PBS as negative group in contrary to be in comparison of the organ of testicle for lab-animal as positive group. Normal and the benign prostate gland proliferation of the sample in situ RT-PCR, AR mRNA signal can be with purple pellet in positive group mainly located in the nearness karyotheca cytoblastema. Report from Liang Lijian research[5] revealed AR could be possible found in both cytoblastema and nucleus. Obvious yellowish brown pellet appears in intranuclear area. We can take the cytoplasma or the cell as the positive expression to determine the AR positive cell with the HPIAS-1000 high resolution pathology chart article analysis system for averaging gradation and luminosity. SPSS 10 software was used for t-test analysis and depicted with average ± STD (x ± s).

3 Results

Yellowish brown pellets can be observed on both pseudostratified cilium cylinder epithelium cells and chondrocytes in the organ of trachea of the rats. We can also observe the yellowish brown pellets in the trachea pseudostratified cilium cylinder epithelium cells in organ of lung of the rats, most of them are in kytoplasm and a few in cell nucleus. In contrary, we can not observe the yellowish brown pellets in control group (replacement of anti-staining by PBS).

3.1 The AR expression in the organ of trachea of male rats

In Table 1, the AR expressions are listed for all animal groups. In comparison with control B (Figure 1a) and group A (Figure 1b), AR expression in group A is higher than in group B ($P < 0.01$). However, no obvious difference can be observed between group C and A ($P > 0.05$) (Figure 1c).

Table 1. The AR expression in the organ of trachea of the rats (x ± s)

Groups	*n*	mean ash density	mean optical density
Control B	12	99.9 ± 7.75	0.293 ± 0.05
ETS A	12	87.0 ± 9.60*	0.358 ± 0.06*
Natural C	12	90.6 ± 6.28**	0.346 ± 0.03**

In comparison with control *: $P < 0.01$; with group C **: $P > 0.05$.

3.2 The AR expression in the organ of lungs of male rats

AR can only expressed in the organ of trachea of the rats, however, no expression in the organ of lung of pulmonary alveoli. The AR expression are listed in Table 2. In comparison with Figure 2a (control), AR expression in group A (Figure 2b) is higher than in group B ($P < 0.05$ or $P < 0.01$) but no difference with group C ($P > 0.05$) (Figure 2c). No positive cells were observed in Figure 3.

Table 2. The AR expression in the organ of lung of the rats (x ± s)

Groups	*n*	mean ash density	mean optical density
Control B	12	140.5 ± 6.04	0.114 ± 0.015
ETS A	12	134.4 ± 5.92*	0.143 ± 0.023**
Natural C	12	135.1 ± 5.29$^{*\Delta}$	0.139 ± 0.017$^{**\Delta}$

In comparison with control *: $P < 0.05$; **: $P < 0.01$; with group C $^{*\Delta}$: and $^{**\Delta}$: $P > 0.05$.

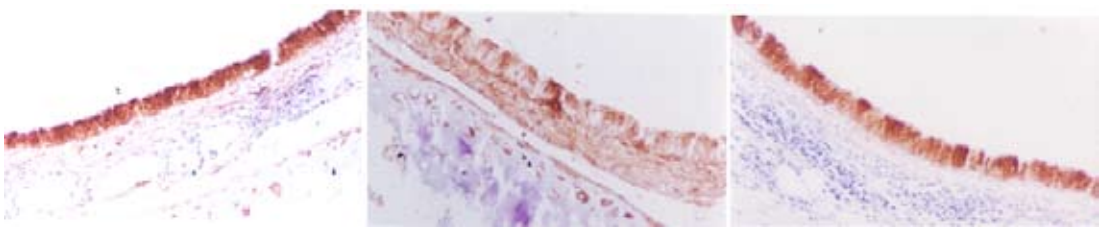

Figure 1. The AR expression in the organ of trachea of the rats (Immunostaining × 200). a: in control group B; b: in group A; c: in group C.

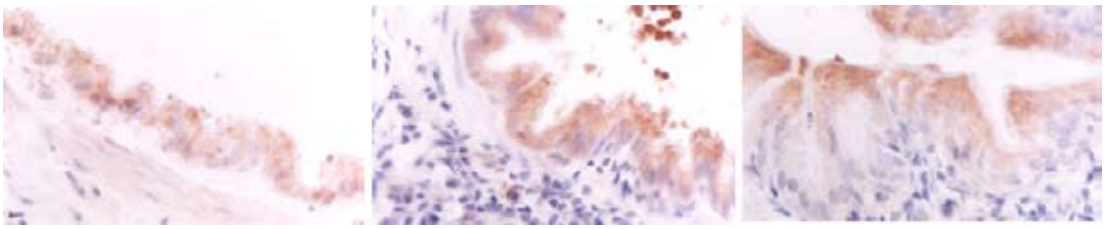

Figure 2. The AR expression in the organ of lung of the rats (Immunostaining × 400). a: in control group B; b: in group A; c: in group C.

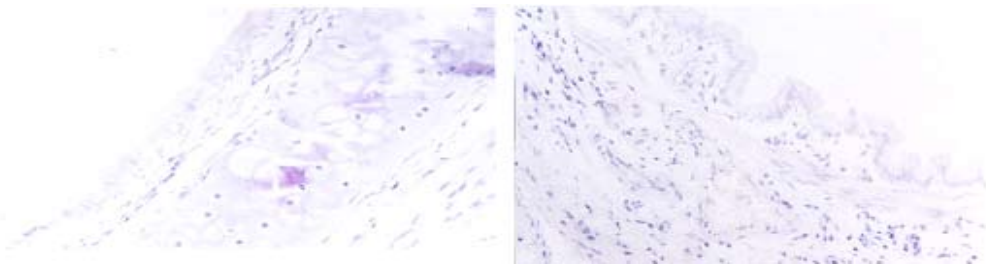

Figure 3. Replace PBS to the antistaining in the organs of trachea (a) and lung (b) of the rats of ETS (Immunostaining × 100).

4 Discussion and Conclusion

The experimental results have shown that the AR expression in the organ of lung and trachea of the rats upon ETS exposure is obvious stronger than in control. The report of Wei Sha Li et al[6] demonstrated smoking may reduce the blood serum androgen standard. Our research revealed the similar result[7]. Extrapolating the low standard of the androgen may possibly cause AR in high expression because the androgen automatically makes the adjustment of AR expression[8]. Thus, ETS can reduce the blood serum androgen standard in the trachea and lung is very obvious. Liang Shu *et al*[9] reported the AR expression for lung cancer patients can be high to 61.7%, also, AR expression of the adenocarcinoma of the lung is higher than lung cancer[10]. AR may participate the carcinogenesis in early stage. The natural did not show too much difference with the experimental group may result that quitting smoke can not help to reduce the expression of the AR in a short time period. However, the mechanism of the promotion of the AR expression and why the target should be the organs of lung and trachea would still be unknown and further research should be conducted.

References

1. Yang GH, Ma JM, Liu NE. The investigation of the smoked and passive smoking population in China. Chinese epidemiology magazine 2005; 26: 77 – 83.
2. Rennard SI. Cigarette smoke in research. Am J Respir Cell Mol Biol 2004; 31: 479 – 80.
3. Zhong C, Jiang SL, Qiu L, *et al*. Urinary cotinine concentration in flight attendants, in relation to exposure to environmental tobacco smoke during intercontinental flights. International Archives of Occupational and Environmental Health 1999; 72(7): 475 – 9.
4. Das SK. Harmful health effects of cigarette smoking. Molecular and Cellular Biochemistry 2003; 253(1): 159 – 65.
5. Zhong C, Jiang SL, Qiu SD. The application of RT-PCR technology for exam AR mRNA in paraffin slide. Anatomy Development 1998; 4(3): 245 – 6.
6. Liang LJ, Lu MD, Huang JF. Naked mouse liver cancer transplant model for study of the anti-androgen treatment. Journal of Chinese Medicine 1998; 7(4): 299 – 300.
7. Wei SL, Zhou SJ, Wang Y. Effect of Smoking to the male seminal parameter, function of the sperm and influence of testosterone research. Chinese Male Scientific Magazine 2000; 14(4): 237 – 9.
8. Wang SL, Chen XF, Cherng S. The endocrine disorder by smoking inhalation. Life Science Journal 2005; 2(1): 37 – 9.
9. Yao GH, Zhou YY, Xu ZH. Research of Androgen control. Research of Life Science 5(3): 202 – 5.
10. Boix L, Castells A, Bruix J, *et al*. Androgen receptors in hepatocellular carcinoma and surrounding liver: relationship with tumor size and recerrence rate after surgical resection. J Hepatology 1995; 22: 216 – 8.

Clinical efficacy study of pelvic floor electrical stimulation for idiopathic detrusor overactivity and urodynamic stress incontinence☆

Huifan Liu[1,2,3], Qingwei Wang[1], Yan Qi[1], Ruili Zhang[2], Shuqiang Zuo[1], Xiaojin Wang[3], Jinxing Wei[1], JianguoWen[2,3]

[1]*Department of Urology*, *The First Affiliated Hospital of Zhengzhou University*, *Zhengzhou*, *Henan* 450052, *China*; [2]*Pediatric Urodynamic Center*, *The First Affiliated Hospital of Zhengzhou University*, *Zhengzhou*, *Henan* 450052, *China*; [3]*Institute of Clinical Medical Research Universities Henan*, *Zhengzhou*, *Henan* 450052, *China*

Received December 19, 2008

Abstract

Objective. To investigate the efficacy of pelvic floor electrical stimulation (PFES) using surface electrode combined with pelvic floor training (PFT) under intensive supervision for female with idiopathic detrusor overactivity (IDO) and urodynamic stress incontinence (USI). *Methods*. PFES using surface electrode and PFT under intensive supervision were performed on 70 women (age ranged from 31 to 64 years, average age 40 ± 7 years old) with IDO and USI for twelve weeks. Urinary diary, International Continence Inquiring Committee's Questionnaire (ICI-Q-SF) scores were recorded and urodynamic study was performed before and after the treatment. *Results*. In total, fifty women (71%) finally completed treatment for twelve weeks, and urinary incontinence disappeared in 8 (16%), detrusor overactivity disappeared in 10 (20%), and leakage was no found in 6 (12%) in leakage point pressure measurement. Moreover, the total time of voiding (72 h), total time of leakage (72 h), total scores of ICI-Q-SF, max detrusor uninhibited contraction pressure and detrusor uninhibited contraction duration were significantly lower than those before treatment; max voided volume, normal desired cystometric capacity, maximum cystometric capacity, Valsalva leak point pressure and max urethral closure pressure were significantly higher than those before treatment ($P < 0.05$). The effective rate following up three months was 60%, not significantly lower than that after treatment ($P > 0.05$). *Conclusions*. PFES using surface electrode combined with PFT under intensive supervision is a useful therapy to treat women with IDO and USI. [Life Science Journal. 2009; 6(2): 43 – 47] (ISSN: 1097 – 8135).

Keywords: urodynamic stress incontinence; idiopathic detrusor overactivity; pelvic floor electrical stimulation; pelvic floor training

1 Introduction

It is well known that urodynamic stress incontinence (USI) is a common and heterogeneous disorder[1]. The overall prevalence of USI among Chinese women is as high as 18% to 55%, moreover, the trend is increasing year by year, seriously affecting their quality of life. The best choice for first-line treatment is mostly behavior therapy mainly including pelvic floor training (PFT) and pelvic floor electrical stimulation (PFES), with advantages of being simple, noninvasive and economic, and only for serious patients surgical treatment can be carried out[2].

However, there are many problems for good outcome of the women with USI in traditional behavior therapy[3]. For one thing, it is important and not easily assured that the validity and duration of the PFT. For anther thing, the vaginal electrode used in the PFES could bring remarkably discomfort[4]. Moreover, no matter what kind of treatment is used, after urodynamic checkup up to 50% of patients are found to be complicated by detrusor overactivity, which is the main reason for no

☆Supported by
*Corresponding author. Tel and Fax: ; Email:

improvement in the quality of lives of the patients after the treatment, but also significantly increases the severity of urinary incontinence[5]. Furthermore, the causes for the women with USI and detrusor overactivity are still not clear, and the clinical treatments and its efficacy are also of much controversy. Therefore, it is imperative to investigate the outcome on the women with USI and detrusor overactivity treated by improved behavior therapy.

The purposes of this study were to prospectively evaluate the efficacy of PFES using surface electrode combined PFT under intensive supervision for female with idiopathic detrusor overactivity (IDO) and USI. We hoped it would provide valuable insights into the pathogenesis and helpful in improving the outcome of them.

2 Materials and Methods

2.1 Patients

In this study, seventy women (mean age 40 ± 7 year, range 31 to 64 year, all had childbearing history by vaginal delivery with an average of 1.2 parities) with USI and IDO were confirmed by urodynamic study, consecutively collected in the Urology and Urodynamic Center of the First Affiliated Hospital of Zhengzhou University from December 2006 to June 2008. The definition of USI and IDO was in according with that of International Continence Society (ICS)[6], which the former is noted during filling cystometry and is defined as the involuntary leakage of urine during increased abdominal pressure, in the absence of a detrusor contraction, the latter is s a urodynamic observation characterised by involuntary detrusor contractions during the filling phase which may be spontaneous or provoked when there is no defined cause. The criteria of patients for inclusion are that the patients have not any treatment since the onset of urinary incontinence, and genital prolapsed within the vaginal orifice when the body examination was carried out. What's more, the exclusive standard was for the patients who were diagnosed to have urinary tract infection, diabetes, bladder vaginal fistula, bladder cancer and trauma, as well as neurogenic bladder dysfunction through the urinoscopy, urography and imaging examination of nervous system. According to the sub-standard of severity of USI[7], this study included 35 mild cases, 23 moderate cases, and 12 cases of severe, and the course of disease was from 6 months to 29 years.

2.2 Method

All the patients were treated by PFES using surface electrode through neuromuscular electrical stimulation instrument (NeuroTrac™ ETS, produced by VML Denmark's company). The patients were asked to lie down, then the skin surface electrode was selected and placed in the perineal area that was besides the line of the vagina and anus. The sequential stimulation programmes were the same as those in previous research[8]. The stimulating cycle was 4S stimulation and 4S rest afterwards. The current strength of stimulus increased by 1% to 5% each time from 0 mA, until the patients had the feelings, while on computer screen electromyologram of perineum and muscle of perineum and anus contraction was observed, but without any significant discomfort. The treatment course was 3 times a week, each time 60 minutes, for 12 weeks.

At the same time, all the patients were given PFT under intensive supervision. First of all, doctors should supervise the patients to identify the correct pelvic floor muscles needing to be trained, by the method that the patients putting the index finger and middle finger in the vagina, they felt pressure around the fingers when anus contracted. In addition, when this method was applied, the contraction from other muscles such as the thighs, back and abdominal muscles should be avoided as far as possible at the same time. PFT program was that after emptying their bladder, the patients were asked to made a quick, maximum and sustained pelvic floor muscles contraction for three times, and then relax the pelvic floor muscles, further a slow, maximum and sustained pelvic floor muscles contraction for three times, and relax the pelvic floor muscles, repeat the above process. The patients should take a rest for 5 to10 seconds after every contraction. PFT lasted for 30 minutes every time, 2 times per day, for 12 weeks. The patients were required to go to the hospital and carried out pelvic floor muscle training in dorsal position at least 4 times a week, and PFES treatment could process at the same time. And the rest of PFT were allowed to carry out at home in dorsal, standing or sitting position.

Urinary diary and International Continence Inquiring Committee's Questionnaire (ICI-Q-SF) scores were recorded and urodynamic study was performed before and after the treatment. The urodynamic study included free uroflowmetry, cystometry, pressure-flow electromyography (EMG), valsalva leak point pressure (P_{VLP}) and static urethral pressure measurement in all patients, using the Duet Logic urodynamic unit (Medtronic Corporation, Denmark) according to the recommendations of ICS[9]. The observation variables of efficiency included the maximum voiding volume (MVV), the total voiding (TOV), the total times of leakage (LT), ICI-Q-SF (total

scores were 21), maximum flow rate (MFR), maximum detrusor uninhibited contraction pressure (MDUCP), detrusor uninhibited contraction duration (DUCD), bladder compliance (BC), normal desired cystometric capacity (NDCC), maximum cystometric capacity (MCC), P_{VLP}, maximum urethral closure pressure (MCP) and the functional urethral length (SFL).

The total efficiency were also followed up immediately and three months after the treatment in out-patient or on the phone. According to the standard[10], the cured were those whose conscious incontinence symptoms disappeared completely; the effective were those whose conscious incontinence symptoms improved significantly, and the leakage times reduced by more than 50%; the ineffective were those whose conscious incontinence symptoms didn't improve obviously, the times of leakage reduced by less than 50%. The effective rate was calculated based on the above cure and effective groups, with the formula (number of cured cases and effective cases)/ total number of cases.

2.3 Statistical analysis

Statistical analyses were carried out by using the Statistical Package for Social Sciences, version 10.0 for windows. The paired samples *t* test and Chi-square test were used. *P*-values of < 0.05 were considered to be statistically significant.

3 Results

3.1 Comparison of the various parameters of women with USI and IDO before and after the treatment

In total, fifty cases (71%) completed 12 weeks of therapy, whose clinical symptoms and urodynamic parameters before and after the treatment were shown in Table 1 and Table 2. Among all the patients, urinary incontinence symptoms completely disappeared in 8 cases (16%), IDO disappeared in 10 cases (20%), no leakage occurrence in 6 cases (12%) during the Valsalva leak point pressure measurement. After treatment, TOV, LT, ICI-Q-SF, MDUCP and DUCD were significantly lower than those before treatment, and MVV, NDCC, MCC, P_{VLP} and MCP were significantly higher than those before treatment ($P < 0.05$).

Table 1. The values of urinary diary and ICI-Q-SF before and after treatment of PFES combined with PFT

	MVV (ml)	TOV(times/72h)	LT (times/72h)	ICI-Q-SF
Before the treatment	159 ± 37	43 ± 8	20 ± 6	17 ± 3
After the treatment	225 ± 48	28 ± 5	10 ± 5	10 ± 3
t	14.671	14.922	10.693	9.076
P	0.000	0.000	0.000	0.000

Table 2. The values of urodynamic variables before and after treatment of PFES combined with PFT

	MFR (ml/s)	MDUCP (cmH_2O)	DUCD (s)	BC (ml/cmH_2O)	NDCC (ml)	MCC (ml)	PVLP (cmH_2O)	MCP (cmH_2O)	SFL (mm)
Before the treatment	29 ± 7	27 ± 9	13 ± 6	45 ± 13	141 ± 39	178 ± 36	81 ± 15	55 ± 8	27 ± 3
After the treatment	30 ± 6	18 ± 8	8 ± 3	47 ± 15	210 ± 48	247 ± 48	94 ± 11	59 ± 8	28 ± 3
t	1.569	5.003	5.849	1.241	10.412	12.392	5.789	2.776	1.008
P	0.123	0.000	0.000	0.220	0.000	0.000	0.000	0.008	0.318

3.2 The efficiency after treatment and follow-up for three months

The assessment of efficiency in the women with USI and IDO immediately after the treatment and follow-up for 3 months is shown in Table 3. The effective rate was 66% immediately after the treatment, and was 60% when following up for 3 months, which the significant difference was not found between them ($P > 0.05$).

Table 3. The efficiency of PFES combined with PFT at post-treatment and follow-up for three months

	Total No. (*n*)	Cured	Effect	Ineffective	Effective rate (%)	χ^2	*P*
After the treatment	50	8 (16)	25 (50)	17 (34)	66	0.386	0.534
Three months after the treatment	50	7 (14)	23 (46)	20 (40)	60		

4 Discussion

USI is one of the most common chronic ailments in the women, some of whom is still poor response to treatment. The dynamic mechanism of USI is that the bladder pressure is higher than urethra pressure during the reserving urine period due to decreased urethra closed capability when a sudden increase of abdominal pressure, and

urethral closure pressure becomes negative. As a result, in order to avoid the urine leakage, the women have to minimize social and sports activities, getting the name "social cancer". It is usually considered to be related with childbirth, birth trauma, aging and declining estrogen levels and so on. These factors might lead to the bladder neck and urethra support structure damage, which made connective tissue surrounding the urethra relaxing, the activities of the urethra enlarging, pelvic floor muscle reflection delaying, the urethral controlled capability declining. The treatment includes conservative therapy and surgery therapy, whose main purposes are to strengthen the pelvic floor tissues to support the pelvic organs, to restore the urethra and bladder neck to the normal anatomic position, to increase the capacity of urethral continence[11]. However, when USI is complicated with IDO, even if there is no sudden increase in abdominal pressure or involuntary detrusor contraction, it can also lead to urine leakage through the lower closure capacity urethra, and then frequency and severity of incontinence of the patients increase significantly. Moreover, even if social and sport activities are limited, it can't avoid occurrence of the leakage, making a significant decline in the quality of life[12]. Furthermore, IDO is also main reason for poor quality of life of USI patients after treatment[13].

So far, there is still controversy about the treatment of the women with USI and IDO. It was suggested by some clinicians that simply treat the USI, and some of the women IDO can self-healing, for the continued existence of the IDO can apply for drugs treatment. For example, Duckett JR[14] reported that the outcome of tension-free vaginal tape (TVT) on 51 women with IDO and USI, and followed up for six months, found that after only 47% of IDO were cured spontaneously, and rest of them who suffered from persistent IDO were given anti-cholinergic drug, but only 22% of the patients released. However, there are also some clinicians holding that IDO should be treated first with oral anticholinergic medication, and then treat USI. Nevertheless, the patients have to endure the pain of urinary incontinence caused by USI during the treatment. Moreover, the side effects of anticholinergic medication is great, IDO is easy to relapse after drug withdrawal[5].

Animal studies have showed that repeated electrical stimulation, causing the passive contraction of pelvic floor muscles, not only increased the contraction capability of pelvic floor muscles, but also feedback inhibited sympathetic reflex to reduce activity of the bladder[15]. Moreover, in the previous studies which the author applied PFES using surface electrodes on female stress incontinence and urge incontinence of young people, the found satisfied effect had been found that symptoms disappeared respectively in 51% and 42% of cases, and it was simple and convenient, non-invasive and clean, and economical[8,16]. Furthermore, PFT also known as Kegel exercise, is a initiative pelvic floor rehabilitation method, and its treating effect have been proved by a large number of meta-analysis and randomized controlled research, making it the first choice for the women with USI of various types[17]. The main principle is that the patients repeated the pelvic floor muscles contraction and relaxation under self conscious, it enhance tension of pelvic floor muscles which support the urethra, bladder, uterus and rectum, increase urethral resistance and restore the pelvic floor muscle relaxation to achieve the goal of curing USI. However, simply pelvic floor muscle training can not ensure the correct and effective pelvic floor muscle contraction training, which resulted in its rare application in the clinic.

In present study, the PFES was combined with PFT under intensive supervision, so that pelvic floor muscles got active and passive contraction training, and then treated IDO and USI at the same time. It was found that IDO and USI can be treated simultaneously. Among all the patients, urinary incontinence symptoms completely disappeared in 8 cases (16%), IDO disappeared in 10 cases (20%), 6 patients' (12%) no leakage occurrence in 6 cases (12%) during the Valsalva leak point pressure measurement. Moreover, after treatment, the TOV, LT, ICI-Q-SF, MDUCP and DUCD were significantly decreased, and MVV, NDCC, MCC, PVLP and MCP were also significantly increased.

PFT was satisfied on the condition that PFT was validity and the duration should be at least 8 weeks. In this study, we applied for PFT under intensive supervision. That is, during 12-week course of treatment, patients were required to go the hospital for professional medical advice at least 4 times a week to ensure the validity of PFT during entire course of treatment, to urge and ensure that their PFT at home was carried out, and to enhance the patients' confidence. In view of the above-mentioned requirements, most of the patients in the study came from the vicinity of our city. This study and Konstantinidou E[18] both found that the efficiency of PFT under intensive supervision for female USI was significantly higher than that of simple family PFT reported in the literature[19]. In addition, in order to improve compliance of the patients, the study carried out PFES using surface electrodes to avoid the side effects of vaginal electrode, such as vaginal infection, bleeding, perineal discomfort and rashes. Moreover, the treatment room was set up and opened all day from Monday to Sunday so that patients

can receive professional medical treatment without a time limit. During the course of treatment, it is important that communication with patients proactively to enhance self-confidence and adjust treatment program timely. In this study, as much as 71% of the patients completed a 12-week treatment and the effective rate after the treatment and following up three months was 66% and 60% respectively.

However, the follow-up time in present study is only three months, the long-term efficacy need further research. Despite these limitations, we believe that our results highlight that PFES using surface electrode and PFT under intensive supervision is a useful therapy to treat women with USI and IDO.

References

1. Nazarishvili G, Gabunia N, Gagua G. Prevalence of urinary incontinence in women population. Georgian Med News 2007; 143: 39 – 42.
2. Rogers RG. Clinical practice. Urinary stress incontinence in women. N Engl J Med 2008; 358(10): 1029 – 36.
3. Choi H, Palmer MH, Park J. Meta-analysis of pelvic floor muscle training: randomized controlled trials in incontinent women. Nurs Res 2007; 56(4): 226 – 34.
4. Amaro JL, Gameiro MO, Kawano PR, Padovani CR. Intravaginal electrical stimulation: a randomized, double-blind study on the treatment of mixed urinary incontinence. Acta Obstet Gynecol Scand 2006; 85(5): 619 – 22.
5. Lai HH, Simon M, Boone TB. The impact of detrusor overactivity on the management of stress urinary incontinence in women. Curr Urol Rep 2006; 7(5): 354 – 62.
6. Abrams P, Cardozo L, Fall M, Griffiths D, Rosier P, Ulmsten U, van Kerrebroeck P, Victor A, Wein A. The standardisation of terminology of lower urinary tract function: report from the Standardisation Subcommittee of the International Continence Society. Neurourol Urodyn 2002; 21(2): 167 – 78.
7. Feng J, Chen GM, Zhang XH, Wang JL. The clinical analysis of stress urinary incontinence treated with bio-feedback and pelvic electronic stimulation. Chin J Clin Obstet Gynecol 2006; 7(1): 5 – 8.
8. Su J, Wen JG, Wang QW, Zhang P, Liu K, Zhang RL. Therapeutic effects and urodynamic changes of patients with genuine stress urinary incontinence after pelvic floor electrical stimulation. Journal of Zhengzhou University (Medical Sciences) 2006; 41(2): 204 – 6.
9. Schäfer W, Abrams P, Liao L, Mattiasson A, Pesce F, Spangberg A, Sterling AM, Zinner NR, van Kerrebroeck P. Good urodynamic practices: uroflowmetry, filling cystometry, and pressure-flow studies. Neurourol Urodyn 2002; 21(3): 261 – 74.
10. Norton P, Brubaker L. Urinary incontinence in women. Lancet 2006; 367(9504): 57 – 67.
11. Hirai K, Sumi T, Kanaoka Y, Ishiko O. Female urinary incontinence: diagnosis, treatment and patients' concerns. Drugs Today (Barc) 2002; 38(7): 487 – 93.
12. Choe JH, Choo MS, Lee KS. The impact of tension-free vaginal tape on overactive bladder symptoms in women with stress urinary incontinence: significance of detrusor overactivity. J Urol 2008; 179(1): 214 – 9.
13. Bump RC, Norton PA, Zinner NR, Yalcin I. Mixed urinary incontinence symptoms: urodynamic findings incontinence severity, and treatment response. Obstet Gynecol 2003; 102(1): 76 – 83.
14. Duckett JR, Tamilselvi A. Effect of tension-free vaginal tape in women with a urodynamic diagnosis of idiopathic detrusor overactivity and stress incontinence. BJOG 2006; 113(1): 30 – 3.
15. Li LK, Song B, Jin XY. An experimental study on the influence of electrical pelvic floor stimulation to the goats' urethral function. Chin J Urol 2002; 23(5): 307 – 9.
16. Su J, Wen JG, Wang QW, Liu K, Zhang P. The Short-term effects of pelvic floor electrical stimulation in treatment of adolescents with idiopathic urgent incontinence using the Neuro Trac5TM. Chinese Journal of Pediatric Surgery 2006; 27(6): 309 – 12.
17. Choi H, Palmer MH, Park J. Meta-analysis of pelvic floor muscle training: randomized controlled trials in incontinent women. Nurs Res 2007; 56(4): 226 – 34.
18. Konstantinidou E, Apostolidis A, Kondelidis N, Tsimtsiou Z, Hatzichristou D, Ioannides E. Short-term efficacy of group pelvic floor training under intensive supervision versus unsupervised home training for female stress urinary incontinence: a randomized pilot study. Neurourol Urodyn 2007; 26(4): 486 – 91.
19. Aukee P, Immonen P, Laaksonen DE. The effect of home biofeedback training on stress incontinence. Int Braz J Urol 2006; 32(4): 462 – 8.

Expression of androgen receptor mRNA affected by the functions of lung and trachea in animal model of Kunming mouse

Shuling Wang[1], Xiufang Chen[2]

[1]*College of Basic Medical Science*, *Zhengzhou University*, *Zhengzhou*, *Henan* 450001, *China*; [2]*Henan Xian Dai Medical Research Hospital*, *Zhengzhou*, *Henan*, *China*

Received January 24, 2009

Abstract

In this article, we demonstrate the experimental results of the expression of androgen acceptor mRNA correlate with the functions of lung and trachea in an animal model. This study depicts androgen acceptor as the connection between lung and kidney in Traditional Chinese Medicine. [Life Science Journal. 2009; 6(2): 48 – 50] (ISSN: 1097 – 8135).

1 Introduction

The function of lung is to breathe for the body. In traditional Chinese medicine, it belongs to gold in five lines. In contrary, kidney belongs to water in the concept of the five elements (of metal, wood, water, fire, and earth) used in ancient Chinese cosmology and later in herb medicine five lines. Based upon the philosophy of Traditional Chinese Medicine, elements in five lines are correlated to each other. Therefore, if the lung and kidney mutually being affected in pathology is true[1,2], the function of sex hormone can be through the special acceptor in target cell cytoblastema[3]. By using the real time polymerase chain reaction (RT-PCR) and the technique of TaqMan fluorescence examination for mouse trachea in lung organization to see if any androgen acceptor/Androgen Receptor (AR) mRNA expression can be found being compared to the AR mRNA founded in mouse testicle organization may be able to reveal the correlation between the lung and kidney. Also, by using immunity histochemical method carries of the AR being in lung is highly correlated to the function of kidney. The androgen level appearing the modification by kidney may be influenced through its acceptor in lung.

2 Materials and Methods

Ten animals of two months old healthy male Kunming mice with body weight 180 g to 200 g for the experiment of checking expression of AR mRNA in lung and trachea were provided by Henan Province Experimental Animal Center. The animal was anaesthetized by abdominal cavity injection with chloramine alkone (3 mg per Kg). Organs of trachea, lung and the testicle were rapidly taken and chopped to preserve in liquid nitrogen at – 70 ºC. Taking 50 mg sample for each organ from the freezer and putting it into 800 μl (10^{-6} liter) reagent A (guanidine thiocyanate-phenol solution) for vibrating 30 seconds, adding 200 μl reagent B (the chloroform: isoamyl alcohol in 24 : 1) for being in 14000 rpm centrifugal for 5 minutes. Supernatant should be carefully drawn 400 μl to mix with 400 μl isoamyl alcohols. Taking 50 μl mixed solution for 14000 rpm centrifugal 10 minutes, we draw off supernatant and added 500 μl 75% ethyl alcohol to sediment shaking uniformly and put it for 14000 rpm centrifugal 5 minutes. Then, we draw supernatant again to get the sediment in dry being ready for use. In the mean time, for each test tube, first making reverse transcript reactive solution by adding 1.5 μm random primer 5'-CTACTGCGCT-3' and 0.3 μm primer 5'-AGGCAGCTGCTCAGGGTGGC-3' mixed with buffer, and then 20 μl solution was taken to mix with 50 μl MLV keeping in 37 ºC incubator for an hour.

For reverse transcript reaction, each tube was added PCR reactive mixture 20 μl and 50 μl MLV-reverse transcriptase. For PCR reaction, making PCR reactive mixture including buffer solution, 2 mM $MgCl_2$, 200 μm

*Corresponding author. Email:

dNTP, 0.3 μM (primer 2) mixed with buffer as well as 0.3 μM 5'-TTACAGCAGAGGCAGGAGACT-3' (primer 1) and 1% off-ion formamide, taking 26 μl reactive mixture solution and 2 μl reverse transcript reactive solution and then added with 2 μl Taq DNA polymerase. Parameters used for the reaction were 94 ºC pre-denaturation for 5 minutes, 94 ºC for 45 seconds, 55 ºC for 45 seconds, 72 ºC for 45 seconds with 35 cycles and expended for 72 ºC for 5 minutes.

After preparing mixture solution by diluting one tenth of the product that was through PCR procedures, 15 μl mixture solutions were taken for 2% Agarose gel electrophoresis checking (0.05% Bromination second grade spindle at voltage of 5 V/cm). To isolate AR, 50 mg sample of mouse testicle was taken for experiment. The segment specificity of the sample can be shown at wavelength of 302 nm under ultraviolet exam. Meanwhile, male specimen has shown 260 bp in size at specificity of DNA segment.

In preparing of DNA specificity segment in tube for centrifuge and lysate being incubated at 37 ºC – 55 ºC for uniformly melting, we can mix 800 μl lysate with DNA, put the mixture in incubation at 55 ºC for 15 minutes, centrifuge at 14000 rpm for thirty minutes, take off supernatant fluid and add 75% alcohol, centrifuge again for another 30 seconds, take off supernatant fluid and add 600 μl TE buffer at 55 ºC gently for 15 minutes, put in 14000 rpm centrifugal for 3 minutes, dilute for 10 times dilution for fluorescent. The PCR amplification can be done by taking 2 μl mixtures for the process. In the mean time, Fluorescence PCR real time reaction for checking system can be performed by taking 2.5 μl buffer, 8 mM $MgCl_2$ and 100 μM dNTP, 2% as well as 3 pM fluorescent probes, 15 pM primer 2, double evaporate 2 μl template being added together with 50 μl distill water.

3 Results

In normal male Kunming mice, we investigated the expression of AR mRNA in trachea, lung tissue and testicles. The lowest expression of AR mRNA was found in lung. Real-time quantitative fluorescence PCR detection results show the *Ct* values at 9.880 ± 8.01, 12.831 ± 5.632 and 22.298 ± 2.35 in testicular and lung (Table 1). From the analysis of gel electrophoresis, size of 260 bp band of AR appearance of the specific segment is revealed.

Figure 1 to Figure 5 depicts the expressions of AR in testis of normal male rat, AR in testis of normal male rat, testis of male normal rat, expression of AR in trachea of normal male rat and the expression of AR in lung of normal male rat.

Table 1. the expression of AR in the trachea and lung of normal male rat

Tissues	*n*	Mean ash density	Mean optical density
Trachea	10	128.1 ± 4.11**	0.225 ± 0.04**
Lung	10	140.98 ± 9.58	0.15 ± 0.05

Compare the trachea with that of lung, **: $P < 0.01$.

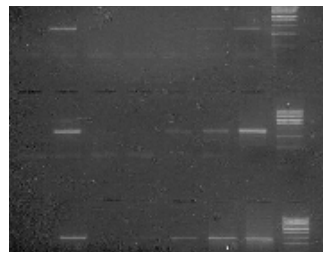

Figure 1. The expression of AR mRNA in the lung, testes and trachea of normal male mice.

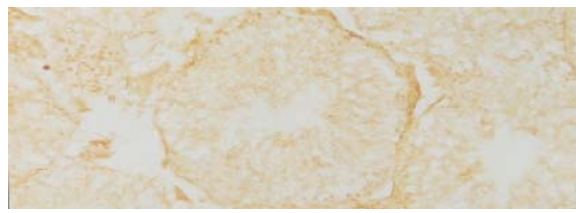

Figure 2. The expression of AR in testis of normal male rat (× 400). AR positive cell mainly appeared in the testis convoluted seminiferous tubule.

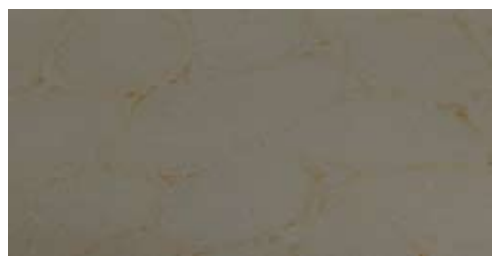

Figure 3. The testis of male normal rat (negative control) (× 400). This is PBS instead of first antibody (There were no AR positive cell in the testis of rat).

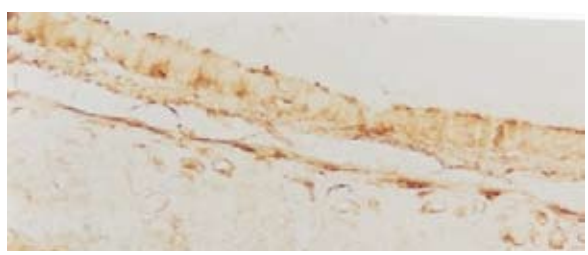

Figure 4. The expression of AR in trachea of normal male rat (× 400). AR positive cells appeared in the pseudo ciliated columnar epithelial cells and cartilage cell of male wistar trachea.

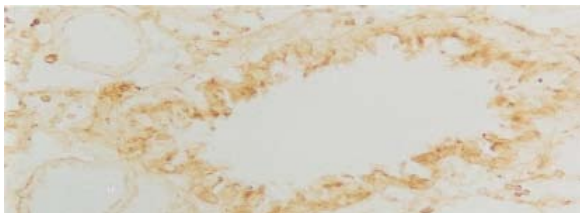

Figure 5. The expression of AR in lung of normal male rat (× 400). AR positive cells appeared in the ciliated columnar cell of each grade bronchus.

4 Discussion

These findings showed the AR mRNA expression can be observed in normal male mouse trachea and lung. Using of RT-PCR and the technology of molecular level, we found the expression of AR mRN in trachea. The AR mRNA expression quantity was stronger in testicle but lower in trachea and lung. The androgen may proliferate to enter the target as well as non-target organization, but only function in the target cells which the androgen receptor exists. Furthermore, the steroid hormone acceptor is located in the cell with AR. The androgen and its acceptor could be the bases of traditional Chinese medicine "the lung kidney mutual promotion of the five elements" and "the kidney host air intake".

The traditional Chinese medicine says that, the lung is the gold in five lines, the kidney is the water in five lines, between the lung kidney the passages through which vital energy circulates is connected. The kidney fine may moisten the lung in cloudy and the kidney may warm the lung. The androgen has the function through its acceptor to the lung and possibly being in the kidney as a warm aspect to the lung. Due to the decrease in the level of androgens, AR directly may affect its target organs for the senior. It may be one of the reasons of chronic bronchitis for senior being significantly higher than that of the incidence of young people[12]. According to the results of this study, many diseases such as asthma, lung cancer and other diseases for the seniors may have occurred with low level sex hormones in the trachea and lungs. Adjust the abnormal level of AR is probably the prevention and treatment of respiratory disease for seniors. Nonetheless, the function of body system is by various factors, and the adjustment mechanism is very complicated. Renal through its receptor on the lungs of androgens can adjust function of "kidney associated".

5 Conclusion

Our study found that the AR mRNA expressions in trachea and lung tissue in male normal mouse. The expression with AR mRNA is highest in testicular but lower in trachea and lowest lung tissue. AR expression in trachea and lung confirmed that trachea and lung are androgen target organ. Adjustment androgen and its acceptor level possibly can be the prevention and treatment for respiratory disease. Therefore, the androgen must have the influence like the traditional Chinese medicine says "the lung kidney mutual promotion of the five elements". The "kidney host air intake" can also possibly be one of material bases through its acceptor to the trachea and the lung to invigorate the kidney as one of the organ affecting respiratory disease.

References

1. Zhu YP, Zhu H, Xu HY, *et al*. 63 example old age masculine chronicity blocking pulmonic bone density and bone metabolism change[J]. China Osteoporosis Magazine 2000; 6(1): 44 – 7.
2. Guo SH, Yang DZ, Xu ZQ, *et al*. Discusses from the chronic bronchitis bone density change for a long time coughs the wound kidney[J]. West China Medicine 1992; 7(1): 46 – 7.
3. Wang M, Yu XY, Xu SD, *et al*. The throat cancer organizes the androgen and the estrogen acceptor determination[J]. Shandong Medical College Journal 1996; 34(4): 27-273.
4. Liu WY, Zhang SF, Hu TZ, *et al*. In young child angioma and blood vessel abnormal organization sex hormone acceptor expression[J]. Chinese Surgical Department Magazine 1999; 37(5): 295 – 7.
5. Cui Xiu is winsome, Zhu Jijiang, wooden village uncle child, *et al*. Epidermis growth factor acceptor and androgen acceptor in human benign prostate gland proliferation sickness immunity localization. China Medical College Journal 1996; 25(6): 595 – 7.
6. Clock Great, Qiu Shudong, Jiang three bright. Benign prostate gland proliferation morphology change andAR mRNA expression difference[J]. Xi'an Medical College Journal 1999; 20(2): 145 – 9.
7. Liang LJ, Lu MJ de, Huang JF, *et al*. Bare mouse person liver cancer transplants the model the anti-androgen treatment. Chinese Medicine Magazine 1998; 78(4): 299 – 300.
8. Friedman MA, Demanes DF, Hoffman PG, *et al*. Hepatomas: hormone receptors and therapy[J]. Am J Med 1982; 73: 362 – 5.
9. Zhao Beautiful jade, Liu ZM, Shao FY, *et al*. Human circumference blood white blood cell androgen acceptor appraisal and significance[J]. Chinese Nuclear Medicine Magazine 1995; 15(1): 51 – 2.
10. Solution Fragrant, Liu Towering, Zhang YL. Androgen acceptor function mechanism[J]. Biochemistry and Biophysics Progress 1999; 26(2): 131 – 4.
11. Earthen mound daphne, Wu GZ, Jin M. Sex hormone to kidney empty patient masculine and feminine elements balance control action[J]. Chinese Medicine Foundation Medicine Magazine 1999; 5(3): 46 – 7.
12. Should Handsome, Yao DH, Zhang QH. Blood serum gao alkone, dissociation gao alkone, double hydrogen gao alkone density and masculine age relations research[J]. Chinese Male Scientific Magazine 2000; 14(1): 13 – 5.

Study of plasma levels of ApoA-I and ApoB for prognosis of acute ischemic stroke

Zhuo Li[1], Yuming Xu[1,*], Song Tan[1], Bo Song[1], Ming Liu[2]

[1]*Department of Neurology*, *The First Affiliated Hospital of Zhengzhou University*, *Zhengzhou*, *Henan* 450052, *China*; [2]*Stroke Clinical Research Unit*, *Department of Neurology*, *West China Hospital*, *Sichuan University*, *China*

Received January 25, 2009

Abstract

Background. The levels of plasma ApoA-I, ApoB and the ratio of ApoA-I/ApoB were reported as risk factors of stroke. However, if they are prognostic factors of stroke is still unknown. This article is to demonstrate the study of plasma levels of ApoA-I and ApoB levels for prognosis of acute ischemic stroke. *Method*. From Aug 24th 2005 to Apr 25th 2007, patients with acute ischemic stroke (AIS) came to Henan Stroke Registry Centre in the First Affiliated Hospital of Zhengzhou University were voluntarily enrolled to this study. Parameters related to prognosis of AIS of these patients were tested at admission counter, such as plasma ApoA-I, ApoB, NIHSS, age, gender. Parameters for patients' self-care ability, such as Modified Rankin Scale (MRS), Barthel Index (BI) were collected one month later. We established MRS < 3 or BI > 60 as patient independence. Then, we used Logistic regression to detect independent predictors for the prognosis of AIS. *Results*. During the 2 years study, we collected 248 patients in all. Of these patients, ApoA-I ranged from 0.20 g/L to 2.30 g/L, and average level was 1.04 ± 0.29 g/L; ApoB ranged from 0.40 g/L to 2.40 g/L, and average level was 0.91 ± 0.32 g/L; ApoA-I/ApoB ratio ranged from 0.21 to 5.50, and its median was 1.17. MRS < 3 was observed in 69% (171/248) of the patients at 1 month follow-up, and BI > 60 in 69.6% (172/248) of the patients. Multivariate analysis showed ApoA-I/ApoB independently associated with MRS score (OR = 0.46, 95%CI = 0.213 – 0.977, $P = 0.043$) and BI score (OR = 0.45, 95%CI = 0.208 – 0.966, $P = 0.040$). *Conclusions*. Our results indicated that ApoA-I/ApoB ratio in AIS patients was independently associated with one month MRS score and BI score. Higher the ApoA-I/ApoB ratio, better the recovery outcome patients would achieve. High ApoA-I/ApoB ratio could be a predictor for good prognosis of AIS. [Life Science Journal. 2009; 6(2): 51 – 56] (ISSN: 1097 – 8135).

Keywords: acute ischemic stroke; ApoA-I; ApoB; Barthel Index

1 Introduction

Stroke is the third leading cause of all disease deaths as well as the first leading cause of severe disability in both developing and developed countries[1]. Finding out predictors for stroke outcome, and interfering in them will improve patients' recovery, and reduce the risk of life threat. Some modifiable predictors, such as blood glucose, blood pressure, and plasma lipids are being studied. So far, hyperglycemia in acute phase has been regarded as a predictor of bad prognosis of stroke[2], and very high or very low, or fluctuating blood pressure in acute phase has also been considered bringing poor outcome. However, the relationship between plasma lipids, lipoproteins and apolipoproteins (Apos) in acute phase and stroke is still not sure. Researches on the relationship of plasma lipids and prognosis of stroke are few and mainly focused on cholesterol, and results always conflict with each other. Some authors' findings suggested that higher levels of cholesterol were associated with a better outcome in the early phase after ischemic stroke[8]; more researchers induced contradictory conclusions[9–11]. In addition, these trials were all retrospective in design. Therefore, it's necessary to study other lipid sub-fractions and stroke using prospective method.

Clinical trails showed statins reduced the risk of ischemic stroke and coronary heart disease nearly to the same

*Corresponding author. Email: xuyuming@zzu.edu.cn

extend. Scandinavian Simvastatin Survival Study (4S)[3] indicated Simvastatin reduced the risk of stroke by 36%; Long-Term Intervention with Pravastatin in Ischemic Disease (LIPID) Study[4] demonstrated that Pravastatin reduced the risk of stroke by 19%, and non-hemorrhagic stroke by 23%. Weak associations between total and low density lipoprotein (LDL) cholesterol and ischemic stroke compared with coronary heart disease (CHD) are at odds with the similar effectiveness of statin drugs in preventing ischemic stroke and CHD, suggesting that other lipid sub-fractions that are affected by statins might be better predictors of ischemic stroke. Plasma ApoA-I, ApoB levels and ApoA-I/ApoB ratio are lipid sub-fractions affected by statins.

Some studies found ApoA-I/ApoB ratio was significantly associated with the occurrence of stroke. AMORIS prospective study[5] linked the ApoB/ApoA-I ratio to the risk of fatal stroke in a similar fashion as myocardial infarction and other ischemic events. Adnan I. Qureshi *et al*[6] reported the ApoA-I/ApoB ratio was inversely associated with both myocardial infarction and stroke and might be an important protective clinical marker for atherosclerosis. A prospective cohort study[7] which enrolled 261 patients with previous TIA and followed up for 10 years found that ApoB and the ApoB/ApoA-I ratio were predictive of ischemic stroke in patients with previous TIA. However, these studies are about ApoA-I, ApoB levels and ApoA-I/ApoB ratio and stroke risk, not stroke outcome. We conducted a small prospective cohort study to investigate plasma ApoA-I, ApoB levels, ApoA-I/ApoB ratio and early outcome of acute ischemic stroke (AIS), aiming at searching for a new predictor of prognosis of AIS.

2 Subjects and Methods

2.1 Subjects

2.1.1 Resources of Subjects. From Aug 24th 2005 to Apr 25th 2007, patients with AIS came to Henan Stroke Registry Centre in the First Affiliated Hospital of Zhengzhou University were voluntarily enrolled to this study.

2.1.2 Diagnostic criteria. 1) The diagnostic criteria for stroke is: Acute onset, focal neurological impairments (some with comprehensive neurological impairments), with signs and symptoms lasting more than 24 hours (or patient die within 24 hours) or rapidly vanishing symptoms with imaging of an acute clinically relevant brain lesion in patients. Exclude non-vascular causes[12]; 2) Exclude hemorrhage by the first time computerized tomography (CT)/magnetic resonance imaging (MRI).

2.1.3 Inclusion criteria. 1) In accordance with the diagnostic criteria above; 2) At any age; 3) Within 15 days since symptoms onset; 4) First stroke, or recurrent stroke with no neurological impairments before onset.

2.2.4 Exclusion criteria. 1) Patients with comorbid hematological diseases or severe renal failure or hepatic failure; 2) Dependence caused by any reason before onset; 3) Inability to give informed consent.

2.2 Methods

2.2.1 Study design. Prognostic study.

2.2.2 Sample size estimation. Empirical formula for sample size estimation of multivariate analysis: sample size = variable number × (5 – 10).

2.2.3 Cases collection. Cases collection included 4 steps: 1) When informed consent got, residents filled out standard stroke registry form for each patient. The form contained patients' age, gender, time from onset to admission, past history, alcohol consumption, smoking status, height, weight, abdomen circumference; first blood pressure on admission, blood chemistry parameters on admission including hemoglobin (HGB), platelets (PLT), hematocrit (HCT), prothrombin time (PT), activated partial thromboplastin time (APTT), fibrinogen (FIB), international normalized ratio (INR), blood urea nitrogen (BUN), creatinine, fasting serum glucose, triglyceride (TG), cholesterol (CHO), LDL, high density lipoprotein (HDL), ApoA-I, ApoB; color ultrasound of carotid artery and heart, brain CT/MRI, transcranial doppler sonography (TCD), Infarction subtype, medications given, rehabilitation care taken, complications and discharge diagnosis. All blood chemistry test were done in the hospital central chemistry lab. Infarction subtype was classified according to Oxford Community Stroke Project (OCSP) stroke classification: total anterior circulation infarction (TACI), partial anterior circulation infarction (PACI), lacunar infarction (LACI), posterior circulation infarction (POCI); 2) Patients' consciousness and neurological impairments were assessed immediately by trained residents using GCS (Glasgow Coma Scale), SSS (Scandinavian Stroke Scale) and NIHSS (National Institute of Health Stroke Scale); 3) On day30 ± 3 after onset, patients received phone calls from residents who didn' participate step 1) and step 2) work. Through telephone, residents evaluated patients' self-care ability using modified Rankin Scale (MRS) and Barthel Index (BI) and recorded the scores; 4) All information collected were saved in SPSS13.0.

2.2.4 Determination of factors probably affecting prognosis of AIS. After checking related studies, we

chose age, gender, infarction subtypes, severity of early neurological impairments (which is evaluated by NIHSS), time from onset to admission, fasting glucose on admission, total cholesterol, plasma ApoA-I, ApoB levels and ApoA-I/ApoB ratio as probable predictors for prognosis of AIS, in accordance with common agreements. These data were all recorded in stroke registry forms, and they were defined as independent variables in statistic analysis. Then, we chose patients' MRS and BI scores at 1 month follow-up as the end point, and they were defined as independent variables in statistic analysis. According to common agreements and related researches, we defined MRS < 3 or BI > 60 as patient independence, MRS ≥ 3 or BI ≤ 60 as dependence, and MRS = 5 and/or BI = 0 is for death.

2.3 Statistical analysis

Analyzing data with SPSS13.0.

3 Results

3.1 General profiles

248 AIS patients documented by CT or MRI were enrolled, and none missed the 1month follow-up. Table 1 and Table 2 demonstrate general data of the patients.

3.2 Relationship between ApoA-I, ApoB, ApoA-I/ApoB and prognosis of AIS

3.2.1 With MRS. We defined gender, age, time from symptom onset to admission, infarction subtype, NIHSS on admission, fasting blood glucose on admission, total cholesterol on admission, ApoA-I, ApoB and ApoA-I/ApoB on admission as concomitant variables, and MRS at 1 month follow up as dependent variable. Then we used multivariate logistic regression analyzing the data. Results showed that ApoA-I/ApoB was significantly associated with MRS (P = 0.042, OR = 0.42, 95%CI (0.182, 0.969)). Every 1 unit increase in ApoA-I/ApoB was associated with 0.42 times reduction in risk of patient dependence at one month (MRS ≥ 3). Other variables associated with one month MRS were age, infarction subtype, NIHSS on admission. However, sex, time from symptom onset to therapy, ApoA-I, ApoB, fasting blood glucose, total cholesterol on admission were not associated with one month MRS (Table 3).

3.2.2 With BI. In this part, BI was defined as dependent variable. Then we used multivariate logisticl regression analyzing the data. Results showed that the ApoA-I/ApoB was significantly associated with BI (P = 0.046, OR = 0.425, 95%CI (0.184, 0.983)). Every 1 unit in crease in ApoA-I/ApoB was associated with 0.425 times reduction in risk of poor outcome after one month (MRS ≥ 3). Other variables associated with BI were age, infarction subtype, NIHSS on admission. However, sex, time from symptom onset to therapy, ApoA-I, ApoB, fasting blood glucose, total cholesterol on admission were not associated with BI (Table 4).

Table 1. Categorical variables

	n	%
Male	146	58.9
Female	102	41.1
Urban	160	64.5
Rural	88	35.5
Hypertension	146	58.9
Diabetes	53	21.4
Hyperlipoidimia	46	18.5
TIA	30	12.1
Migraine	11	4.4
Smoke	87	35.1
Alcohol	63	25.4
Previous stroke	60	24.2
TACI	8	3.2
PACI	72	29.0
LACI	121	48.8
POCI	47	19.0
MRS < 3	171	69.0
3 ≤ MRS < 5	77	31.0
BI > 60	79	69.3
0 < BI ≤ 60	77	30.7
MRS = 5 and BI = 0	7	2.8

Table 2. Ccontinuous variables

variable	Sum total	Minimal value	Maximal value	Mean ± SD
Age	248	23	93	62.46 ± 12.71
Time form symptom onset to admission	248	0.1	360.0	7.5
NIHSS on admission	248	1	56	4
FBG on admission	248	3.26	17.58	5.39
TC on admission	248	2.38	11.95	5.09 ± 1.26
ApoA-I on admission	248	0.20	.30	1.04 ± 0.29
ApoB on admission	248	0.40	2.40	0.91 ± 0.32
ApoA-I/ApoB	248	0.21	5.50	1.17

4 Discussion

Table 3. Results of Logistic regression analysis 1

	B	SE	Wald	Sig	Exp (B)	95%CI for EXP(B)	
						Lower	Upper
Age	0.050	0.016	9.347	0.002*	1.051	1.018	1.086
Infarction subtypes			12.888	0.005*			
NIHSS on admission	0.234	0.044	27.747	0.000*	1.263	1.158	1.378
ApoA-I/ApoB	– 0.867	0.426	4.137	0.042*	0.420	0.182	0.969
Sex				0.387			
Time from symptom onset to treatment				0.421			
FBG on admission				0.099			
TC on admission				0.395			
ApoA-I on admission				0.318			
ApoA-I on admission				0.980			

B = LnOR, Wald = Walds test value, OR = odds ratio, 95%CI Lower = 95% lower limit of confidence interval, Upper = 95% upper limit of confidence interval. $P < 0.05$ and 95%CI ≠ 1 had statistical significance, Sig = *P* value.

Table 4. Results of Logistic regression analysis 2

	B	SE	Wald	Sig	Exp (B)	95%CI for EXP(B)	
						Lower	Upper
Age	0.059	0.017	12.146	0.000*	1.060	1.026	1.096
Infarction subtypes			12.443	0.006*			
NIHSS on admission	0.226	0.044	26.843	0.000*	1.254	1.151	1.366
ApoA-I/ApoB	– 0.855	0.428	3.996	0.046*	0.425	0.184	0.983
Gender				0.352			
Time from symptom onset to treatment				0.312			
FBG on admission				0.080			
TC on admission				0.318			
ApoA-I on admission				0.493			
ApoA-I on admission				0.519			

B = LnOR, Wald = Walds test value, OR = odds ratio, 95%CI Lower = 95% lower limit of confidence interval, Upper = 95% upper limit of confidence interval. $P < 0.05$ and 95%CI ≠ 1 had statistical significance, Sig = *P* value.

4.1 The function of Apos in lipids metabolism

Basic researches reveal that Apos plays important roles in lipids metabolism. ApoA-I is the major Apo in HDL, and it is probably important in protecting against premature atherosclerosis. Genetic defects that cause the inability to synthesize ApoA-I cause very low plasma concentrations of HDL cholesterol and premature coronary artery disease in the fourth and fifth decades[13–16]. Conversely, an increased rate of ApoA-I production causes high plasma levels of HDL cholesterol and may be associated with protection from premature coronary artery disease based on familial longevity[17]. Furthermore, overexpression of human ApoA-I in transgenic mice inhibits the development of atherosclerosis[18]. ApoB is the major Apo in chylomicrons, VLDL, intermediate-density lipoprotein, and LDL. It is an essential structural part in these lipoprotein particles. For example, the genetic inability to secrete ApoB causes the absence of these lipoproteins in plasma[19]. Furthermore, mutations in the ApoB gene can cause low levels of ApoB and LDL cholesterol and may be associated with protection from premature coronary artery disease[20]. In addition, ApoB acts as a ligand for the LDL receptor, mediating the cellular uptake and degradation of LDL[21]. Only one molecule of ApoB exists per lipoprotein particle, and thus the quantity of ApoB in fasting plasma is a measure

of the number of LDL and VLDL particles. In fact, the plasma levels of "non-HDL cholesterol", which includes both LDL and VLDL, are correlated with plasma ApoB levels[22,23]. However, in contrast to the constant 1 : 1 molar ratio of ApoB per LDL and VLDL particle, the amount of cholesterol in these lipoproteins varies widely. Therefore, plasma ApoB levels may be a better assay of the concentration of atherogenic lipoprotein particles than are LDL cholesterol or non-HDL cholesterol levels[24,25].

4.2 The association between ApoA-I/ApoB and outcome of AIS

Avogaro *et al*[26] considered Apos better discriminators than lipids for atherosclerosis. AMORIS[5] study found no significant relevance between ApoA-I, ApoB and risk of stroke. A community-based cohort study in Taiwan-Chin-Shan Community Cardiovascular Study[27], as one of the few studies on plasma ApoA-I, ApoB and stroke in Chinese people, reported ApoA-I but not ApoB levels might serve as an effect modifier of hypertension for the risk of stroke events. However, these studies were all about stroke risk, and no article on plasma levels of ApoA-I, ApoB, ApoA-I/ApoB and prognosis of AIS has been published yet. This study found no significant relevance between plasma ApoA-I, ApoB levels and short-time outcome of AIS, with no contradiction with previous researches on plasma ApoA-I, ApoB levels and risk of AIS.

More and more concerns has been attracted by ApoA-I/ApoB ratio, a novel predictor for high risk of atherosclerosis. A study[28] showed high ApoB and a high ApoB/ApoA-I ratio were strongly related to increased coronary risk, while high ApoA-I was inversely related to risk. Walldius and Jungner[29] reviewed articles recently published on ApoB/ApoA-I ratio and risk of atherosclerosis and concluded that the cholesterol balance determined as the ApoB/ApoA-I ratio has repeatedly been shown to be a better marker than lipids, lipoproteins and lipid ratios. In all, results indicated that the ApoB/ApoA-I ratio was a simple, accurate and new risk factor for CV disease – the lower the ApoB/ApoA-I ratio, the lower the risk. As a prognostic study, this research showed higher ApoA-I/ApoB ratio was associated with better outcome at 1 month follow-up, suggesting a potential protective role higher ApoA-I/ApoB played in the neurofunction recovery post stroke.

Mechanism of neuroprotective function of higher ApoA-I/ApoB ratio probably lies in the fact that ApoB/ApoA-I ratio is a better marker than lipids, lipoproteins and lipid ratios to evaluate the balance of atherogenic and antiatherogenic lipoproteins. Antiatherogenic lipoprotein HDL activities include endothelium protection, anti-inflammation, anticoagulation, antioxidation, as well as diminishing brain injury by inhibiting inflammation, oxidative stress post-stroke[30–33]. In addition, HDL, mainly ApoA-I, increases the resistance of endothelial cells against oxidized LDL and prevents its toxic (apoptotic) effect by blocking the pathogenic intracellular signaling (culminating in sustained Ca^{2+} rise) involved in cell death[34].

4.3 Other factors and outcome of AIS

The relationship between lipids and stroke is not clear yet. Some large sample prospective study found the elevation of plasma lipids, including TG, CHO, and LDL were not able to predict the occurrence of stroke[35–38]. Some authors' findings suggested that higher levels of cholesterol were associated with a better outcome in the early phase after ischemic stroke8; more researchers induced contradictory conclusions[9–11]. This study showed no significant association between CHO and short-time outcome of AIS, in accordance with most similar researches.

Unlike previous studies, this study didn't conclude that fasting glucose on admission was relevant to outcome of AIS. The possible reason is that glucose fluctuates frequently in the superacute phase of AIS. Previous researches on glucose and stroke enrolled patients who admitted to hospital mainly within 3 days since onset; this study enrolled patients admitted to hospital within 15 days, whose glucose levels couldn't represent the level in the superacute phase.

5 Conclusions

ApoA-I/ApoB ratio is significantly associated with short-time prognosis of AIS. Higher ApoA-I/ApoB ratio might be a predictor of good outcome of AIS. As this is a small-sample pilot study, further large sample researches are needed.

References

1. Yusuf S, Reddy S, Ounpuu S, *et al*. Global burden of cardiovascular diseases. Part I. General considerations, the epidemiologic transition, risk factors and impact of urbanisation. Circulation 2001; 104: 2746 – 53.
2. Stollberger C, Exner I, Finsterer J, *et al*. Stroke in diabetic and non-diabetic patients: course and prognostic value of admission serum glucose. Ann Med 2005; 37(5): 357 – 64.
3. Vauthey C, de Freitas GR, van Melle G, *et al*. Better outcome after stroke with higher serum cholesterol levels[J]. Neurology 2000;

54(5): 1944 – 8.
4. Weir CJ, Sattar N, Waiters MR, *et al*. Low triglyceride, not low cholesterol concentration, independently predicts poor outcome following acute stroke[J]. Cerebrovasc Dis 2003; 16(1): 76 – 82.
5. Dziedzic T, Slowik A, Gryz EA, *et al*. Lower serum triglyceride level is associated with increased stroke severity[J]. Stroke 2004; 35(6): 151 – 2.
6. Bhatia RS, Garg RK, Gaur SPS, *et al*. Predictive value of routine hematological and biochemical parameters on 30-day fatality in acute stroke[J]. Neurology India 2004; 52(2): 220 – 3.
7. Scandinavian Simvastafin Surviv8l Study Group. Randomised trial of cholesterol lowering in 4 44 patients with coronary heart disease: the Scandinavian Simvastatin Survival Study (4S) J J Lancet 1994; 344: 1383 – 9.
8. White HI, Simes RJ, Anderson NE, *et al*. Pm astatin therapy and the risk of strokel. J N Engl J Med 2000; 343: 317 – 26.
9. Walldius G, Aastveit AH, Jungner I. Stroke mortality and the apoB/apoA-I ratio: results of the AMORIS prospective study. J Intern Med. 2006; 259(3): 259 – 66.
10. Qureshi AI, Giles WH, Croft JB, *et al*. Apolipoproteins A-1 and B and the likelihood of non-fatal stroke and myocardial infarction -- data from The Third National Health and Nutrition Examination Survey. Med Sci Monit 2002; 8(5): CR311 – 6.
11. Bhatia M, Howard SC, Clark TG, *et al*. Apolipoproteins as predictors of ischemic stroke in patients with a previous transient ischemic attack. Cerebrovasc Dis 2006; 21(5 – 6): 323 – 8.
12. Guidelines for Prevention of Stroke in Patients With Ischemic Stroke or Transient Ischemic Attack. A Statement for Healthcare Professionals From the American Heart Association/American Stroke Association Council on Stroke: Co-Sponsored by the Council on Cardiovascular Radiology and Intervention: The American Academy of Neurology affirms the value of this guideline. Stroke 2006; 37: 577 – 617.
13. Norum RA, Lakier JB, Goldstein S, *et al*. Familial deficiency of apolipoproteins A-I and C-III and precocious coronary-artery disease. N Engl J Med 1982; 306: 1513 – 9.
14. Schaefer EJ, Heaton WH, Wetzel MG, *et al*. Plasma apolipoprotein A-1 absence associated with a marked reduction of high density lipoproteins and premature coronary artery disease. Arteriosclerosis 1982; 2: 16 – 26.
15. Matsunaga T, Hiasa Y, Yanagi H, *et al*. Apolipoprotein A-I deficiency due to a codon 84 nonsense mutation of the apolipoprotein A-I gene. Proc Natl Acad Sci USA 1991; 88: 2793 – 7.
16. Ng D, Leiter L, Vezina C, *et al*. Apolipoprotein A-I Q(–2)Xcausing isolated apolipoprotein A-I deficiency in a family with analphalipoproteinemia. J Clin Invest 1994; 93: 223 – 9.
17. Rader DJ, Schaefer JR, Lohse P, *et al*. Increased production of apolipoprotein A-I associated with elevated plasma levels of high-density lipoproteins, apolipoprotein A-I, and lipoprotein A-I in a patient with familial hyperalphalipoproteinemia. Metabolism 1993; 42: 1429 – 34.
18. Rubin EM, Krauss RM, Spangler EA, *et al*. Inhibition of early atherogenesis in transgenic mice by human apolipoprotein A-I. Nature 1991; 353: 265 – 7.
19. Rader DJ, Brewer HB Jr. Abetalipoproteinemia. New insights into lipoprotein assembly and vitamin E metabolism from a rare genetic disease. JAMA 1993; 270: 865 – 9.
20. Linton MF, Farese RV Jr, Young SG. Familial hypobetalipoproteinemia. J Lipid Res 1993; 34: 521 – 41.
21. Brown MS, Goldstein JL. A receptor-mediated pathway for cholesterol homeostasis. Science 1986; 232: 34 – 47.
22. Vega GL, Grundy SM. Does measurement of apolipoprotein B have a place in cholesterol management? Arteriosclerosis 1990; 10: 668 – 71.
23. Levinson SS, Wagner SG. Measurement of apolipoprotein B-containing lipoproteins for routine clinical laboratory use in cardiovascular disease. Arch Pathol Lab Med 1992; 116: 1350 – 4.
24. Brunzell JD, Sniderman AD, Albers JJ, *et al*. Apoproteins B and A-I and coronary artery disease in humans. Arteriosclerosis 1984; 4: 79 – 83.
25. Sniderman AD, Silberberg J. Is it time to measure apolipoprotein B? Arteriosclerosis 1990; 10: 665 – 7.
26. Avogaro P, Bon GB, Cazzolato G, *et al*. Are apolipoproteins better discriminators than lipids for atherosclerosis? Lancet 1979; 1: 901 – 3.
27. Kuo-Liong Chien, Fung-Chang Sung, Hsiu-Ching Hsu, *et al*. Apolipoprotein A-I and B and Stroke Events in a Community-Based Cohort in Taiwan: Report of the Chin-Shan Community Cardiovascular Study. Stroke 2002; 33: 39 – 44.
28. The apoB/apoA-I ratio is better than the cholesterol ratios to estimate the balance between plasma proatherogenic and antiatherogenic lipoproteins and to predict coronary risk. Clin Chem Lab Med 2004.
29. Walldius G, Jungner I. The apoB/apoA-I ratio: a strong, new risk factor for cardiovascular disease and a target for lipid-lowering therapy--a review of the evidence. J Intern Med 2006; 259(5): 493 – 519.
30. Navab M, Berliner JA, Subbanagounder G, *et al*. HDL and the inflammatory response induced by LDL-derived oxidized phospholipids. Arterioscler Thromb Vasc Biol 2001; 21(5): 481 – 8.
31. Gordon T, Castelli WP, Hjortland MC, *et al*. High density lipoprotein as a protective factor against coronary heart disease. A m J Med 1997; 62(5): 707 – 14.
32. Viswambharan H, Ming XF, Zhu S, *et al*. Reconstituted high-density lipoprotein inhibits thrombin-induced endothelial tissue factor expression through inhibition of RhoA and stimulation of phosphatidylinositol 3-kinase but not Akt/endothelial nitric cxide synthase. Circ Res 2004; 95(7): 918 – 25.
33. O'Connell BJ, Genest J Jr. High-density lipoproteins and endothelial function. Circulation 2001;104(16): 1978 – 83.
34. Isabelle Suc; Isabelle Escargueil-Blanc; Muriel Troly; *et al*. HDL and ApoA Prevent Cell Death of Endothelial Cells Induced by Oxidized LDL. Arteriosclerosis, Thrombosis, and Vascular Biology 1997; 17: 2158 – 66.
35. Harmsen P, Rosengren A, Tsipogianni A, *et al*. Risk factors for stroke in middle-aged men in Goteborg, Sweden. Stroke 1990; 21: 223 – 9.
36. Kannel WB, Dawber TR, Sorlie P, *et al*. Components of blood pressure and risk of atherothrombotic brain infarction: the Framingham Study. Stroke 1976; 7: 327 – 31.
37. Kagan A, Popper JS, Rhoads GG, *et al*. Dietary and other risk factors for stroke in Hawaiian Japanese men. Stroke 1985; 16: 390 – 6.
38. Kannel WB, Gordon T, Dawber TR. Role of lipids in the development of brain infarction: the Framingham Study. Stroke 1974; 5: 679 – 85.

Somatic embryogenesis and *in vitro* regeneration of an endangered medicinal plant sarpgandha (*Rauvolfia serpentina* L.)

Prabhat Singh, Anand Singh, Arvind K. Shukla, Lalit Singh, Veena Pande, Tapan K. Nailwal*

Department of Biotechnology, *Kumaun University*, *Nainital*, *Uttarakhand*-263001, *India*

Received March 7, 2009

Abstract

Objective. An efficient protocol for *in vitro* regeneration of endangered medicinal plant *Rauvolfia serpentina* has been developed. *Methods and Results*. The juvenile leaf explants were transferred to MS medium containing different combinations of PGRs. Among the various combinations of BAP (1.0 – 3.0 mg/L) and IAA (0.1 – 0.5 mg/L) the intensity of callus induction was highest in 2.5 mg/L BAP + 2.0 mg/L IAA and 1.0 mg/L BAP + 0.5 mg/L IAA. The frequency of callus induction was highest 77.77% in 1.0 mg/L BAP + 0.5 mg/L IAA. During organogenic callus formation, different types of calli with variation in colour and texture were noticed and among them, the light green, fragile calli responded well for the induction of shoots. Among the various combinations of BAP and IAA used the frequency of shoot regeneration was highest 75% in 2.5 mg/L BAP + 0.4 mg/L IAA. For elongation of shoot 1 ppm GA-3 was also used, this provides a better result. The shoot was transferred to MS medium for root regeneration containing PGRs: BAP (2.5 mg/L) + IAA (0.3 – 0.5 mg/L) + NAA (0.3 – 0.5 mg/L). The frequency of root regeneration was 100% in MS medium containing BAP (2.5 mg/L) + IAA (0.5 mg/L) + NAA (0.5 mg/L). After rooting on shoots the plantlets were shifted to sterile soil field pots for acclimatization. The survival percentage of plants after hardening was 67%. *Conclusion*. The protocol was optimized by manipulations of different PGRs for enhanced multiplication. Protocol explained in this research paper provides a rapid plant regeneration system which could be used for the somaclonal variation; shoot induction and producing transgenic plants in *Rauvolfia* through *Agrobacterium* and biolistic methods. [Life Science Journal. 2009; 6(2): 57 – 62] (ISSN: 1097 – 8135).

Keywords: *Rauvolfia serpentina*; regeneration; *in vitro*; induction

1 Introduction

Medicinal plants have been the subjects of man's curiosity since time immemorial (Constable, 1990). Almost every civilization has a history of medicinal plant use (Ensminger *et al*, 1983). Approximately 80% of the people in the world's developing countries rely on traditional medicine for their primary health care needs, and about 85% of traditional medicine involves the use of plant extracts (Vieira and Skorupa, 1993). *In vitro* cell and tissue culture methodology is envisaged as a mean for germplasm conservation to ensure the survival of endangered plant species, rapid mass propagation for large-scale revegetation, and for genetic manipulation studies. Combinations of *in vitro* propagation techniques (Fay, 1992) and cryopreservation may help in conservation of biodiversity of locally used medicinal plants.

Rauvolfia serpentina L. commonly known as sarphgandha is an important medicinal shrub of family Apocynaceae (Nathan Kline, 1954). The snake-weed genus includes about 50 species, this has fairly wide area of distribution, including the tropical part of the Himalayas, the Indian peninsula, Sri Lanka, Burma, and Indonesia. The plant is indigenous to India, Bangladesh and other regions of Asia and found to grow in the wild in many places around the country (Ghani, 1998). Its roots contain 0.15% resperine-rescinnamine group of alkaloids (Anonymous, 1969). It also contains a number of bioactive chemicals, including ajmaline, deserpidine, rescinnamine and yohimbine (Lewis WH, 2003). This herbal plant is used as medicine for high blood pressure, insom-

*Corresponding author. Email: tapannailwal@gmail.com

nia, anxiety and other disorders of the central epilepsy (Ghani, 1998).

Rauvolfia is threatened in India due to indiscriminate collection and over exploitation of natural resources for commercial purposes to meet the requirements of pharmaceutical industry, coupled with limited cultivation (Nayar and Sastry, 1987; Gupta, 1989). IUCN has kept this plant under endangered status. The chemical resperine is an alkaloid first isolated from roots of *Rauvolfia serpentina* and is used to treat hypertension (Ford RV *et al*, 1953; Vida F, 1953). Although, for centuries they have been used empirically in India for a variety of conditions that they were effective in relief of hypertension was first commented on by Bhatia in 1942. Subsequently, other clinical investigators working in India confirmed the effectiveness of *Rauvolfia serpentina* for that purposes (Chakraverti NK *et al*, 1951; Gupta JC, 1942). In a short term study, a significant decrease in systolic as wall as diastolic blood pressure of patients to whom the drug was given was observed (Vakil, 1949). Insanity, Snakebite and Cholera can also be treated by use of this alkaloid (Wild R, 1994). The pectic polysaccharide named rauvolfian RS was obtained from the dried callus of *Rauvolfia serpentina* L. by extraction with 0.7% aqueous ammonium oxalate and it was found to posses some anti-inflammatory effect (Popov SV *et al*, 2007).

In approximately 60% of medicinal plants used in traditional medicines, roots are the principal source of drug preparation (Kamboj, 1988). The development of fast growing culture system can offer an opportunity for producing drugs from the roots in the laboratory with out having to depend solely on field cultivation (Sudha and Seeni, 2003).

In vitro regeneration of sarphgandha has been done from several genotypes. Micropropagation has been achieved from explant of *Rauvolfia micrantha* Hook F cultures (Sudha and Seeni, 1996). Micropropagation can be considered as an important tool for the production of higher quality plant based medicines (Debnath M, 2006). In view of this, there is an urgent need to apply *in vitro* culture methods for the micropropagation and conservation of this valuable endangered plant. Here efforts have been made to define efficient protocol for the recovery of plants through organogenesis of Rauvolfia serpentina. *In vitro* regeneration of *Rauvolfia* has been reported by many authors (Butenka, 1964; Mitra and Kaul, 1964; Vollosovich and Butenka, 1970; Kukreja *et al*, 1989; Roy *et al*, 1994). The present study was undertaken to develop a more efficient protocol for rapid in vitro multiplication of *Rauvolfia serpentina* using leaf explant as an initial plant material.

2 Materials and Methods

2.1 Plant material

Plantlets of *Rauvolfia serpentina* were obtained from Corbett Jadibuti Udhyan Kaladhungi, Nainital, Uttarakhand and grown in sterile vermiculite at 25 ºC – 30 ºC in light. All the explants were taken from these donor plants for present investigation. Leaf explants from 2 months old donor plant was kept for 2 hours in systemic fungicide Bavistin (VIMCO pesticides, Gujarat) and Tween-80, an antimicrobial agent, prior to surface sterilization. For surface sterilization, chemicals such as $HgCl_2$ (0.1%), NaOCl (1%), H_2O_2 (1%) and ethanol (70%) was used. Juvenile leaves were washed thoroughly in running tap water for 30 minutes and then with distilled water three times. Leaves were treated with bavistin solution for 4 – 5 minutes, and then rinsed thoroughly with sterile distilled water. The leaves were subjected to 0.1% $HgCl_2$ for 30 seconds, washed with distilled water and then placed in 70% ethanol for 1 minute and again washed with distilled water, followed by addition of three drops of antibiotic solution (cefotaxime) in laminar airflow cabinet. In the antibiotic solution, all leaves were dissected into small pieces and treamed so that maximum part can be exposed to media. All the chemicals used were purchased from Hi-media unless stated otherwise.

2.2 Culture media and growth condition

The medium comprised of macro and micro elements according to Murashige and Skoog (1962) with mesoinosotol (100 mg/L), thiamine-HCl (0.5 mg/L), pyridoxine-HCl (1 mg/L), nicotinic acid (0.5 mg/L) and sucrose (30 g/L), solidified with 0.6% agar. The plant growth regulators used were 6-benzyl-aminopurine (BAP), α-naphthalene acetic acid (NAA) and indole acetic acid (IAA). All experiments were carried out in culture tubes (150 × 25 mm) containing 30 ml of culture medium. The pH of media were adjusted to 5.8 prior to autoclaving at 121 ºC at 15 lbs pressure for 20 minutes. Cultures were incubated under 16 hours/8 hours light/dark cycles (artificial light, 80 μM per m^2/s).

2.3 Callus induction and shoot regeneration

For callus induction juvenile leaf section (3 – 5 mm in length) with cut end surface in contact with culture medium were placed on MS medium supplemented with various concentrations of PGRs BAP and IAA. After 20 days of culture, the leaves cultured on MS basal medium supplemented with 3% (w/v) sucrose, BAP (1.0 ppm) and IAA (0.5 ppm) were found to give profuse callusing and when callusing was observed in entire explant, the

callus was cut into small pieces transferred to MS media having BAP and IAA in same concentration as for callus induction. Subculturing was done after every 1 – 2 weeks. After 3 – 4 weeks of subculturing first shooting is observed in callus.

2.4 Regeneration of roots and development of complete plantlets

For initiation of roots the 6 – 8 weeks old shoots (2.5 – 4.0 cm in length) were cultured on half strength MS basal medium supplemented with 2% (w/v) sucrose and different concentration of PGR were tested BAP (2.5 ppm) : IAA (0.3 ppm) : NAA (0.3 ppm), BAP (2.5 ppm) : IAA (0.4 ppm) : NAA (0.4 ppm), and BAP (2.5 ppm) : IAA (0.5 ppm) : NAA (0.5 ppm), for 2 – 3 weeks. The shoots were also tested on hormone free full and half strength MS basal medium with 3% sucrose (w/v) for root initiation.

The complete rooted plantlets (6 – 10 weeks old) were washed free of agar and dipped in 0.2% bavistin fungicide for 5 – 10 minutes, and potted in small plastic pots containing sterilized soilrite. The plantlets were covered with polythene bags to maintain high humidity. These were acclimatized at 25 ± 3 ºC less than 16 hours photoperiod and watered regularly. After 3 – 4 weeks, the polythene bags were removed and established plantlets were transplanted to earthen pots in a greenhouse.

3 Results and Discussion

The smaller size of explants were chosen due to fact that smaller size of explants provide less chance of contamination, as well as longer leaves showed total loss of morphogenic potential (Mujib A, 2003). Initiation of calluses from leaf explants did not pose a major problem. During initiation the explants did not show any leaching or browning of tissues. MS basal medium was the most effective for callusing of leaf explants. The explants cultured on MS basal medium supplemented with different combinations of BAP and IAA showed varied response for callusing (Table 1). Leaf explants culture on MS basal medium without any PGR supplementation showed only swelling of explants that were not significant for callusing. This was possibly due to significant role of PGR over callusing. In the media supplemented with BAP and IAA, the leaf segments remain green for long period with very slow process of callus induction (Figure 1). Further transfer into media containing BAP and IAA rapidly showed callus induction because the excretion of phenolic compounds from explants to the medium was strictly avoided by regular sub-culturing of callus (Figure 2).

Callus is an unorganized mass of plant cells and its formation is controlled by growth regulating substances present in the medium (auxins and cytokinins) (Shah *et*

Table 1. Effect of different concentrations of PGR added to MS medium on induction of callus from leaf in *R. serpentina* (Observation after 27 days)

PGR (mg/L)		Intensity of callus induction	Nature of callus
IAA	BAP		
0.1	–	–	No callus formation
0.1	1.0	++	White coloured, fragile
0.1	1.5	+	Green coloured, fragile
0.2	0.0		No callus formation
0.2	1.0	++	Light green coloured, fragile
0.2	1.5	+	Light green coloured, fragile
–	2.0	–	No callus formation
–	2.5	–	No callus formation
–	3.0	–	No callus formation
0.1	2.0	+	White coloured, fragile
0.1	2.5	–	No callus formation
0.1	3.0	–	No callus formation
0.2	2.0	–	No callus formation
0.2	2.5	+++	White coloured, fragile
0.2	3.0	–	No callus formation
0.3	–	–	No callus formation
0.3	1.0	++	Green coloured, fragile
0.3	1.5	+	Light green coloured, fragile
0.3	2.0	–	No callus formation
0.3	2.5	++	Light green coloured, fragile
0.3	3.0	–	No callus formation
0.4	–	–	No callus formation
0.4	1.0	+	Light green coloured, fragile
0.4	1.5	+	Light green coloured, fragile
0.4	2.0	–	No callus formation
0.4	2.5	++	Light green coloured, fragile
0.4	3.0	–	No callus formation
0.5	–	–	No callus formation
0.5	1.0	+++	Light green coloured, fragile
0.5	1.5	+	Green coloured, fragile
0.5	2.0	++	Light green coloured, fragile
0.5	2.5	–	No callus formation
0.5	3.0	–	No callus formation
–	–	–	Swelling of the explant observed

al, 2003). The specific concentration of plant regulators needed to induce callus, varies from species to species and even depends on the source of explant (Charriere *et al*, 1999). It has been demonstrated in many cases that 2,4-D is usually the choice of auxin for callus induction and subculture of grasses (Bhaskaran and Smith, 1990; Chaudhury and Qu, 2000). Lately more and more experimental results indicate that the addition of a low concentration of cytokinin in callus culture medium often enhances callus regeneration (Alpeter and Posselty, 2000; Chaudhury and Qu, 2000; Cho *et al*, 2000; Bai and Qu, 2001; Bradely *et al*, 2001). Minimal cytokinins and auxins in culture media would avoid somaclonal variation and efficiently produce true to type plantlets (Edson *et al*, 1996).

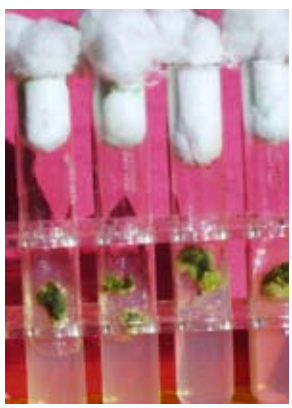

Figure 1. Callus induction in *R. sepentina* from leaf explants in MS media containing 1.0 mg/L BAP and 0.5 mg/L IAA.

Figure 2. Shoot regeneration from callus on 2.5 mg/L BAP + 0.4 mg/L IAA MS media.

The success of micropropagation largely relies on the selection of suitable plant part, which is to be used as the starting material for the experiment. In the present experiment leaf explants was best fit for purposes. The best callusing was observed in media having BAP : IAA in concentration ratio of (1.0 : 0.5 ppm). In the media supplemented with only BAP and IAA the callus induction was very significant (Figure 2). This remains in accordance with previous reported work of (Mathur *et al*, 1987). Different types of calli with variation in colour and texture were noticed (Table 1) and among them, the light green, fragile calli responded well for the induction of shoots.

This study further demonstrates that shoot regeneration from callus was very earlier in media supplemented with BAP and IAA in concentration ratio of (2.5 : 0.4 ppm), in comparison to 2.5 : 0.3, 1.0 : 0.5 or 2.0 : 0.5 (Table 2 and Figure 3). Thus, the PGR concentrations have significant impact on shoot regeneration. This is basically due to endogenous level of growth regulators. For elongation of shoot 1ppm GA-3 was also used, this provides a better result (Figure 4).

Table 2. Effect of different concentration of PGRs added to MS medium on induction of callus and regeneration of shoots from leaf of *R. serpentina*

PGR (mg/L)		Days for callus formation (day)	Days of shoot regeneration after callusing (day)	Frequency of callusing (%)	Frequency of shoot regeneration (%)
BAP	IAA				
2.5	0.4	24	18	72.00	75
2.5	0.3	24	36	40.00	45.03
1.0	0.5	24	37	77.77	52
2.0	0.5	24	38	70.00	39.45

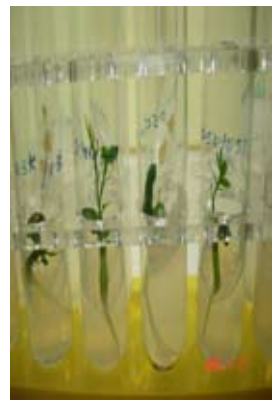

Figure 3. Rooting regeneration on 2.5 mg/L BAP + 0.5 mg/L IAA + 0.5 mg/L NAA MS media.

No root could be induced in either basal medium of full or half strength MS media. However, when 2.5 – 4.0 cm elongated shoots were placed on half strength MS

basal medium supplemented with BAP, IAA and NAA in concentration ratio of (2.5 : 0.5 : 0.5 ppm) roots were induced in nearly 100% of shoots within 2 weeks (Figure 5). Other concentration BAP, IAA and NAA (2.5 : 0.4 : 0.4 and 2.5 : 0.3 : 0.3) induce rooting in slightly lower percentage (Table 3). Basal media supplemented with NAA was found to be better for root regeneration this was in accordance with previous reported work of Kumar *et al* (1993).

Figure 4. *In vitro* regeneration of complete plantlets of *R. serpentina* from leaf explant.

Figure 5. Hardening of plantlet to mixture of sterile soil, sand and vermicompost.

Taking care of root regeneration data it can be concluded that the standard protocol developed for regeneration of *Rauvolfia* was nearly 100% efficient but in accordance with hardening data (Table 4) there is a need for further standardization and work to increase the efficiency, during hardening so that this medicinally important plant could be propagate at larger scale and its medicinal importance properties could be utilized for well being of human population. This further become important due to advancement in commercialization of plant tissue cultured plantlets by commercial sectors have led to continued exponential growth within the industry in terms of numbers of new units as well as numbers of plants produced by the units (Govil S and Gupta SC, 1997). The development of a reliable *in vitro* protocol are of great importance for producing plant material and for conservation of rare plant species, and offset the pressure on the natural populations as well as plant medicinal purposes.

Table 3. Effect of different concentration of PGR added to MS medium for root regeneration from shooted callus of *R. serpentina*

PGR (mg/L)			Days of rooting (day)	Frequency of rooting (%)
BAP	IAA	NAA		
2.5	0.3	0.3	12	85
2.5	0.4	0.4	15	96
2.5	0.5	0.5	10	100

Table 4. Estimated survival of plants after hardening

Number of pots containing plants	Number of plants survived	Percentage of survival (%)
5	3	60
3	2	67
4	2	50

4 Conclusion

The present study describes a well documented and reliable protocol of *R. serpentina* from leaf explants with much higher rate of multiplication. This protocol can be used as a basic tool for commercial cultivation of sarphgandha plant.

References

1. Anonymous. In: The Wealth of India. Raw Materials. Vol. III, Publication and Information Directorate, CSIR, New Delhi, India. 1969.
2. Alpeter F, Posselt UK. Improved regeneration from cell suspensions of commercial cultivars, breeding and in bred lines of perennial ryegrass (*Lolium perenne* L.). J Plant Physiol 2000; 156: 790 – 6.
3. Bai Y, Qu R. Factors influencing tissue culture responces of mature seeds and immature embryos in turf-type tall fescue (*Festuca arundinacea* schreb.). Plant Breeding 2001; 120: 239 – 42.
4. Bhaskaran S, Smith RH. Regeneration in cereal tissue culture: a review. Crop Sci 1990; 30: 1328 – 36.
5. Bhatia BB. On the use of *Rauvolfia serpentina* in high blood pressure. J Ind Med Assn 1942; 11: 262.

6. Butenka RG. Isolated tissue culture and physiology of plant morphogenesis. Nauka, Moscow. 1964.
7. Bradley DE, Bruneau AH, Qu R. Effect of cultivar, explant treatment and medium supplements on callus induction and plantlet regeneration in perennial ryegrass. Int Turfgrass Soc Res J 2001; 9: 152 – 6.
8. Chakraverti NK, Rai Chudjuri MN, Chaudjuri RN. *Rauvolfia serpentina* in essential hypertension. Ind Med Gazette 1951; 86: 348.
9. Chaudhury A, Qu R. Somatic embryogenesis and plant regeneration of truf-type bermudagrass: effect of 6-benzaldehyde in callus induction medium. Plant cell tiss Org Cult 2000; 60: 113 – 20.
10. Charriere F, Sotta B, Miginiac E, Hahne G. Induction of adventitious shoots or somatic embryos on invitro culture. Plant Physiol Biochem 1999; 37(10): 752 – 7.
11. Constable F. Medicinal plant biotechnology. Planta Med 1990; 56: 421 – 5.
12. Edson JL, Leege-Brusven AD, Everett RL, Wenny DL. Minimizing growth regulators in shoot culture of an endangered plant, *Hackelia ventusa* (Boraginaceae). *In Vitro* Cell Dev Biol Plant 1996; 32: 267 – 71
13. Ensminger AH, Ensminger ME, Konlande JE, Robson JRK. Food & Nutrition Encyclopedia. Pegus Press, Clovis, California, U.S.A. 1983; 2: 1427 – 41.
14. Fay MF. Conservation of rare and endangered plants using *in vitro* methods. *In Vitro* Cell Dev Biol Plant 1992; 28: 1 – 4.
15. Ford RV, Moyer JH. Extract of *Rauvolfia serpentina* in hypertension. Genl Practice 1953; 8: 51.
16. Ghani A. Medicinal plants of Bangladesh. Chemical constituents and uses. Asiatic Society of Bangladesh, Ed. 2nd 1998; 36.
17. Govil S, Gupta SC. Commercialization of plant tissue culture in India. Plant Cell, Tissue and Organ Culture 1997; 51: 65 – 73.
18. Gupta JC. Alkaloids of *Rauvolfia serpentina*. Rep Adv School Bd, Ind Res Fund Assn 1942; 70.
19. Gupta R. Indian J Plant Genet Resources 1989; 1: 98 – 102.
20. Kukreja AK, Mathur AK, Ahuja PS, Thakur RS. Tissue Culture and Biotechnology of Medicinal and Aromatic Plants. ICSIR, Lucknow, India. 1989.
21. Kumar KP, Soniya EV, Lawrence B, Nair GM. Micropropagation of *Clitoria terntea* L. (Paplionaceae) through callus regeneration and shoot tip multiplication. Journal of Species and Aromatic Crops 1993; 2: 41 – 6.
22. Mitra GC, Kaul KN. *In vitro* culture of root and stem callus of *Rauwolfia serpentina* Benth. for reserpine. Indian J Exp Biol 1964; 2: 49 – 51.
23. Mujib A, Das S, Dey S. Free cell culture, organization and plant regeneration in *Santalum album* L. Plant tissue culture 1997; 7: 63 – 9.
24. Murashige T, Skoogs F. A revised medium for rapid growth and bioassays with tobacco tissue cultures. Physiol Plant 1962; 15: 473 – 9.
25. Popov SV, Vinter VG, Patova OA, Markov PA, Nikitina IR, Ovodova RG, Popova GY, Shashkov AS, Ovodov YS. Chemical characterization and anti-inflammatory effect of rauvolfin, a pectic polysaccharide of *Rauvolfia* callus. Biochemistry (Mosc) 2007; 72(7): 778 – 84.
26. Roy SK, Hossain MZ, Islam MS. Mass propagation of *Rauvolfia serpentina* by *in vitro* shoot tip culture. Plant Tissue Cult 1994; 4(2): 69 – 75.
27. Shah MI, Jabeen M, Ilahi I. *In vitro* callus induction, its proliferation and regeneration in seed explants of wheat (*Triticum aestivum* L.) var. Lu-26S. Pak J Bot 2003; 35(2): 209 – 17.
28. Vakil RJ. A clinical trial of *Rauvolfia serpentina* in essential hypertension. Brit Heart J 1949; 11: 350.
29. Vida F. Behandlung der Hypertonie mit der indischen *Rauvolfia serpentina*. Die Med 1952; 20(37): 1157 – 9.
30. Vieira RF, Skorupa LA. Brazilian medicinal plants gene bank. Acta Hort 1993; 330: 51 – 8.
31. Vollosovich AG, Butenka RG. Tissue culture of *Rauwolfia serpentina* as a resource of alkaloids. In: Butenka RG (Ed). Culture of Isolated Organs, Tissues and Cells of Plant. Nauka, Moscow. 1970; 253 – 7.

Study of the risk factors of postoperative upper gastrointestinal bleeding of percutaneous coronary interventional therapy

Zhenxiang Zhang*, Wei Zheng, Junling Li

The Second Affiliated Hospital of Zhengzhou University, *Zhengzhou*, *Henan* 450014, *China*

Received January 21, 2009

Abstract

Objective. Investigate the risk factors of postoperative upper gastrointestinal bleeding of percutaneous coronary interventional (PCI) therapy. *Methods*. From March of 2005 to 2008, application of Logistic multiple stepwise regression analysis and forecasting factor screening Fishers discrimination mode, we have studied 152 cases for postoperative upper gastrointestinal bleeding of PCI therapy in the Second Affiliated Hospital of Zhengzhou University. *Results*. The incidence of upper gastrointestinal bleeding is 0.3% (5/152). Meanwhile, Logistic regression analysis showed that the risk factors of upper gastrointestinal bleeding are associated with elderly age and postoperative using heparin and Tirofiban. *Conclusion*. Early identification of risk factors can reduce the risk of gastrointestinal bleeding of PCI for postoperative patients. [Life Science Journal. 2009; 6(2): 63 – 64] (ISSN: 1097 – 8135).

Keywords: coronary heart disease; angioplasty; upper gastrointestinal bleeding; PCI

1 Introduction

Manoukian *et al* reported[1] that up to 30% patients of acute coronary syndrome and of coronary heart disease with percutaneous coronary intervention (PCI) treatment are in suffering of bleeding complications. Patients with immediate bleeding and the long-term poor prognosis with hemorrhage is closely related[2,3]. Both Anticoagulation and antiplatelet therapy are the must in the treatment of patients with coronary heart disease to reduce the occurrence of ischemia but also may increase the tendency of bleeding. This report demonstrated 152 case-studies on gastrointestinal bleeding risk factor of PCI patients with coronary artery disease were retrospectively analyzed and discussed.

2 Cases Study

From March 2005 to 2008, 152 PCI (88 of male and 64 of female aged from 37 to 77 years old patients) cases were studied. Among the patients, there are 63 cases for acute myocardial infarction, 56 cases for unstable angina pectoris, and 13 cases for remote infarct as well as 20 cases for ischemic cardiomyopathy excluding ischemic heart valve disease, serious, myocarditis, arrhythmia, liver function is not complete, chronic obstructie pulmonary emphysema, etc. However, patients were administrated with nitrate, beta blockers and calcium channel blockers, statins, aspirin, clopidogrel and other drugs with PCI therapy.

Clinical observation. Before the operation for routine PCI platelet counts, blood clotting time, prothrombin were carefully recorded and measured for all the cases. In the use of heparin and Tirofiban, platelet counts, blood coagulation time, thrombinogen reaction time and fecal occult blood test with specific criteria, such as blood platelet count test must be less than 20×10^9/L and APTT test must be longer than 180 seconds etc., all carefully being performed has obviously shown the bleeding tendency. Moreover, positive fecal occult blood test indicated the early gastrointestinal bleeding. Clinically, we observed the bleeding of gums indicating the administration of heparin and Tirofiban may cause early bleeding being observed. Administration of heparin and Tirofiban may also cause the bleeding tip coagulated time longer

*Corresponding author. Email:

than regular 2 to 3 minutes for intravenous administration and much dressings oozed blood or local hematoma for the PCI postoperative care,

3 Results

Recording age, gender, alimentary basic diseases, PCI duration and complications preoperative and postoperative, side effects of using heparin and Tirofiban, proton pump inhibitors, platelet count and blood clotting PT and PTT as the data base, by using SPSS and Logistic regression analysis, we set up parameters and proposed a model for bleeding risk factor calculation as following:

$P = \exp(-14.253 + 0.152 \times \text{age} + 2.602 \times \text{concentration of heparin and Tirofiban})/[1+\exp(-14.253 + 0.152 \times \text{age} + 2.602 \times \text{heparin and Tirofiban})]$

According to the model, we conclude the ROC curve at 0.961 (95% CI: 0.911 – 1.010) and standard error is 0.025. In the mean time, increasing age may increase the risk of bleeding of PCI therapy.

Table 1. The risk factors of postoperative upper gastrointestinal bleeding of PCI therapy

parameters	B	SE	Wald	*P*	Exp (B)	95% CI
Age	0.152	0.067	5.214	0.022	1.164	1.022 – 1.326
Heparin and tirofiban	2.602	1.032	6.357	0.012	13.487	1.7859 – 101.931
Constant	– 14.253	4.851	8.634	0.003	< 0.0001	

B: partial regression coefficient; SE: standard error of partial regression coefficient; Exp (B): relative risk RR.

If substitute age, heparin and Tirofiban (two risk factors) to Fisher formula, we can get the discriminant function

$Y = 0.647 \times \text{age} + 0.774 \times \text{concentration of heparin and Tirofiban}$

By using cross validation to evaluate the reliability, we can get the accuracy of discriminant function of 84.2%.

4 Discussion

In order to avoid the PCI postoperative stent acute thrombosis, Heparin and Tirofiban can be used for therapy. Through the anticoagulant III enzyme, heparin can inhibit the function of II a, IX a, X a plasma thromboplastin component (PTC) and therefore within 10 minutes of injection can significantly prolong the blood clotting, thrombin enzyme activity and hemoglutination[4,5]. Through inhibiting platelet by glycoprotein II b/III receptor to exert the function of antiplatelet agents, Tirofiban can provide the function of anticlotting. Anticlotting drugs can directly cause gastrointestinal mucosa bleeding[6]. For senior patients, due to the physiological degradation, heparin and Tirofiban combination therapy may have high risk of gastrointestinal bleeding which truly match the calculation from our prediction model.

References

1. Manoukian SV, Voeltz MD, Eikelboom J. Bleeding complications in acute coronary syndromes and percutaneous coronary intervention: predictors, prognostic significance, and paradigms for reducing risk[J]. Clin Cardiol 2007; 30(Suppl 2): II24 – 34.
2. Feit F, Voeltz MD, Attubato MJ, *et al*. Predictors and impact of major hemorrhage on mortality following percutaneous coronary intervention from the REPLACE-2 Trial[J]. Am J Cardiol 2007; 100: 1364 – 9.
3. Chin MW, Yong G, Bulsara MK, *et al*. Predictive and protective factors associated with upper gastrointestinal bleeding after percutaneous coronary intervention: a case-control study[J]. Am J Gastroenterol 2007; 102: 2411 – 6.
4. Qiu BF, Shi W. Digestive disease – Consultant rounds of upper gastrointestinal bleeding [J]. Chinese PracticalJournal of Rural Doctors 2008; 15(4): 52 – 4.
5. Yao MH, Yao LX. Běijīng rénmín weishēng chū bǎn shè ,2001:273.
6. Lǐ Jiàn. Drug-induced digestie disease [M]. Běijīng: Kēxué chū bǎn shè, 2001:104.

The effect of high frequency stimulation on intracellular Ca^{2+} in sympathetic PC12 cells☆

Yan Wo#, Rong Xia#, Feng Li, Wenlong Ding*

Department of Anatomy, *School of Medicine*, *Shanghai Jiao Tong University*, *Shanghai* 200025, *China*

Received December 11, 2008

Abstract

Objective. This study were designed to compare the impact of instant high frequency stimulation (HFS) and 3-day continuous HFS on the intracellular Ca^{2+} volume in sympathetic PC12 cells and to define the role of Nifedipine(NIF) in this process. *Methods.* The cells were randomly divided into two groups, namely instant HFS and 3-day continuous HFS. Using a line scanning technique under a Laser Scanning Microscope (LSM) at 1.2 ms – 1.25 ms intervals for 60s, we found that the intracellular Ca^{2+} fluorescence intensity changes between conduction of HFS and after termination of HFS. *Results.* The intracellular Ca^{2+} fluorescence intensity rapidly declined instantly after HFS on the sympathetic PC12 cells and the range of declination observed through line scanning was 47.7%. HFS was conducted continuously for 3 days, 3 hours per day. After discontinuing HFS, Ca^{2+} fluorescence intensity increased sharply with a 60% inclination. This effect was weakened by Ca^{2+} channel inhibitor Nifedipine (NIF). *Conclusion.* These data indicates that the variation of Ca^{2+} volume induced through HFS has a significant effect on sympathetic PC12 cells. On commencing instant HFS, Ca^{2+} fluorescence intensity increased significantly and decreased sharply after 3-day continuous HFS was terminated. However, NIF can partially counteract the inhibitory effect of HFS on PC12 cells, instead of complete blockage. [Life Science Journal. 2009; 6(2): 65 – 70] (ISSN: 1097 – 8135).

Keywords: PC12 cells; high frequency stimulation; Nifedipine; laser scanning microscope

1 Introduction

The treatment of Parkinson's disease (PD) is a difficult process that currently remains partially explored. Now, high frequency stimulation (HFS) of the subthalamic nucleus (STN) has become one of the main global surgical techniques in the treatment of PD[1,2]. In clinical conditions, HFS of STN neurons in PD is empirically applied at > or = 100 Hz (130 – 185 Hz), with pulses of short duration (60 – 100 micros) and 1 – 3 mA amplitude[3,4]. And more recently, a double effect hypothesis, implying both an inihibition of pathological neural activity and the induction of a new rhythm by periodic electrical stimulation[5,6]. This experiments attempts to enhance understanding of HFS effect mechanisms in treating PD and to observe changes in cellular function under stimulation more effectively, in particular Ca^{2+} as the second messenger which partakes widely in a large range of cellular functions such as cellular movement, secretion, metabolism and differentiation[7], as well as Ca^{2+} mediated cells also have significant tuning effects on responses to external stimulation[8]. This experiment utilizes pheochromocytoma cells (PC12 cells) that are similar to neurons in cellular anatomy, physiology and biochemistry, and possess common attributes with neurons and neurosecretory cells[9], when induced by nerve growth factor (NGF) in particular, the PC12 cell differentiates toward sympathetic neurocytes[10,11]. We applied HFS on continuous sympathetic PC12 cells by currents acting on medium, and using a laser scanning microscope (LSM) observed changes in sympathetic PC12 intracellular Ca^{2+} under the effect of HFS, and through the use of Nifedipine (NIF), prove that changes can be induced in sympathetic PC12 intracellular Ca^{2+} through HFS. We expect these results would benefit further exploration of possible effect mechanisms HFS has on the treatment of

☆Supported by Shanghai Leading Academic Discipline Project (Grant No. S30201).

*Corresponding author. Email: dingwl500@sina.com.cn

#These authors contributed equally to this work.

PD, and provide more reliable theoretical support for the appropriate use of HFS in the clinical treatment of PD.

2 Materials and Methods

2.1 High frequency stimulation method

Cells were inoculated in a Poly-L-Lysine hydrobromide (PLL) (Sigma, USA) coated 24-hole culture plate or a 3.5 cm culture dish and incubated for 24 hours in a 37 ºC incubator with 5% CO_2. Titanium wires were aligned parallel across adjacent holes in the 24 hole culture plate, two titanium wires were aligned parallel in the 3.5 cm culture dish, with ends respectively connected to positive and negative currents and stimulated with high frequency electrical currents. Square wave was generated by a stimulus generator and run through the isolator to stimulate cell population. HFS parameters were: 130 Hz frequency, 500 μA current, 60 μs pulse widths.

2.2 Incubation of sympathetic PC12 cells and cellular identification experiment

Undifferentiated PC12 cells were provided by the Nuclear Medicine Lab, College of Medicine, Shanghai Jiao Tong University. Incubation fluid contained 88% Dulbecco's modified Eagle's medium (DMEM) (GIBCO, USA), 10% fetal bovine serum (Zhejiang Hangzhou Sijiqing Biotech Co., China), 1% Penicillin streptomycin (GIBCO, USA) and 1% L-Glutamine (GIBCO, USA). PC12 cells were incubated in a 37˚C incubator with 5% CO_2; Cells were inoculated in a 24-hole culture plate at a density of 0.5×10^4 units/cm^2 or which were inoculated in a 3.5 cm culture dish at a density of 0.8×10^4 units /cm^2. 72 hours before commencing the experiment, sympathetic neurocytes obtained by inducing and differentiating PC12 cells through NGF (Promega, USA) were added at a final concentration of 50 ng/ml[11,12]. The cells were left overnight using 1 : 4000 TH-16 (Sigma, USA) at 4 ºC, with anti-mouse-HRP (Shanghai Changdao Biotech Co., China) incubation at 37 ºC for 1 hour to conduct immunohistochemical staining. The positive results of tyrosine hydroxylase (TH) which secreted by PC12 sympathetic neurocytes were yellow-brown particles.

2.3 Instant high frequency stimulation

2.3.1 Changes in intracellular Ca^{2+} in PC12 cells. Cells were inoculated at a density of 0.8×10^4 units/cm^2 in a PLL coated 3.5 cm culture dish containing 3 ml of fluid culture. NGF was added at a final concentration of 50 ng/ml to induce differentiation in PC12 cells. After cells have adhered, 0.5 mM of Fluo-4/AM (Molecular Probes, USA) with a final concentration of 2.5 μM was added to monitor PC12 intracellular Ca^{2+}. Cells were then incubated for 30 minutes in an incubator with 5% CO_2 at 37 ºC. The culture dish was placed under scanning stage of laser scanning microscope (510) (Zeiss Co., German) at × 10 objective and excited by an argon ion laser with excitation wavelength 488nm and emission wavelength BP 500-550 nm. Images were recorded via photomultiplier and image resolution was 52 × 52 using imaging software Time Series v.4.0. Line scanning was conducted at 1.2 ms – 1.25 ms intervals, with a total of 50000 scans over a total time of 60 seconds. HFS (parameters same as above) was conducted 14.4 seconds after commencing line scan and changing trends in intracellular Ca^{2+} fluorescence were dynamically recorded.

2.3.2 The effect of NIF on intracellular Ca^{2+} in PC12 cells. Cells are differentiated using NGF and identified by the TH-16 immunohistochemical method, then inoculated in a 3.5 cm culture dish at 0.8×10^4 units/cm^2. PC12 intracellular Ca^{2+} were measured with Fluo-4/AM and cells were incubated for 30 minutes in an incubator with 5% CO_2 at 37 ºC, then incubated with NIF (Calbiochem Co., USA) (final concentration 2 μM) for 5 minutes under the same conditions. Changes in intracellular Ca^{2+} fluorescence upon commencing HFS were observed under a LSM using the same scanning parameters as above.

2.4 Three-day continuous high frequency stimulation

2.4.1 Changes in intracellular Ca^{2+} in PC12 cells. Cells were differentiated through NGF and identified with the TH-16 immunohistochemical method, then inoculated in a 3.5 cm culture dish at 0.8×10^4 units/cm^2. After cells have adhered, HFS was applied continuously for 3 hours at fixed times daily for three days. HFS (parameters same as above). 30 minutes before terminating the 3-day stimulation period, PC12 intracellular calcium ions were measured with Fluo-4/AM and cells were incubated in an incubator with 5% CO_2 at 37 ºC, and scanned under a LSM at 1.2 ms – 1.25 ms intervals, with a total of 50000 scans over a total time of 60 seconds. HFS (parameters same as above) was conducted 14.4 seconds after commencing line scan and changing trends in intracellular Ca^{2+} fluorescence were dynamically recorded.

2.4.2 The effect of NIF on intracellular Ca^{2+} in PC12 cells. Cells were differentiated using NGF and identified by the TH-16 immunohistochemical method, then inoculated in a 3.5 cm culture dish at 0.8×10^4 units/cm^2. After cells have adhered, HFS (parameters as above) was applied continuously for 3 hours at fixed times daily for three days. 30 minutes before terminating the 3 day stimu-

lation period, PC12 intracellular Ca^{2+} were measured with Fluo-4/AM and cells were incubated for 30 minutes in an incubator with 5% CO_2 at 37 ºC, then incubated with NIF (final concentration 2 μM) for 5 minutes in an incubator with 5% CO_2 at 37 ºC, and scanned under a LSM (same scanning parameters as above) to observe effects of NIF on changes and trends in intracellular Ca^{2+} fluorescence values instantly after the 3-day HFS period was terminated.

2.5 Statistical analysis

Data drawn from cell form and cellular identification were analyzed using imaging software RS IMAGE PRO V.4.5; Laser scanned images were analyzed using imaging software Time Series. Data drawn from the experiment, in-group differences before and after HFS in the instant stimulation group and termination of the 3-day continuous stimulation group were tested using the one-way ANOVA. Differences between the instant stimulation group and 3-day continuous stimulation group were tested using the independent *t*-test and analyzed using SPSS 11.0.

3 Results

3.1 PC12 sympathetic neuron cell identification results

PC12 cells are differentiated by NGF to become sympathetic neurocytes. After HFS, the metabolic level of intracellular tyrosine hydroxylase is tested using the TH-16 immunohistochemical method. This method stains PC12 sympathetic neurocytes yellow-brown and serves to identify PC12 sympathetic neurocytes after HFS (Figure 1).

3.2 Changes in intracellular Ca^{2+} in PC12 cells after instant HFS

After Fluo-4/AM has been combined with free Ca^{2+} in PC12 sympathetic neurocytes, it could be observed using the LSM that intracellular fluorescence was evenly distributed. After commencing instant HFS, the strength of intracellular fluorescence weakened (Figure 2 A & B); it could be observed through line scanning that with the progression of stimulation time, intracellular Ca^{2+} fluorescence decreased sharply (Figure 3), with range of decline reaching 47.7% (Figure 4).

3.3 NIF on intracellular Ca^{2+} in PC12 cells after instant HFS

After adding NIF (2 μM), cells were incubated for 5 minutes before HFS. Change in intracellular fluorescence in the instant HFS group was not apparent before and after commencing HFS (Figure 5 A & B). It could be observed through line scanning method that intracellular fluorescence did not weaken significantly as stimulation time progressed (Figure 3), with range of only 4.8%, compared with groups without NIF ($P < 0.01$) (Figure 4). This indicated NIF had suppressed Ca^{2+} outflow induced by HFS.

3.4 Changes in intracellular Ca^{2+} in PC12 cells after 3-day continuous HFS

It could be observed that after HFS was terminated for the 3-day HFS group, there was a gradual increase in intracellular fluorescence (Figure 2 C & D). It could be observed through line scanning that after HFS was terminated, intracellular Ca^{2+} fluorescence increased rapidly (Figure 6) at range of 60% (Figure 7). Despite the speed and short time between line scan intervals that may cause fluorescence annihilation, line scanning still showed the more significant increase in Ca^{2+} fluorescence. After HFS was terminated for the 3-day continuous HFS group, intracellular Ca^{2+} fluorescence increased. This may have been caused by the inflow of extra-cellular Ca^{2+} or the release of intracellular calcium storage.

3.5 NIF on intracellular Ca^{2+} in PC12 cells after 3-day continuous HFS

After adding NIF (2 μM), cells of the 3-day HFS group were incubated for 5 minutes before HFS. Change in intracellular fluorescence was not apparent after HFS was terminated (Figure 5 C & D). It could be observed through line scanning method that intracellular fluorescence did not weaken significantly (Figure 6), with range of only 17.2% compared with the group without NIF ($P < 0.01$) (Figure 7). This indicated NIF had inhibited Ca^{2+} outflow induced by HFS in the 3-day HFS group, but from the data it is shown that NIF did not completely suppress changes that occurred in intracellular Ca^{2+}.

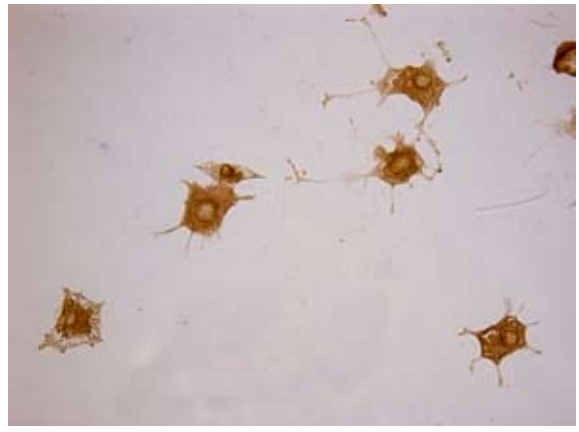

Figure 1. TH in PC12 sympathetic neurocytes was stained yellow-brown by TH-16 immunohistochemical method (DAB, × 400).

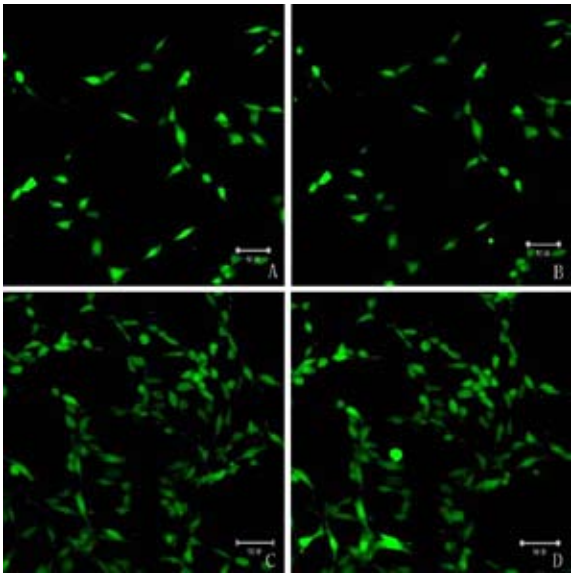

Figure 2. The effect of high frequency stimulation on intracellular Ca^{2+} in sympathetic PC12 cells. A: Before commencing instant HFS. B: After commencing instant HFS. C: Before terminating 3-day HFS. D: After terminating 3-day HFS.

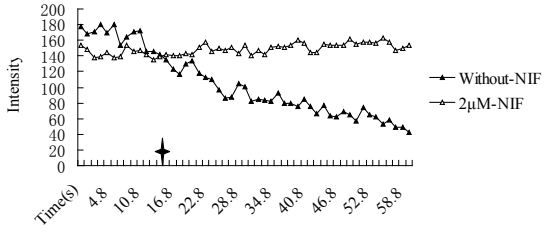

Figure 3. Line scanning of instant HFS. With commencing instant HFS, and without-NIF intracellular Ca^{2+} fluorescence decreased sharply; 2 μM-NIF intracellular Ca^{2+} fluorescence did not weaken significantly. †:Instant HFS was conducted 14.4 seconds.

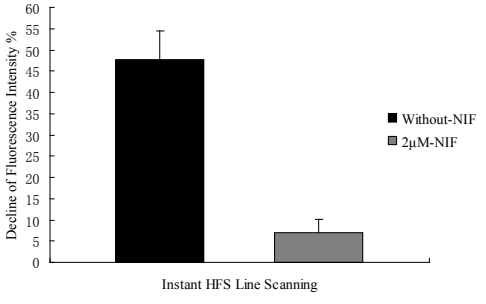

Figure 4. The effect of NIF on intracellular Ca^{2+} in PC12 cells after commencing instant HFS. With commencing instant HFS, and without-NIF intracellular Ca^{2+} fluorescence decreased sharply, with ranges of decline reaching 47.7% through line scanning;2μM-NIF intracellular fluorescence did not weaken significantly, with range of only 4.8%. **: $P < 0.01$ *vs.* the without-NIF group.

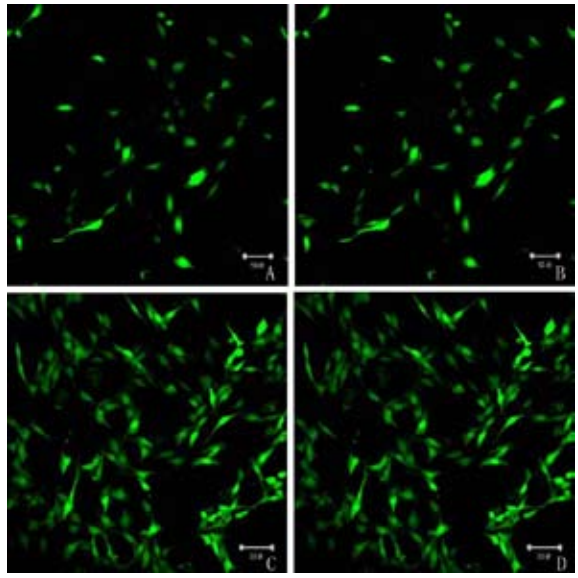

Figure 5. The effect of L-voltage sensitive Ca^{2+} channel blocker NIF on intracellular Ca^{2+} in PC12 sympathetic neurocytes after HFS. A: Before commencing instant HFS; B: After commencing instant HFS; C: Before terminating 3-day HFS; D: After terminating 3-day HFS.

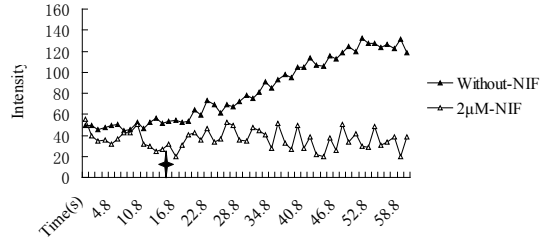

Figure 6. Line scanning of instant 3-day HFS.With terminating 3-day HFS, and without-NIF intracellular Ca^{2+} fluorescence increased rapidly;2μM-NIF intracellular Ca2+ fluorescence did not weaken significantly; :3-day HFS period was terminated 14.4 seonds.

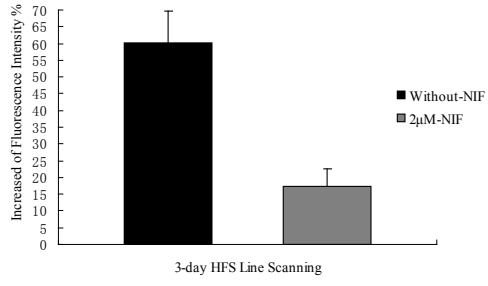

Figure 7. The effect of NIF on intracellular Ca^{2+} in PC12 cells after terminationg 3-day HFS. With terminating 3-day HFS, and without-NIF intracellular Ca^{2+} fluorescence increased rapidly at range of 60% through line scanning;2 μM-NIF intracellular fluorescence did not weaken significantly,with range of only 17.2% .**: $P < 0.01$ *vs.* the without-NIF group.

4 Discussion

Since TH is a rate-limiting enzyme organically composed by catecholamines as well as a key enzyme in the formation of such substances as dioxyphenylalanine and adnephrin, an important role in the organic synthetic tuning of substances such as dioxyphenylalanine. A range of abnormal changes generally occur in the genetic expression, apoenzyme levels and enzymatic activity of animal PD models and PD sufferers[13,14], and it was also found that TH levels increase significantly in PC12 cells that have been NGF differentiated[15]. The high frequency electrical currents act on cells' body by cells' medium[16]. Based on this, this experiment tests the metabolic level of intracellular TH using the TH-16 immunohistochemical method, which serves to determine whether NGF differentiated PC12 cells are sympathetic neurocytes and provides basis for successive experiments. The changes in intracellular Ca^{2+} fluorescence before and after commencing/terminating HFS was observed.

Intracellular Ca^{2+} plays the role of the second messenger; its temporary changes are determined by extracellular Ca^{2+} density and unpolarized cellular membrane level[17,18,19]. This experiment shows that there is a close relationship between HFS and intracellular Ca^{2+} fluorescence. Significant changes could be observed in intracellular Ca^{2+} fluorescence at the instant of commencing or terminating HFS. Upon commencing HFS, Ca^{2+} fluorescence increased significantly and decreased sharply after HFS was terminated. It is speculated that under stimulated conditions, the Ca^{2+} channel located on the PC12 cellular membrane is activated by the intra/extra-cellular voltage difference generated by instant HFS. This could cause the Ca^{2+} channel located on the PC12 cellular membrane to open, resulting in the rapid outflow of cytoplasm Ca^{2+}. Related research lends proof to the fact that electrical stimulation can cause changes in single calcium channel dynamics[20].

Through line scanning, this experiment showed that there is a regressive time-strength relationship between HFS and intracellular Ca^{2+} fluorescence. The decline rate of Ca^{2+} fluorescence which is caused by line scan is 47.7%. It is shown that instant HFS induces a stronger intracellular Ca^{2+} outflow for a short time after it commences, which subsides as time progresses. Upon termination of stimulation repeated daily at fixed times and frequencies for 3 days, Ca^{2+} located outside and in the cell organ may both be motivated to enter the cytoplasm. Not only extracellular free Ca^{2+} inflow but also the release of intracellular calcium storage cause localized calcium signals in Ca^{2+} in the cytoplasm to strengthen. Similarly, observations from line scanning techniques, it was shown that the increase rate of Ca^{2+} fluorescence caused by line scan is 60%. It can be seen that HFS also caused more obvious Ca^{2+} fluorescence signal in a short time and Ca^{2+} inflow subsides as time progresses after HFS has been terminated. Meanwhile, this effect is closely tied to the L-voltage sensitive Ca^{2+} channel, despite the fact that this channel plays a secondary role in the release of neurotransmitters[21]. The results of this experiment lend experimental evidence to the release of HFS induced intracellular Ca^{2+} via the L-voltage sensitive Ca^{2+} channel. When the channel inhibitor NIF is used in conjunction with HFS[22], it brings about significant changes in intracellular Ca^{2+} fluorescence, in which no apparent changes occurred at the instant commencing HFS and 3-day continuous terminating HFS. It is speculated that the Ca^{2+}channel inhibitor altered cell response toward different mediate signals. However, further research is needed to determine whether the increase and decrease of intracellular Ca^{2+} fluorescence upon commencing/terminating HFS are caused entirely by the opening of L-voltage sensitive calcium channels, and whether the strength of this effect is tied to NIF concentration.

5 Conclusion

This experiment shows that there is a close relationship between HFS and intracellular Ca^{2+} volume in PC12 cells. Significant changes in intracellular Ca^{2+} fluorescence intensity could be observed at the instant of commencing or terminating HFS. Upon commencing HFS, Ca2+ fluorescence intensity increased significantly while decreased sharply after HFS was terminated. And the NIF can partially counteract the inhibitory effect of HFS on PC12 cells, instead of complete blockage.

Acknowledgment

We thank Jinjia Hu, Hao Zhu and Wenjin Wang for their technical assistance. This study was supported in part by the Department of Nuclear Medicine from Shanghai Jiao Tong University.

References

1. Soulas T, Gurruchaga JM, Palfi S. Attempted and completed suicides after subthalamic nucleus stimulation for Parkinson's disease.Neurol Neurosurg Psychiatry 2008; 79(8): 952 – 4.
2. Voges J, Koulousakis A, Sturm V. Deep brain stimulation for Parkinson's disease. Acta Neurochir Suppl 2007; 97(Pt 2): 171 – 84.
3. Garcia L, Alessandro DG, Fernagut PO. Impact of high-frequency stim-

ulation parameters on the pattern of discharge of subthalamic neurons. Neurophysiol 2005; 94(6): 3662 – 9.
4. Moro E, Esselink RJ, Xie J. The impact on Parkinson's disease of electrical parameter settings in STN stimulation. Neurology 2002; 59(5): 706 – 13.
5. Garcia L, Allessandro DG, Bioulac B. High frequency stimulation in Parkinson's disease: More or less? Trends Neurosci 2005; 28(4): 209 – 16.
6. Galati S, Scarnati E, Mazzone P. Deep brain stimulation promotes excitation and inhibition in subthalamic nucleus in Parkinson's disease. Neuroreport 2008; 19(6): 661 – 6.
7. Teruel MN, Chen W, Persechini A. Differential codes for free Ca^{2+}-calmodulin signals in nucleus and cytosol. Curr Biol 2000; 10(2): 86 – 94.
8. Katz E, Verbitaky M, Rothlin C. High calcium permeability and calcium block of the alpha9 nicotinic acetylcholine receptor. Hear Res 2000; 141(1–2): 117 – 28.
9. Das PC, McElroy WK, Cooper RL. Potential mechanisms responsible for chlorotriazine-induced alterations in catecholamines in pheochromocytoma (PC12) cells. Life Sci 2003; 73(24): 3123 – 38.
10. Zachor DA, Moore JF, Brezausek C. Cocaine inhibits NGF-induced PC12 cells differentiation through D1-type dopamine receptor. Brain Res 2000; 869(1–2): 85 – 97.
11. Greene LA, Tischler AS. Establishment of a noradrenergic clonal line of rat adrenal pheochromocytoma cells which respond to nerve growth factor. Proc Natl Acad Sci USA 1976; 73(7): 2424 – 8.
12. Vaudry D, Stork PJ, Lazarovici P. Signaling pathways for PC12 cell differentiation: making the right connections. Science 2002; 296(5573): 1648 – 9.
13. Shiman R, Akino M. Solubilization and partial purification of tyrosine hydroxylase from bovine adrenal medulla. Biol Chem 1971; 246(5): 1330 – 40.
14. Czyzyk Krzeska MF, Paulding W, Toska K. Tyrosine hydroxylase and Parkinson's disease. Neurobiol 1998; 16(3): 285 – 309.
15. Edel T, Kavanagh, John P. Functionality of NGF-protected PC12 cells following exposure to 6-hydroxydopamine. Biochemical and Biophysical Res 2006; 351(4): 890 – 5.
16. Xia R, Berger F, Piallat B. Alteration of hormone and neurotransmitter production in cultured cells by high and low frequency electrical stimulation. Acta Neurochir (Wien) 2007; 149(1): 67 – 73.
17. Birch BD, Eng DL, Kocsis JD. Intranuclear Ca^{2+} transients duringneurite regeneration of an adult mammalian neuron. Proc Natl Acad Sci USA 1992; 89(17): 7978 – 82.
18. Berridge MJ, Bootman MD. Calcium signaling: dynamics, homeostasis and remodeling. Nat Rev Mol Cell Biol 2003; 4(7): 517 – 29.
19. Friel DD, Chiel HJ. Calcium dynamics: analyzing the Ca^{2+} regulatory network in intact cells. Trends Neurosci 2008; 31(1): 8 – 19.
20. Marchionni I, Paffi A, Pellegrino M. Comparison between low-level 50 Hz and 900 MHz electromagnetic stimulation on single channel ionic currents and on firing frequency in dorsal root ganglion isolated neurons. Biochim Biophys Acta 2006; 1758(5): 597 – 605.
21. Pancrazio JJ, Viglione MP, Kim YI. Effects of Bay K 8644 on spontaneous and evoked transmitter release at the mouse neuromuscular junction. Neuroscience 1989; 30(1): 215 – 21.
22. Green KN, Taylor SC, Smithand IF. Differential coupling of voltage-gated Ca^{2+} channels to catecholamine secretion from separate PC12 cell batches. Neuroscience Lett 2001; 301(1): 13 – 6.

Study on phylogenetic relationship of freshwater planarians (Turbellaria: Tricladida: Paludicola) in nine Chinese localities using RAPD method☆

Hecai Zhang[1], Guangwen Chen[1,2,*], Xiaojuan Sun[1], Cunshuan Xu[1,2]

[1]*College of Life Sciences*, *Henan Normal University*, *Xinxiang*, *Henan* 453007, *China*; [2]*Key Laboratory for Cell Differentiation Regulation*, *Xinxiang*, *Henan* 453007, *China*

Received December 13, 2008

Abstract

Objective. China is rich in freshwater planarian resource. In order to investigate phylogenetic relationships, Random Amplified Polymorphic DNA (RAPD) technique was applied to analyze RAPD pattern variations in planarians collected from nine Chinese localities, which belong to *Dugesia japonica* and *Seidlia sinensis*, respectively. *Methods.* Among 60 arbitrary primers (10 bp) under predetermined optimum reaction conditions, 27 primers were informative and yielded a total number of 314 clear and reproducible bands. The patterns show polymorphic variations among and within species. RAPD data were used to calculate Nei and Li similarity coefficient and genetic distance. Molecular systematic evolution tree was reconstructed by Nearest-Neighbor method via program SPSS 10.0. *Results.* The results showed that samples of *D. japonica* collected from eight localities clustered first, and then clustered with *S. sinensis*. In the clade of *D. japonica*, three branches are further divided. *Conclusion.* This clustering pattern coincides with the results drawn from the cytogenetical study, and also relates to their geographic distribution. [Life Science Journal. 2009; 6(2): 71 – 75] (ISSN: 1097 – 8135).

Keywords: freshwater planarian; RAPD; phylogenetic relationship; China

1 Introduction

Planarians are the earliest free-living platyhelminthes with triploblast and bilateral-symmetry, and also the important animal group which transits from water-inhabitation to land. Therefore, they play an important role in studying the systematic evolution of animals. Moreover, because of their powerful regenerative abilities, they are the ideal materials for studying the molecular mechanism of cell differentiation and redifferentiation. Researches on planarian have already been carried out to molecular level in Europe and the United States recently. For example, the molecular phylogenetics on the higher level were studied[1,2]. And the origin and evolution of planarian brain have been studied[3] and some genes about regeneration, such as Hox gene, Pax-6 gene have been cloned and expressed[4,5]. Though planarians distribute widely in China and the resources are rich, it is a pity that the study is weak in our country and few scientists are working in this field. Till now, we have just made some progress in Paludicola (Tricladida) and reported 14 species belonging to five genera, three families[6].

As a method for DNA fingerprinting based on the Polymerase Chain Reaction (PCR), the Random Amplified Polymorphic DNA (RAPD), which developed by Williams *et al*[7], Welsh & McClelland[8], and Welsh *et al*[9], is currently receiving particular attention. Because of its simplicity, it has been extensively used as a powerful tool for gene-mapping, population and pedigree analysis, phylogenetic study and bacterial strain identification[10–12]. The basic strategy involves the PCR amplification of random fragments of genomic DNA with single

☆Supported by the National Natural Sciences Foundation of China (Nos. 30670247, 30170119, 30870368), the Doctor Point Foundation for Universities of Education Ministry (No. 200804760003), the Outstanding Young Scientists Foundation of Henan Province (No. 0312001100), Universities Innovation Talent Foundation of Henan Province (No. 2005126) and the Foundation of Doctor Scientific Research Startup of Henan Normal University (No. 0713).

*Corresponding author. Email: chengw0183@sina.com

or multiple primers of arbitrary sequence. Polymorphism between individuals (or strains) is detected as differences between the patterns of DNA fragments amplified from the different DNAs using a given primer.

The taxonomic standard of planarian is mainly based on the morphology of copulatory organs[13]. This study used RAPD technique with enough random primers, and the evidence of genome level for the phylogenetic and taxonomic research of freshwater planarians in nine Chinese localities was obtained.

2 Materials and Methods

2.1 Experimenal animals

The experimental planarians are collected from nine localities in China, which belong to *Dugesia japonica* (*D. joponica*) and *Seidlia sinensis* (*S. sinensis*), respectively (Figure 1 and Table 1).

Figure 1. The geographic distribution of samples.

2.2 Reagents

The reagents include Genomic DNA Minipreps kit, 10 bp random primers, TaqDNA polymerase, 10 × PCR buffer, 25 mmol/L $MgCl_2$, dNTP Mix, RNase A and Proteinase K. RNase A was from Beijing DingGuo Biotech. Co. Ltd. (Beijing, China). Proteinase K was from Qiagen. Other reagents were all from Shanghai Sangon Biological Engineering Technology and Services Co., Ltd. (Shanghai, China).

2.3 Preparation of DNA template

Genomic DNA was extracted with the genomic DNA Minipreps kit (Shanghai, China). Then DNA was resuspended in TE solution after being dried in air, keeping storage in 4 ºC for use.

Table 1. List of localities of samples

Locality	Code	Species
Yingtaogou, Beijing City	D-1	*Dugesia japonica*
Luanchuan County, Henan	D-2	*Dugesia japonica*
Hangzhou City, Zhejiang	D-3	*Dugesia japonica*
Stone-man Mountain, Henan	S-4	*Seidlia sinensis*
Lushan County, Henan	D-5	*Dugesia japonica*
Xiuwu County, Henan	D-6	*Dugesia japonica*
Yangcheng County, Shanxi	D-7	*Dugesia japonica*
Jiyuan City, Henan	D-8	*Dugesia japonica*
Xin County, Henan	D-9	*Dugesia japonica*

2.4 Amplification conditions

According to the pre-experiments, the optimum conditions are as follows: amplification reactions were performed in a total volumes of 25 μl, containing 1 × PCR buffer, 2.0 mmol/L $MgCl_2$, 0.2 μmol/L primer, 0.2 mmol/L dNTPs, 20 ng of DNA template and 1.0 U of Taq DNA polymerase. Samples were subjected to PCR in a Little Genious Thermal Cycler (Guangzhou Fangtong Biotech. Co. Ltd. Guangzhou) using 40 cycles of 1 min at 94 ºC, 1 min at 37 ºC, 2 min at 72 ºC with pre-denaturation at 94 ºC for 5 min before the first cycle and final extention at 72 ºC for 5 min after the last cycle[14].

2.5 Agarose gel electrophoresis

Amplification products were analyzed on a 1.5% agarose gel containing EB (ethidium bromide) with 1 × TAE buffer for 2.5 h under the condition of 5 v/cm and room temperature. Then the electropherograms photographed under GIS-1000 Gel Auto-phtotograph System.

2.6 Statistical analysis

Presence and absence of a given fragment that amplified from genomic DNA were represented by "1" and "0" characters, respectively. Clear or weak and reproducible bands were recorded as "1". No or weak and non-reproducible bands were recorded as "0". Thus a matrix of characters was obtained for phylogenetic analysis as initial data. According to the formula $S = 2Nxy/(Nx+Ny)$[15], the similarity coefficients were calculated, where Nxy is the number of similar bands between two samples. The coefficient allows a value of the similarity between any two samples. This analysis provided data about the genomic distances between different samples. The coefficient was used because it is recommended for routine computation of genetic similarities using RAPD data[16]. The coefficients gave similarity values in the range 0 to 1 and were converted to genetic distance (D) as $D = 1 - S$.

Cluster analysis was made for these nine samples and the molecular systematic tree was reconstructed by Nearest Neighbor method via SPSS 10.0.

3 Results

3.1 RAPD results

Nine samples were screened using 60 10-mer primers, 27 of them generated clear and reproducible fingerprintings interest. See Table 2 for sequences of these 27 primers and numbers of RAPD bands.

The total number of bands amplified with 27 primers is 314, and the average number of each primer is 11.6. Primers S10, S90 amplified the most bands, both are 15. Primers S13, S66 and S77 all amplified the fewest bands with the number of eight. Therefore, there is notable difference in amplification products among different primers. Figure 2 shows profiles obtained with primers S10 and S82, respectively.

3.2 Genetic distance and cluster analysis

To show genetic affinity, the genetic distances among these nine samples were calculated via the formula D = 1 – S, and the distance matrix was shown in Table 3. Figure 3 shows the dendrogram reconstructed by Nearest Neighbor method via SPSS 10.0.

4 Discussion

Researches on the molecular systematics of planarians

Table 2. List of 27 primer sequences and numbers of RAPD bands amplified with each primer for nine samples

Primer sequence	D-1	D-2	D-3	S-4	D-5	D-6	D-7	D-8	D-9	Total
S5 (5'-TGCGCCCTTC-3')	0	3	4	2	3	2	1	2	6	10
S8 (5'-GTCCACACGG-3')	2	3	5	4	6	2	1	3	5	12
S10 (5'-CTGCTGGGAC-3')	2	5	7	5	6	8	5	4	5	15
S13 (5'-TTCCCCCGCT-3')	0	3	3	2	5	1	2	1	2	8
S15 (5'-GGAGGGTGTT-3')	3	1	3	3	3	4	4	3	4	12
S16 (5'-TTTGCCCGGA-3')	1	2	2	3	3	1	2	2	5	10
S17(5'- GGGAACGAG-3')	4	2	4	1	4	5	4	4	6	10
S18 (5'-CCACAGCAGT-3')	4	8	6	5	3	7	6	5	3	12
S20 (5'-GGACCCTTAC-3')	1	3	7	5	3	8	5	6	2	11
S62 (5'-GTGAGGCGTC-3')	3	4	3	2	3	5	2	5	2	11
S64 (5'-CCGCATCTAC-3')	3	4	4	2	4	6	4	5	3	11
S65 (5'-GATGACCGCC-3')	4	3	5	5	3	8	10	8	2	14
S66 (5'-GAACGGACTC-3')	2	2	2	3	3	4	4	2	3	8
S70 (5'-TGTCTGGGTG-3')	4	4	6	4	4	5	3	4	5	11
S71(5'-AAAGCTGCGG-3')	2	1	3	2	2	3	3	3	1	8
S75 (5'-GACGGATCAG-3')	5	3	4	8	5	5	2	4	2	13
S78 (5'-TGAGTGGGTG-3')	3	2	6	5	3	3	4	4	3	12
S79 (5'-GTTGCCAGCC-3')	3	1	3	5	4	3	3	3	5	11
S80 (5'-ACTTCGCCAC-3')	4	4	3	3	3	4	5	2	5	12
S82(5'-GGCACTGAGG-3')	2	5	5	6	7	3	5	6	3	13
S83 (5'-GAGCCCTCCA-3')	3	1	7	5	5	5	4	5	2	12
S84 (5'-AGCGTGTCTG-3')	4	6	6	5	6	7	5	5	3	12
S85(5'-CTGAGACGGA-3')	3	0	4	5	5	6	5	6	5	13
S88 (5'-TCACGTCCAC-3')	4	5	3	4	6	4	5	4	3	12
S89 (5'-TGCCCAGCCT-3')	4	5	8	5	4	4	7	8	5	14
S90 (5'-AGGGCCGTCT-3')	3	4	3	5	3	7	8	6	3	15
S93 (5'-CTCTCCGCCA-3')	7	7	7	3	7	6	6	6	8	12
Total	80	91	123	105	115	126	115	116	101	314

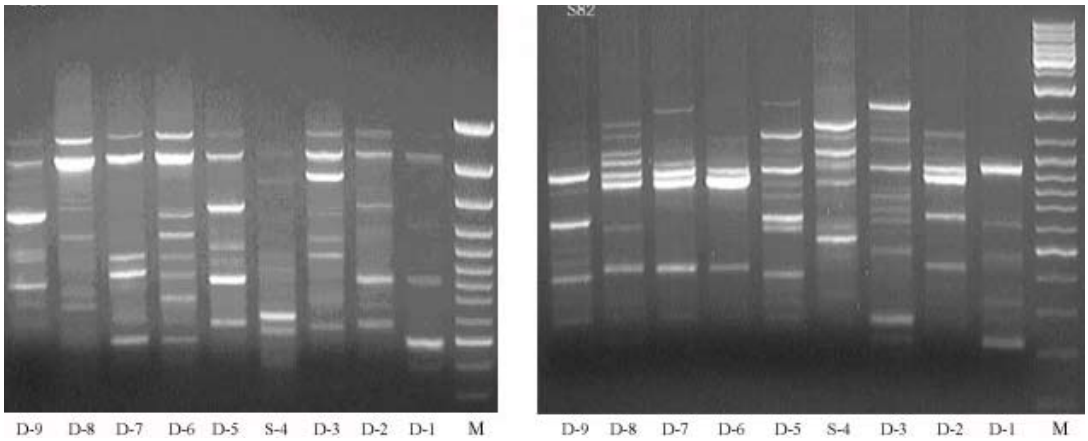

Figure 2. Electrophoresis patterns of RAPD products of freshwater planarian from nine localities in China (primer S10, S82, respectively). M: Molecular size marker, Gene Ruler™ 100 bp DNA Ladder Plus.

Table 3. Genetic distance between freshwater planarians from nine localities in China

	D-1	D-2	D-3	S-4	D-5	D-6	D-7	D-8	D-9
D-1	0								
D-2	0.4791	0							
D-3	0.6355	0.5607	0						
S-4	0.6865	0.6429	0.6228	0					
D-5	0.6615	0.4369	0.6303	0.7545	0				
D-6	0.6602	0.5853	0.5422	0.5844	0.6515	0			
D-7	0.6821	0.5340	0.5798	0.6182	0.6087	0.2863	0		
D-8	0.5816	0.5362	0.5732	0.6199	0.6450	0.3471	0.3247	0	
D-9	0.6133	0.5000	0.6429	0.7184	0.4074	0.6476	0.6296	0.6959	0

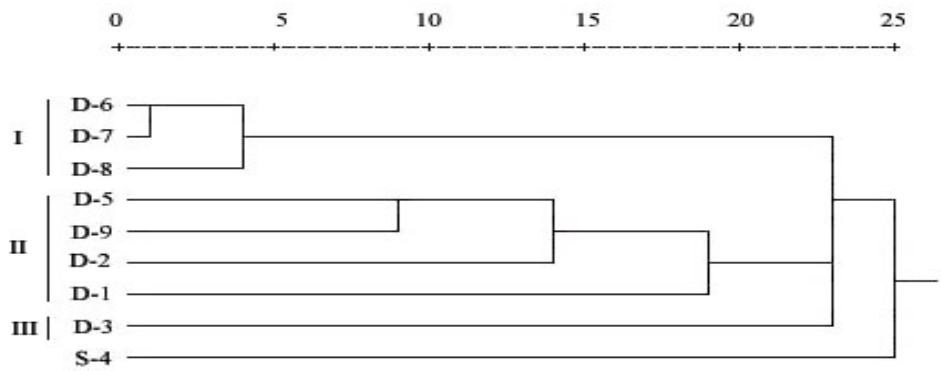

Figure 3. Dendrogram reconstructed for freshwater planarians from nine localities in China via SPSS 10.0.

using RAPD method have not been reported in China yet. In this paper, we studied the phylogenetic relationship among nine samples belonging to *D. japonica* and *S. sinensis*, respectively, using RAPD technique.

There are two clades in the dendrogram. The first clade can be divided into three branches. In branch I, D-6 (from Xiuwu County, Henan Province) and D-7 (from Yangcheng County, Shanxi Province) clustered first, and then clustered with D-8 (from Jiyuan City, Henan Province). In branch II, D-2 (from Luanchuan County, Henan Province) clustered with D-5 (from Lushan County, Henan Province) and D-9 (from Xin County,

Henan Province) after the latter two clustering together, then they three clustered with D-1(from Beijing City). At last, branch I and II clustered with branch III (D-3 from Hangzhou City, Zhejiang Province), forming the first clade of *D. japonica*. Then the first clade clustered with the second clade of *S. sinensis* (from the Stone-man Mountain, Henan Province). Populations of the same species are closer in relationship than those belonging to different genera, which indicate indirectly that the taxonomic positions of these samples are correct at least at genus level.

The clustering pattern within *D. japonica* also coincides with their geographic distribution. Xiuwu County, Yangcheng County and Jiyuan City are close in latitude, belonging to Taihang Mountain Area. As all of them belong to Palearctic realm in fauna, they are similar to a great extent and planarians from these three localities are close in relationship. Lushan County, Luanchuan County and Xin County belong to Funiu Mountain Area and Dabie Mountain Area, respectively. They are close in latitude, and lower than the former three. They belong to the transitional area of Palearctic region to Oriental region, so the planarians in these three areas are close. Beijing City belongs to Palearctic region, higher in latitude. Hangzhou City belongs to subtropical zone, Oriental region in the fauna, lower in latitude. So the populations from these two cities are remotest in relationship than to the other six populations.

Furthermore, the results from cytogenetics also support this RAPD analysis. In branch II, *D. japonica* from Lushan County, Xin County and Luanchuan County are all triploid, having 24 chromosomes. And *D. japonica* with the karyotype formula of 2n = 2x = 16 = 16m forming branch III. In branch I, the cluster results also coincide with cytogenetical results, but there is a little disagreement. The karyotype formulae of planarians from Xiuwu County are 2n = 2x = 16 = 16m and 2n = 3x = 24 = 24m, while that of planarians from Yangcheng County is 2n = 3x = 24 = 3m + 15sm + 3st + 3T. Those from Jiyuan City are 2n = 3x = 24 = 3m + 18sm + 3st (more), and 2n = 2x = 16 (fewer)[17]. While *S. sinensis* possesses 42 chromosomes which differentiate greatly from those of *D. japonica* in quantity and shape, constructing the second clade of the dendrogram.

From above, it is confirmed that the relationships of different populations of *D. japonica* are closer than those between *Dugesia* and *Seidlia*. Our research, at genome level, supports the results drawn from morphology and cytogenetics. Meanwhile, it also indicates that RAPD technique holds considerable promise for the population genetic, systematic evolution and classification of freshwater planarians.

Acknowledgment

We are grateful to Yingli Wang for her revising the manuscript.

References

1. Carranza S, Littlewood DTJ, Clough KA, *et al*. A robust molecular phylogeny of the Tricladida (Platyhelminthes: Seriata) with a discussion on morphological synapomorphies. Proceedings of the Royal Society of London (B) 1998; 265(1396): 631 – 40.
2. Carranza S, Baguñă J, Riutort M. Origin and evolution of paralogous rRNA geneclusters within the flatworm family Dugesiidae (Platyhelminthes, Tricladida). Journal of Molecular Evolution 1999; 49(2): 250 – 9.
3. Masumi N, Francesc C, Katsu hiko M, *et al*. Search for the evolutionary origine of a brain: Planarian brain characterized by microarry. Molecular Biology and Evolution 2003; 20(5): 784 – 91.
4. Bayascas JR, Castillo E, Munoz-Marmol AM, *et al*. Planarian Hox genes: novel patterns of expression during regeneration. Development 1997; 124(1): 141 – 8.
5. Callaerts P, Munoz-Marmol AM, Glardom S, *et al*. Isolation and expression of a Pax-6 gene in the regenerating and intact planarian Dugesia (G) tigrina. Proceedings of the National Academy of Science U.S.A. 1999; 96(2): 558 – 63.
6. Chen GW, Lu JQ, Ma JY. Report on freshwater planarians from China. Acta Zoologica Sinica 2001; 47 (Suppl): 9 – 12.
7. Williams JGK, Kubelik AR, Livak KJ, *et al*. DNA polymorphisms amplified by arbitrary primers are useful as genetic markers. Nucleic Acids Research 1990; 18(22): 6531 – 5.
8. Welsh J, McClelland M. Fingerprinting genomes using PCR with arbitrary primers. Nucleic Acids Research 1990; 18(24): 7213 – 8.
9. Welsh J, Peterson C, McClelland M. Polymorphism generated by arbitrarily primed PCR in the mouse: application to strain identification and genetic mapping. Nucleic Acids Research 1991; 19(2): 303 – 6.
10. Bando SY, do Valle GRF, Martinez MB, *et al*. Characterization of enteroinvasive *Escherichia coli* and Shigella strains by RAPD analysis. FEMS Microbiological Letters 1998; 165(1): 159 – 65.
11. Oliveira CM, Mota M, Monte-Corvo L, *et al*. Molecular typing of Pyrus based on RAPD markers. Scientia Horticulturae 1999; 79: 163 – 74.
12. Lin W, Zhang CF, Zhang YD, *et al*. Using RAPD method on systematic evolution of four species in anura. Zoological Research 2001; 22 (4): 332 – 6.
13. Liu DZ. Chinese Freshwater Turbellarians. Beijing: Beijing Normal University Press. 1993.
14. Zhang HC, Chen GW, Li YC, *et al*. Optimization of reaction conditions for RAPD analysis of freshwater planarians in China. Acta Biologae Experimentalis Sinica 2004; 37(4): 330 – 6.
15. Nei M, Li WH. Mathematical model for studying genetic variation in terms of restriction endonucleases. Proceedings of the National Academy of Science U.S.A. 1979; 76(10): 5269 – 73.
16. Lamboy WF. Computing genetic similarities using RAPD data: the efforts of artifacts. Genome Research 1994; 4: 31 – 7.
17. Xiong CL. Studies on the taxonomy and karyotype of freshwater planarian in China. Dissertation of Henan Normal University for the Degree of Master of Science. 2003.

Therapeutic effect of L-carnitine on sialic acid, soluble Fas (sFas) and other biochemical variables in hyperinsulinemic rats

Mohamed H. Mahfouz[1,*], Hala M. Ghanem[2], Mona A. Mohamed[3]

[1]*Department of Biochemistry*, *National Institute of Diabetes and Endocrinology (NIDE)*, *Cairo*, *Egypt*; [2]*Department of Biochemistry*, *Faculty of Science*, *Ain Shams University*; [3]*Biochemistry Division*, *Chemistry Department*, *Faculty of Science*, *Al-Azhar University*

Received December 29, 2008

Abstract

Background. Rats fed "high-fructose diet" (60 g/100 g diet) (FRU) were used as a model of insulin resistance in this context. *Objective.* The aim of this study was to evaluate the modulator effect of L-carnitine (CAR) on oxidative stress, lipid profile, inflammatory (sialic acid) and apoptotic (soluble Fas) markers in blood of rats fed "high-fructose diet". *Materials.* Male Wistar rats of body weight 120 – 160 g were divided into 5 groups of 6 rats each. Groups 1 and 2 animals received starch as control diet, while groups 3, 4 and 5 rats were fed a "high-fructose diet". Groups 2, 4 and 5 animals additionally received intraperitoneal CAR (300 mg/kg body weight) for 30 days. Group 4 rats received CAR on first day of the experiment (to study the prophylactic effect), while group 5 rats received CAR on after 15th day of the experiment (to study the therapeutic effect of CAR). *Methods.* At the end of the experimental period, levels of glucose, insulin, lipid profile, sialic acid and sFas in serum and glycosylated Hb (HbA1c) in whole blood were determined, in addition total antioxidant capacity (TAC) and malondialdehyde (MDA) were assayed. *Results.* Fructose feeding to rats caused significant elevations in the serum levels of glucose, insulin, triacylglycerol, HDL-c, sialic acid, sFas and MDA, while the level of serum TAC was significantly reduced as compared to controls. Intraperitonial administration of CAR to fructose-fed rats, alleviated the effect of fructose and these rats showed near normal levels of the parameters studied. *Conclusion.* Exogenous CAR to fructose-fed rats improves insulin resistance, reduces lipo- and glucotoxicity and attenuates oxidative stress, inflammatory and apoptotic markers. These effects suggest that CAR supplementation may have some benefits in patients suffering from insulin resistance. [Life Science Journal. 2009; 6(2): 76 – 82] (ISSN: 1097 – 8135).

Keywords: L-carnitine (CAR); fructose-fed rats; insulin resistance; sialic acid; soluble Fas

1 Introduction

Rats consuming a "high-fructose diet" induces insulin resistance accompanied by deleterious metabolic consequences including hyperinsulinemia, hyperglycemia, glucose intolerance, hypertriglyceridemia and hypertension in rats and these metabolic effects are similar to those observed in the human multimetabolic syndrome X and in which a cluster of disorders are described[1,2]. Studies have reported that hyperglycemia and insulin resistance could also promote inflammation by increased oxidative stress[3,4] and alteration in lipid metabolism in rat tissues[5].

Furthermore, the serum sialic acid (N-acetyl neuraminic acid) concentration is one of the markers for acute-phase response[6] and an inflammatory marker and predictor of microvascular complications in type 2 diabetic patients[7].

Inflammatory and resident cells (endothelial and vascular smooth muscle cells) release different proteins (sFas and sFas L) that can generate a chronic inflammatory re-

*Corresponding author. Tel: 002-106868481; Email: mhesham5@yahoo.com

sponse and to play an important role in apoptotic signaling[8]. Oxidative stress in a critical part of the apoptoting agent, antioxidants can inhibit or delay oxidative stress induced apoptosis[9].

L-carnitine (CAR, β-hydroxy-γ-trimethyl amino butyrate), has been described as a conditionally essential nutrient for humans. It is formed by biosynthesis from lysine and methionine in the body. CAR may acts as antioxidant either having a primary antioxidant activity (inhibiting free radical generation, scavenging the initiating free radicals, and terminating the radical propagation reactions) or more likely, functioning as a secondary antioxidant (repairing oxidized polyunsaturated fatty acids estrified in membrane phospholipids[10]. CAR functions to transport long-chain fatty acids across the inner mitochondrial membrane into the matrix for β-oxidation and has effects on oxidative metabolism of glucose in tissues[11]. Considering all these, the present study was to evaluate the therapeutic effect of CAR on oxidant-antioxidant balance, lipid profile, inflammatory (sialic acid) and apoptotic (sFas) markers in blood of rats fed "high-fructose diet".

2 Materials and Methods

2.1 Chemicals and drugs

CAR, other chemicals and solvents were of analytical grade and were purchased from Sigma Chemical Company.

Animals and treatment: Adult male Wistar rats of body weight ranging from 120 – 160 g were used in this study. They were purchased from the breeding unit of the Egyptian Organization for Biological Products and Vaccines (Helwan, Egypt). They were housed 2/cage under controlled condition 12 h light/12 h dark cycle. All animals received standard pellet diet for one week and water *ad libitum*. Approval had been taken from the research ethics committee of General Organization of teaching Hospitals & Institutes, Cairo, Egypt.

Insulin resistance was induced by feeding high-fructose diet (60 g/100 g). After acclimatization, the animals were divided into 5 groups consisting of 6 rats each and were maintained as follows:

Group 1: CON/control animals received the control diet containing corn starch (60%) as a sole source of carbohydrate and tape water *ad libitum*.

Group 2: (CON + CAR)/control animals received the control diet and intraperitonial CAR (300 mg/kg body wt /day).

Group 3: FRU/fructose-fed animals received the fructose enriched diet (60%) and tap water *ad libitum*.

Group 4: (FRU + CAR on 1st day)/fructose-fed animals received the fructose-diet and intraperitonial CAR (300 mg/kg body wt/day) on 1st day of experimental period (prophylactic or prevention effect).

Group 5: (FRU + CAR on 16th day)/fructose-fed animals received the fructose-diet and intraperitonial CAR (300 mg/kg body wt/day) on 16th day of experimental period (therapeutic effect).

The diet composition was given in Table 1. The animals were maintained in their respective groups for 30 days and body weight changes were measured weekly.

Table 1. Composition of diet (g/100 g)[5]

Ingredients	Control diet	High-fructose diet
Corn starch	60	–
Fructose	–	60
Casein (fat free)	20	20
Methionine	0.7	0.7
Groundnut oil	5	5
Wheat bran	10.6	10.6
Salt mixture*	3.5	3.5
Vitamin mixture**	0.2	0.2

*: The composition of mineral mix (g/kg) contained 30.5 g $MgSO_4 \cdot 7H_2O$, 65.2 g NaCl, 105.7 g KCl, 200.2 g KH_2PO_4, 3.65 g $MgCO_3$, 38.8 g $Mg(OH)_2 \cdot 3H_2O$, 40.0 g $FeC_6H_5O_7 \cdot 5H_2O$, 512.4 g $CaCO_3$, 0.8 g KI, 0.9 g NaF, 1.4 g $CuSO_4 \cdot 5H_2O$, 0.4 g $MnSO_4$ and 0.05 g $CONH_3$. **: One kilogram of vitamin mix contained 3.0 g thiamine mononitrate, 3.0 g riboflavin, 3.5 g pyridoxine HCl, 15 g nicotinamide, 8.0 g d-calcium pantothenat, 1.0 g folic acid, 0.1 g d-biotin, 5 mg cyanocobalamin, 0.6 g vitamin A acetate, 25 g α-tocopherol acetate and 10 g choline chloride.

2.2 Blood sampling and processing

On day 29th, rats were fasted overnight, about 4 ml of blood was drawn from the animal retina under ether anesthesia. A part of blood sample was taken on EDTA as whole blood sample for determination of glycosylated hemoglobin (HbA1c) using Chromatographic-Spectrophotometric methods[12]. Another part of blood collected was taken on a plain tube without anticoagulant for separation of serum by centrifugation at 3000 rpm for 10 min. Serum glucose was assayed by glucose oxidase method[13], total cholestrol was determined by the enzymatic method[14], triacylglycerol was assayed by peroxidase-coupled method[15] and HDL-c by the enzymatic method after precipitation of other lipoproteins with $MgCl_2$ and dextran sulphate[16]. LDL-c was calculated by the Friedwald formula[17]. Atherogenic index was calculated from ratio of total cholesterol/HDL-c[18]. The remaining part of serum was stored at – 80 °C until analysis of insulin,

malondialdehyde (MDA), sialic acid, total antioxidant capacity (TAC) and sFas. Levels of serum insulin was assayed by monoclonal immunoradiometric assay using kit supplied by Diagnostic Products Corporation (DPC)[19]. Lipid peroxidation product, MDA concentration was determined fluorometrically with excitation at 515 nm and emission at 550 nm after isobutyl alcohol extraction[20]. Serum sialic acid was measured by a spectrophotometric assay[21]. Total antioxidant capacity was determined according to the method of Koracevic *et al*[22]. Plasma sFas concentration was assessed using the enzyme-linked immunosorbent assay (ELISA) kit (Research & Diagnostic Systems, Minneapolis, U.S.A.) according to the manufacturer's instructions. Model Assessment (HOMA) correlates positively with insulin-resistance, and was calculated according to Matthews *et al*[23].

2.3 Statistical analysis

All results were expressed as the mean ± SD. Statistical analysis was performed with Statistical Package for the Social Science for Windows (SPSS, version 11.0, Chicago, IL, USA). The data were analyzed by one-way analysis of variance (ANOVA). To compare the difference among the groups, post hoc testing was performed by the Bonferroni test. Pearson's correlation analysis was used to determine the correlation among the parameters assessed. The *P*-value less than 0.05 was considered statistically significant[24].

3 Results

The body weights of the animals increased progressively during the experimental period. The percentage change in the body weight gain in rats of studied groups did not vary significantly as compared to controls.

The levels of serum glucose, insulin, HOMA index and glycosylated hemoglobin are shown in Table 2. There were significant elevations in glucose, insulin levels and HOMA index after 30 days of fructose-fed rats (FRU group) ($P < 0.0001$ for each) compared to control animals.

CAR supplementation to fructose-fed rats (group 5) caused a significant reduction in the levels of glucose, insulin and HOMA index ($P < 0.0001$ for each) as compared to fructose diet fed rats, while administration of CAR from the first day of the experiment (group 4) has no statistically effect on insulin level but it induced pronounced decrease in serum glucose level ($P < 0.003$) and HOMA index ($P < 0.0001$) compared to FRU-group. Rats fed control diet, CAR administration had no marked effects on the studied parameters.

Table 3 demonstrates that high-fructose diet (FRU) induced marked elevation in serum level of triacylglycerol which amounted (161.0 ± 1.5, $P < 0.0001$) as compared to control diet fed rats. Whereas the levels of cholesterol, low density lipoprotein cholesterol (LDL-c) and atherogenic index did not show any significant alteration in FRU group compared to control rats. Significantly decreases in triacylglycerol and atherogenic index ($P <$ 0.003, 0.005 respectively) and marked increase in HDL-c level ($P < 0.005$) were observed in group 5 as compared to group 3. The level of triacylglycerol in group 4 showed slight significant decrease ($P < 0.01$) as compared to group 3. For animals fed control diet, exogenous CAR caused a significant reduction in atherogenic index only ($P < 0.003$) as compared to control group.

Fed high-fructose diet to rats induced significant increases in serum levels of sialic acid (1.75 ± 0.51), sFas (27.6 ± 1.9) and MDA (15.33 ± 2.4) ($P < 0.0001$ for each), while TAC level represent a marked reduction (0.53 ± 0.22, $P < 0.0001$) as compared to rats fed control diet (Table 4). In fructose-fed rats the serum sialic acid levels positively correlated with serum triacylglycerol ($r = 0.048$), and serum insulin ($r = 0.342$), while negative correlation was observed between sialic acid and not only glucose ($r = – 0.386$), but also sFas ($r = – 0.468$). Good correlation was observed between sialic acid and HDL-c ($r = 0.939$, $P = 0.005$) in high fructose fed rats (Figure 1). The significant negative correlation was observed between sFas and triacylglycerol in FRU group (*r*

Table 2. Serum levels of glucose, insulin, HOMA index and HbA1c in control and experimental animals (Means ± SD)

Parameters	Experimental groups				
	1	2	3	4	5
F. Glucose (mg/dl)	83.8 ± 19.0	66.3 ± 17.6	134.2 ± 17.4[a]	92.8 ± 12.7[b]	66.0 ± 15.2[c]
Insulin (μIU/ml)	16.0 ± 2.3	14.2 ± 1.9	35.8 ± 4.4[a]	32.5 ± 4.3	21.3 ± 3.3[c]
HOMA index	3.23 ± 0.76	2.26 ± 0.40	11.82 ± 2.75[a]	7.64 ± 0.92[c]	3.38 ± 0.68[c]
HbA1c (%)	4.2 ± 0.12	4.1 ± 0.12	4.3 ± 0.1	4.2 ± 0.24	4.2 ± 0.098

[a]: $P < 0.0001$ *vs.* CON (1), [b]: $P < 0.003$ *vs.* FRU (3), [c]: $P < 0.0001$ *vs.* FRU (3).

Table 3. Serum lipid profile in control and experimental animals (Means ± SD)

Parameters	Experimental groups				
	1	2	3	4	5
Cholesterol (mg/dl)	70.7 ± 7.2	62.0 ± 7.4	81.5 ± 10.8	75.2 ± 9.7	70.7 ± 10.4
Triacylglycerol (mg/dl)	69.2 ± 7.1	90.2 ± 13.1	161.6 ± 60.5[a]	104.7 ± 25.5[b]	98.0 ± 14.2[c]
HDL-c (mg/dl)	31.2 ± 1.2	34.2 ± 1.7	37.2 ± 1.5[d]	38.3 ± 3.6	43.0 ± 3.9[e]
LDL-c (mg/dl)	25.8 ± 1.3	24.0 ± 0.63	26.7 ± 1.9	25.2 ± 2.4	26.2 ± 2.0
T. cholesterol/HDL-c	2.3 ± 0.23	1.8 ± 0.18[d]	2.18 ± 0.29	1.97 ± 0.14	1.65 ± 0.27[e]

[a]: $P < 0.0001$ *vs.* CON (1), [b]: $P < 0.01$ *vs.* FRU (3), [c]: $P < 0.003$ *vs.* FRU (3), [d]: $P < 0.003$ *vs.* CON (1), [e]: $P < 0.005$ *vs.* FRU (3).

Table 4. Serum levels of sialic acid, sFas, TAC and MDA in control and experimental animals (Means ± SD)

Parameters	Experimental groups				
	1	2	3	4	5
Sialic acid (mmol/L)	0.32 ± 0.067	0.25 ± 0.055	1.75 ± 0.51[a]	0.76 ± 0.31	0.35 ± 0.06[b]
sFas (ng/ml)	19.1 ± 1.1	16.2 ± 1.8	27.6 ± 1.9[a]	23.8 ± 2.1	17.2 ± 3.5[b,c]
TAC (mM/L)	0.82 ± 0.068	0.69 ± 0.085	0.53 ± 0.22[a]	0.69 ± 0.071	0.75 ± 0.095[c]
MDA (nmol/ml)	7.56 ± 1.57	8.32 ± 2.68	15.33 ± 2.4[a]	10.8 ± 2.97[d]	5.85 ± 1.62[b]

[a]: $P < 0.0001$ *vs.* CON (1), [b]: $P < 0.0001$ *vs.* FRU (3), [c]: $P < 0.024$ *vs.* FRU (3), [d]: $P < 0.008$ *vs.* FRU (3), [e]: $P < 0.008$ *vs.* FRU + CAR on 1st day (4).

= – 0.832, $P = 0.04$) (Figure 2). Intraperitoneal injection of CAR to fructose-fed rats improved these parameters toward the control levels after 2 weeks of treatment. In fructose-fed rats treated with CAR on 16th day, there was negative correlation between sialic acid and triacylglycerol (r = – 0.583), glucose (r = – 0.106) and insulin (r = – 0.72), while sFas level correlated with serum sialic acid (r = 0.435), fasting glucose (r = 0.200) and negative correlation with HDL-c (r = – 0.98), also there was a significant positive correlation between serum insulin and HDL-c level (r = 0.928, P = 0.008) (Figure 3).

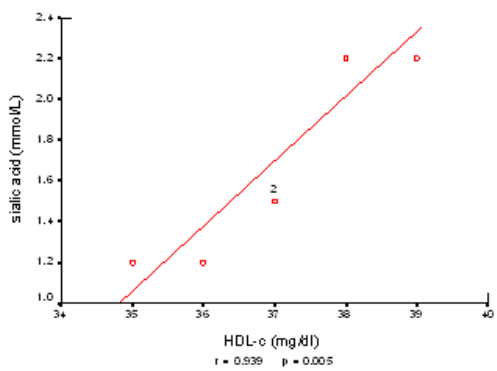

Figure 1. Correlation between serum sialic acid and HDL-c in fructose-fed rats.

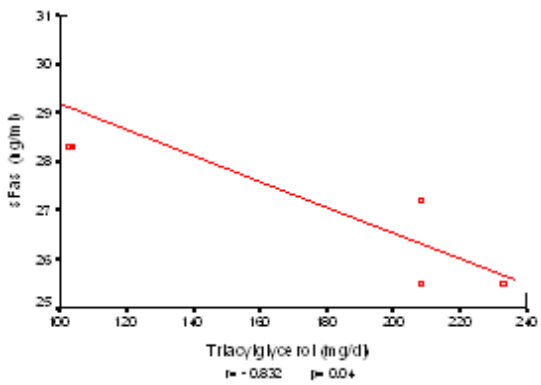

Figure 2. Correlation between serum sFas and serum triacylglycerol in fructose- fed rats.

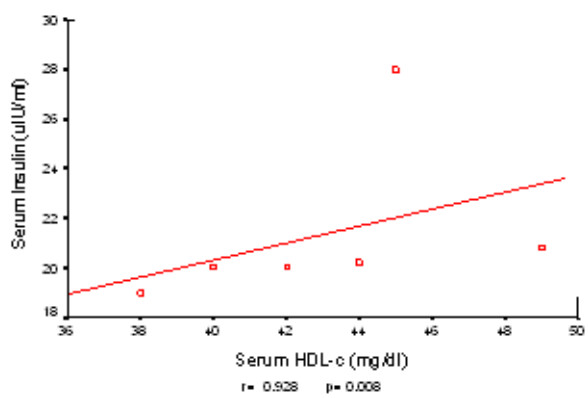

Figure 3. Correlation between serum insulin and HDL-c in fructose-fed rats treated with CAR.

4 Discussion

The development of insulin resistance in high fructose fed rats is well documented in the literature[2], and has been established in the present study. The degree of insulin resistance was higher in fructose-fed rats (FUR group) as indicated by significant elevation of serum glucose, insulin levels and higher value of HOMA index as compared with control fed rats. Insulin resistance has been attributed to how level of insulin-stimulated glucose oxidation due to modifications in the post-receptor cascade of insulin action[25]. Several metabolic hypotheses has been advanced to explain insulin resistance in fructose-fed rats. It has been shown that chronic fructose feeding alters the activity of several enzymes regulating hepatic carbohydrate metabolism, including decreasing the activity of glucokinase and increasing glucose-6-phosphatase activity leading to hepatic insulin resistance[26].

The present study demonstrated non significant changes in HbA1c in the studied groups, this may be due to insufficient of time duration of the experiment. Rajasekar et al[27] illustrate that rats fed high-fructose diet for six weeks showed significant alterations in the RBC membrane composition, which membrane-bound ATPases were significantly lower while MDA and lipid hydroperoxide were significantly higher in high fructose fed rats than those of control rats. Consequently, this explain the unaffected HbA1c level in FRU group. High fructose fed rats reduced the adverse effects of fructose load on glucose and insulin levels, where glucose and HOMA were improved. CAR reduces intramitochondrial acyl-COA/COA ratio, promotes oxidative glucose utilization, lowers intracellular glucose levels, and improves insulin sensitivity[5].

Varying the type of dietary carbohydrate has a profound influence on insulin action[28] and could cause changes in the metabolism of lipids[29]. Fructose when fed as the sole source of dietary carbohydrate induces dyslipidaemia which observed in the present study. The results revealed significant elevation of serum levels of triacylglycerol and HDL-c. These results may be attributed to the induction of various lipogenic enzymes by feeding fructose and can be associated with impaired insulin action. In this study, there were no significant alterations in total cholesterol and LDL-c concentration in fructose-fed rats compared to control diet fed animals. These findings are consistent with those of Dai and McNeill[30] who found no significant alteration in serum cholesterol in fructose-fed rats. These results agree with those of Nandhini *et al*[29]. On the contrary, Hallfrisch *et al*[31] demonstrated higher plasma cholesterol and LDL-c levels in rats fed fructose for 4 weeks. Nandhini *et al*[29] reported that hypertriglyceridemia may be due to reduction of lipoprotein lipase activity which is an important enzyme responsible for hydrolysis of triglyceride, this leads to hypertriglyceridemia.

In the present study, there was impairment of the antioxidant defense system in rats fed high-fructose diet. This indicated by pronounced decrease in serum total antioxidant capacity (TAC), while lipid peroxidation as MDA was statistically increased compared to control rats. These findings are in agreement with the suggestion of Ceriello *et al*[32] who found that acute hyperglycemia provokes oxidative capacity. It is well known that fructose itself can create oxidative stress by its metabolism[5]. They reported also that in fructose-fed rats, free radical production can be enhanced during hyperinsulinemia and hyperglycemia by mechanisms such as autoxidation of glucose, enhanced glycation, and altered polyol pathway[33]. These free radicals can catalyzed lipid peroxidation. Other potential mechanisms of oxidative stress include the reduction of antioxidant defense, MDA is one of the well-known secondary products of lipid peroxidation after exposure to reactive oxygen species and free radicals, it may be used to evaluate oxidative damage[34].

The dyslipidemia and production of free radicals resulting from fructose- fed rats was attenuated by CAR supplementation in the present study. The intraperitonial injection of CAR to fructose-fed rats improved the antioxidant defense system by increasing the total antioxidant capacity and decreased the MDA levels toward the normal values. This improvement is more pronounced in the group 5 than the values of group 4 of the experimental period.

Reduction of MDA may be due to the enhancement of the fatty acid transport by CAR into mitochondria for energy production, thereby lowering the availability of lipids for peroxidation. The modulatory effect of CAR on dyslipidemia was indicated by decreased the triacylglycerol level and increased the HDL-c level significantly compared with FUR group. The rise in serum HDL-c concentration by CAR treated rats after two weeks of fructose feeding (group 5) (therapeutic effect) may be due to delayed clearance and increased synthesis of HDL constituents, stimulation of lipoprotein lipase levels to rise in HDL production and reduction of VLDL constituents[29]. In fructose-fed rats treated with CAR (group 5), serum insulin significantly positive correlated with HDL-c level (Figure 3).

Rajasekar and Anuradha[5] reported that exogenous CAR improves insulin sensitivity, reduces both lipo- and gluco-toxicity and attenuated oxidative stress in skeletal

muscle. The benefits could be attributed to its effect on glucose disposal, antioxidative mechanisms, lipid profile and oxidative stress after two weeks of fructose- fed rats. As mention above, under certain conditions increased generation of ROS and/or reduction of the antioxidative capacity leads to enhanced ROS activity and oxidative stress which cause cellular injury and tissue damage by promoting several cellular reactions (e.g. lipid peroxidation, DNA damage)[35,36].

The present results revealed that feeding high-fructose diet to rats induced significant elevations in the levels of both inflammatory (sialic acid) and apoptotic (sFas) markers compared to those fed control diet. With regard to the result of sFas, its increasing level may be associated with hypertension which induced by chronic fructose feeding; this result was in agreement of reports of Park *et al*[3] who reported that rats fed high-fructose diet represent an animal model for insulin resistance and hypertension. Ceriello *et al*[37] reported that high serum glucose may produce myocardial damage and cardiac cell apoptosis through a formation of nitrotyrosine, which leads to increase the Fas/Fas-ligand system in uncontrolled apoptosis.

It has been reported that sFas concentration are increased and sFas-L are decreased in subjects of high cardiovascular risk compared with healthy subjects and also demonstrated that sFas and sFas-L concentrations are related to different cardiovascular risk factors such as diabetes, metabolic syndrome or hypertension, suggesting that these proteins may be novel markers of vascular injury[38,39]. The significant negative correlation was observed between sFas and triacylglycerol in fructose-fed rats (Figure 2).

With respect to the inflammatory marker, the present research indicates that there was a significant increase in serum sialic acid concentration in rats fed high fructose compare to control diet fed rats. Sialic acid is a component of cell membranes[1] and elevated levels may indicate excessive cell membrane damage but more specifically to the cells of vascular tissue. Sialic acid can be used as a measurement of acute phase response because many of the proteins of the immune response are actually glycoproteins which have sialic acid as the terminal sugar of their oligosaccharide chain[40]. In high fructose feeding rats, good correlation was observed between sialic acid and important cardiovascular risk factors such as HDL-c. Several research studies have shown that the concentration of sialic acid in serum is elevated in pathological states when there is damage to tissue, tissue proliferation and inflammations[41].

5 Conclusion

It is concluded that intraperitoneal administration of CAR to fructose-fed rats alleviated the oxidative stress, lipid profile, inflammatory (sialic acid), apoptotic (sFas) markers and may be helpful in overcoming of these abnormalities as therapeutic effect.

References

1. Thorburn AW, Storlien LH, Jenkins AB, Khouri S, Kraegen EW. Fructose- induced *in vivo* insulin resistance and elevated plasma triglyceride levels in rats. Am J Clin Nutr 1989; 49(6): 1155 – 63.
2. Reaven GM. Insulin resistance, hyperinsulinemia, hypertriglyceridemia, and hypertension: parallels between human disease and rodent models. Diabetes Care 1991; 14(3): 195 – 202.
3. Park OJ, Cesar D, Faix D, Wu K, Shackleton CH, Hellerstein MK. Mechanism of fructose-induced hypertriglyceridaemia in the rats. Activation of hepatic pyruvate dehydrogenase through inhibition of pyruvate dehydrogenase kinase. Biochem J 1992; 282: 753 – 7.
4. Baynes JW, Thorpe SR. Role of oxidative stress in diabetic complications: a new perspective on an old paradigm. Diabetes 1999; 48(1): 1 – 9.
5. Rajasekar P, Anuradha CV. Effect of L-carnitine on skeletal muscle lipids and oxidative stress in rats fed high-fructose diet. Exp Diabetes Res 2007; 2007:72741
6. Pickup JC, Mattock MB, Chusney GD, Burt D. NIDDM as a disease of the innate immune system: association of acute-phase reactants and interleukin-6 with metabolic syndrome X. Diabetologia 1997; 40(11): 1286 – 92.
7. Nayak BS, Roberts L. Relationship between inflammatory markers, metabolic and anthropometric variables in the Caribbean type 2 diabetic patients with and without microvascular complications. J Inflamm (Lond) 2006; 22: 3 – 17.
8. Nagata S. Fas ligand- induced apoptosis. Ann Rev Genet 1999; 33: 29 – 55.
9. Jabs T. Reactive oxygen intermediates as mediators of programmed cell death in plants and animals. Biochem Pharmacol 1999; 1;57(3): 231 – 45.
10. Liu J, Head E, Kuratsune H, Cotman CW, Ames BN. Comparison of the effects of L-carnitine and acetyl-L-carnitine on carnitine levels, ambulatory activity, and oxidative stress biomarkers in the brain of old rats. Ann N Y Acad Sci 2004; 1033: 117 – 31.
11. Broderick TL, Quinney HA, Lopaschuk GD. Carnitine stimulation of glucose oxidation in the fatty acid perfused isolated working rat heart. J Biol Chem 1992; 267(6): 3758 – 63.
12. Bisse E, Abraham A, Stallings M, Perry RE, Abraham EC. High-performance liquid chromatographic separation and quantitation of glycosylated hemoglobin A2 as an alternate index of glycemic control. J Chromatogr 1986; 24;374 (2): 259 – 69.
13. Barham D, Trinder P. An important colour reagent for the determination of blood glucose by the oxidase system. Analyst 1972; 97: 142 – 5.
14. Allain CC, Poon LS, Chan CSG, Richmond W, FU, P.C. Enzymatic determination of total serum cholesterol. Clin Chem 1974; 20(4): 470 – 5.
15. Fossati P, Prencipe L. Serum triglycerides determined colorimetrically with an enzyme that produces hydrogen peroxide. Clin Chem 1982; 28(10): 2077 – 80.
16. Finley PR, Schifman RB, Williams RJ, Lichhti DA. Cholesterol in high-density lipoprotein: use of Mg^{2+}/dextran sulphate in its enzymatic measurement. Clin Chem 1978; 24: 931 – 3.
17. Friedewald WT, Levy RI, Fredrickson DS. Estimation of the concen-

tration of low-density lipoprotein cholesterol in plasma, without use of the preparative ultracentrifuge. Clin Chem 1972; 18(6): 499 – 502.
18. Wilson PW, Garrison RJ, Castelli WP, Feinleib M, McNamara PM, Kannel WB. Prevalence of coronary heart disease in the Framingham Offspring Study: role of lipoprotein cholesterols. Am J Cardiol 1980; 46(4): 649 – 54.
19. Marschner I, Bottermann P, Erhardt. Group experiments on the radioimmunological insulin determination. Hormone and Metabolic Research 1974; 6: 293 – 6.
20. Li XY, Chow CK. An improved method for the measurement of malondialdehyde in biological samples. Lipids 1994; 29(1): 73 – 5.
21. Warren L. The thiobarbiturate assay for sialic acid. J Biol Chem 1959; 234: 1971 – 5.
22. Koracevic D, Koracevic G, Djordjevic V, Andrejevic S and Cosic V (): method for the measurement of antioxidant activity in human fluids. Clin Pathol 2001; 54: 356 – 61.
23. Matthews DR, Hosker JP, Rudenski AS, Naylor BA, Treacher DF, Turner RC. Homeostasis modelassessment: insulin resistance and beta-cell function from fasting plasma glucose and insulin concentrations in man. Diabetologia 1985; 28(7): 412 – 9.
24. Dawson B, Trapp RG. Basic and clinical biostatistics, third edition , pbl. Lange Medical Books/McGraw-Hill .U.S.A. 2001.
25. Catena C, Giacchetti G, Novello M, Colussi G, Cavarape A, Sechi LA. Cellular mechanisms of insulin resistance in rats with fructose-induced hypertension. Am J Hypertens 2003; 16(11 Pt 1): 973 – 8.
26. Faure P, Rossini E, Lafond JL, Richard MJ, Favier A, Halimi S. Vitamin E improves the free radical defense system potential and insulin sensitivity of rats fed high fructose diets. J Nutr 1997; 127(1): 103 – 7.
27. Rajasekar P, Balasaraswathi K, Anuradha CV. Effects of L-carnitine on RBC membrane composition and function in hyperinsulinemic rats. Ital J Biochem 2007; 56(1): 53 – 60.
28. D'Alessandro ME, Chicco A, Karabatas L, Lombardo YB. Role of skeletal muscle on impaired insulin sensitivity in rats fed a sucrose-rich diet: effect of moderate levels of dietary fish oil. J Nutr Biochem 2000; 11(5): 273 – 80.
29. Nandhini AT, Balakrishnan SD, Anuradha CV. Taurine improves lipid profile in rats fed a high fructose-diet. Nutrition Research 2002; 22: 343 – 54.
30. Dai S, McNeill JH. Fructose-induced hypertension in rats is concentration- and duration-dependent. J Pharmacol Toxicol Methods 1995; 33(2): 101 – 7.
31. Hallfrisch J, Reiser S, Prather ES. Blood lipid distribution of hyperinsulinemic men consuming three levels of fructose. Am J Clin Nutr 1983; 37(5): 740 – 8.
32. Ceriello A. Acute hyperglycaemia and oxidative stress generation. Diabet Med 1997; 14(Suppl 3): S45 – 9 (Review).
33. Paolisso G, Giugliano D. Oxidative stress and insulin action: is there a relationship? Diabetologia 1996; 39(3): 357 – 63 (Review).
34. Karatas F, Karatepe M, Baysar A. Determination of free malondialdehyde in human serum by high-performance liquid chromatography. Anal Biochem 2002; 1;311(1): 76 – 9.
35. Yu BP. Cellular defenses against damage from reactive oxygen species. Physiol Rev 1994; 74(1): 139 – 62.
36. Maxwell SR. Prospects for the use of antioxidant therapies. Drugs 1995; 49(3): 345 – 61 (Review).
37. Ceriello A, Quagliaro L, D'Amico M, Di Filippo C, Marfella R, Nappo F, Berrino L, Rossi F, Giugliano D. Acute hyperglycemia induces nitrotyrosine formation and apoptosis in perfused heart from rat. Diabetes 2002; 51(4): 1076 – 82.
38. Cosson E, Bringuier AF, Paries J, Guillot R, Vaysse J, Attali JR, Feldmann G, Valensi P. Fas/Fas-Ligand pathway is impaired in patients with type 2 diabetes. Influence of hypertension and insulin resistance. Diabetes Metab 2005; 31: 47 – 54.
39. Blanco-Colio LM, Martín-Ventura JL, de Teresa E, Farsang C, Gaw A, Gensini G, Leiter LA, Langer A, Martineau P, Hérnandez G, Egido J. Increased soluble Fas plasma levels in subjects at high cardiovascular risk: Atorvastatin on Inflammatory Markers (AIM) study, a substudy of ACTFAST. Arterioscler Thromb Vasc Biol 2007; 27(1): 168 – 74.
40. Pickup JC. Inflammation and activated innate immunity in the pathogenesis of type 2 diabetes. Diabetes Care 2004; 27(3): 813 – 23 (Review).
41. Hangloo VK, Kaul I, Zargar HU. Serum sialic acid levels in healthy individuals. J Postgrad Med 1990; 36(3): 140 – 2.

Using technique of Video-Assistant Thoracic Surgery (VATS) and small incision for diagnosis and treatment of pleura-pulmonary diseases under local anesthesia

Yanzheng Song[1,*], Karni S. Moshal[2], M.J. Krasna[3]

[1]*Department of Thoracic Surgery*, *Henan Chest Hospital*, *Zhengzhou*, *Henan* 450003, *China*; [2]*Department of Physiology and Biophysics*, *School of Medicine*, *500 S Preston Street*, *University of Louisville*, *Louisville*, *Kentucky*, *USA*; [3]*Department of Thoracic Surgery*, *University of Maryland Medical Center*, *USA*

Received January 19, 2009

Abstract

Background. Thoracotomy is one of the hardest surgical incisions to deal with and easy leading to atelectasis or pneumonia. Investigation of minimally invasive techniques has been the major concern for surgeons. To explore the feasibility of local anesthesia in thoracotomy including minithoracotomy and Video-Assistant Thoracic Surgery (VATS) for diagnosis and treatment of Pleura-pulmonary diseases is demonstrated in this article. *Methods*. Forty patients under local anesthesia in surgery were divided into performing thoracotomy and non-thoracotomy as two major groups. Thoracotomy group contains two sub-group including minithoracotomy and VATS, where minithoracotomy was performed on both open and closed pneumothorax for diagnosis and treatment of pleura-pulmonary diseases. In the meantime, performing non-thoracotomy was only for local wrapped pleura diseases and chest wall diseases. *Results*. In minithoracotomy group, biopsy of pleura for thirteen patients were performed. Ten of them were diagnosed as metastasis, one was amyloidosis and two were proliferation of pleura. Biopsy of three of patients of diffuse pulmonary diseases resulted two cases of interstitial fibrosis and one pulmonary tuberculosis II. In the VATS group, except one patient had serious pleural adhesion with performing minithoracotomy under general anesthesia, all other cases were performed biopsy bullarectomy for recurrent pneumothorax and pleurodesis for intractable pleuaral effusion under local anesthesia. Performing diagnostic thoracoscope under local anesthesia revealed four cases of pleural effusion and one case of liver-related pleural effusion. Meanwhile, ten patients under remedial thoracoscope revealed eight cases of malignant pleural effusion with undergoing pleurodesis and two cases of recurrent pneumothorax with undergoing bullarectomy and pleurodesis as well. In the non-thoracotomy group, five cases of thoracic tuberculosis were investigated, three cases of local wrapped empyema and two cases of benign tumor of rib were found. None of severe complications and death were seen. *Conclusion*. Minithoracotomy and VATS under local anesthesia can be performed safely for pleural-plumonary disease and chest wall lesions, which is less cost procedure for clinical applications. [Life Science Journal. 2009; 6(2): 83 – 87] (ISSN: 1097 – 8135).

Keywords: Local anesthesia; Video-Assistant Thoracoscopic Surgery

1 Introduction

Open thoracic biopsy must be considered for diagnosis of pleural-plumonary diseases, pulmonary sarcoidosis and primary plerual thickening. However, this operation is usually with general anesthesia in high risk for patients. In Clinical, a novel method with less traumatic and lower cost diagnosis and treatment is demonstrated in this article.

2 Patients and Methods

2.1 Patients

40 patients aged between 30 and 77 years old were

*Corresponding author. Email: yanzhengsong@163.com

studied, 26 of male, 14 female. Patients were divided into two groups, one for thoracotomy which includes minithoracotomy and Video-Assistanted thoracic surgery group respectively, and another one non-thoracotomy group. In thoracotomy group, 16 cases of the minithoracotomy group, three of them was found diffuse pulmonary diseases underwent biopsy at local anesthesia, 2 cases of interstitial fibrosis, one case of pulmonary tuberculosis. 13 patients with Biopsy of pleura under local anesthesia revealed different degrees of pleural thickening by chest X-ray, 10 cases were diffused and 3 cases were localized uneven. All cases occurred unilaterally with 7 left and 6 right. All 13 patients had performed B-ultrasound-guided or CT-guided biopsy of pleura check in one year, no positive results were obtained with pleural effusion pathological examination; Video-Assistanted Thoracic Surgery was performed on 14 cases in thoracotomy group, 4 cases was diagnosed as malignant pleural effusion by diagnostic thoracoscope, 1 was found liver-related pleural effusion. Meanwhile, 10 cases was performed by remedial thoracoscope with 8 cases maligant pleural effusion being done for pleurodesis, 2 cases of recurrent pneumothorax for bullarectomy and pleurodesis. There are 10 cases in the non-thoracotomy group including 5 cases of thoracic tuberculosis, 3 cases of local wrapped empyema, 2 cases of benign tumor of rib. Diagnosis and treatment of the above cases were performed all under Local anesthesia.

2.2 Methods

2.2.1 Thoracotomy group

2.2.1.1 Minithoracotomy group. In order to understand the location of pleura lesion and determine the coverage of pleural thickening, the fluoroscopy, X-ray and B-ultrasonography of chest were in examination routinely before operation. 5% double diluted Lidocaine (stock solution was not exceed 20 ml) was injected into the rib periosteum and its surroundings as infiltration anesthesia after routine sterilization and bespreading on skin of diseased region.

Biopsy of pleura: About 3 cm long incision was made firstly, the skin, subcutanceous tissues were cut in turn, the direction of the rib with felt and based on that the muscles of chest wall were cut until to the rib periosteum, ribs were adequately exposed and inflitration anesthesia was performed there, then the periosteum was stripped about 2 cm and the exposed rib was cut (Figure 1).

Abnormal pleural located under the cut ribs, compared with the normal pleural which was felt soft and pink in color, it was felt a little hard, and was in dark color, After the diseased region was confirmed, infiltration anesthesia was performed on the pleura to be removed, meanwhile the aspiration was tried to observe if there was any liquid or gas, a few anesthetic drugs was injected into thoracic cavity to lessen the response of pleural to gas after chest open, the depth of cut was also estimated.

Figure 1. Biopsy of pleura.

Open pneumothorax formed after a piece of full-thickening pleural was cut. The leak was blocked interruptedly with fingers, and patients were asked to hold breath after deep inspiration, and the changes were observed to decide tube intubation.The patients who had pleural fluid was aspirated slowly with aspirator.

Biopsy of diffused pulmonary diseases: the incision was chosen according to chest CT examination, the length of incision was about 5cm,the skin, subcutaneous tissue,muscle of chest wall were cut in turn along intercostal direction, the thoracic cavity was open after middle intercostal muscles were cut,the bleeding was stopped and intercostal muscles were sutured without knot.A small-sized army navy retractor was used to open thoracic cavity, lung was pulled out with ring forceps, the biopsy site was found and resected about 2 cm × 2 cm × 1 cm, then the incompleted lung surface was sutured and intercostal muscles were ligated with the last knot completed at the time of long inflation, no chest tube was placed. Antiphlogistic,analgesic and antibiotics were administered after operation.

2.2.1.2 Video-assistanted thoracoscope group. The patients were asked to fast for 4 h, empty bladder before operation. They were performed on continuous electrocardiogram and oxygen saturation monitoring, 50 mg dolantin, 25 mg diprozin and 10 mg codeine were in-

tramuscular injected. After then the patients were let lie on the operating table at lateral position on healthy side, ventilated with oxygen, sterilized and bespreaded as routine.

5% double diluted Lidocaine was injected into the seventh intercostal space between middle and posterior axillary line of the diseased side for local infiltration anesthesia, about 1cm incision was made, a channel into the cavitas pleuralis was made with straight blood vessel forcep, following with a canula (diameter was 105 mm) insertion, after that the inner core of which was pulled out and the opening was blocked by a cotton pad.

Ensuring the saturation of blood oxygen did not decrease obviously, cotton pad was open interruptedly, letting gas enter into thoracic cavity slowly, kept diseased lung collapse. The finger part of latex glove with a small opening at the end was used to cover canula, and Video-Assistanted thoracoscope was inserted to observe around the canula. Another 2 incisions were made according to the diseased region under the monitoring and guide of thoracoscope. The canulas were inserted with the same anesthesia, and were covered with latex gloves. Pleura adhesion was treated as follows: if it was a small streak adhesion,it could be fulgurized and cut by endoscopic scissor; if it was a small membranous puff adhesion, it could be bluntly dissected by thoracoscopic grasper; if the area of adhension was large and difficult to separate, it was converted to general anesthesia.

Diagnostic thoracoscope: the chest fluid of those patients who had pleural effusion should be aspirated completely, then the pleura, diaphragm, cervical pleura were observed, but pericardium was hard to observe. If nodules were found in the pleura, local infiltration anesthesia was applied and the nodule was cut for biopsy.

Remedial thoracoscope: the patients who were diagnosed definitely with malignant pleural effusion or recurrent pneumothorax could take pleurodesis induced by talc, if the lung expand was ascertained preoperatively. The method was the same as pleurodesis under general anesthesia.When no active bleeding was proved, a thoratic drainage tube was placed with thoracoscope.

The patients were asked to cough or were given oxygen with mask, letting lung expand gradually.During the operation,the saturation of blood oxygen should be cared, when it was low the operation sould be stopped and ask patients to cough, or supply oxgen with mask, reoperated until it was back to normal.

2.2.2 Non-thoracotomy group. Preoperative preparation has shown that location was the most important concern, especially those patients with multiple localized encapsulated pleural effusion, such as tuberculoma or nodular of pleura,pleural endotheliomas, etc. CT examination was performed before the operation to fix the lesion area of the patient roughly, then B-Ultrasonic localization was used to mark the incision. The incision we adopted is open and close on diseased chest wall so that the movement of upper extremities could influence the location of incision mark. The best choice for patient's body position in operation may keep similar as that in B-Ultrasonic examination. 2 – 3 incisions were designed according to different diseased regions found by B-Ultrasonic examination. It's easy to locate the thoracic tuberculosis so did other chest wall masses. It's easier to locate fluid lesion than soft-tissue masses like tuberculosis granulation tissue. Sufficient anaesthesia was performed on the superior, inferior margin and internal, external surface of ribs during the operation to relieve patients' painful feeling. The operation in localized encapsulated pleural effusion was the same to routine surgery. Pleura should not be injured to cause pneumothorax and infection, notably the cut of ribs and whether changed to localiz thoracic surgery relying on the size of lesions. The thoracic tuberculosis was treated as conventional operation.

3 Results

In thoracotomy group, three patients of diffuse pulmonary diseases were done for minithoracotomy, two of them had interstitial fibrosis, one had pulmonary tuberculosis II. Biopsy of pleura were performed on thirteen patients, ten of them had pleural metastasis, one had amyloidosisas and two had proliferation of pleura. No complications and death were seen. The removed pleura lesion was about from 0.5 cm × 0.5 cm × 0.3 cm to 1.5 cm × 1 cm × 0.5 cm, the thickest of which was 1.5 cm. Little effect of open pneumothorax on patients' respiration was found in 10 cases of diffused pleural thickening after thoracotomy, another 3 cases of localized partial pleural thickening were found with slight cough after thoracotomy.

One patient was misdiagnosed as tuberculosis of pleura for not performing full pleurotomy, exploratory surgery was done again to confirm the pleural metastasis of the lung cancer. Intrathoracic drain tube and the open pneumothorax should not be detained more than 5 days and 2 – 5 min respectively. In VATS group, except one patient was converted to general anesthesia due to serious pleural adhesion, other patients were performed under local anesthesia.

Pleural metastatic nodules were found in 4 cases of malignant pleural effusion by diagnostic thoracoscope,

the final diagnosis was made after biopsy. 1 case of liver-related pleural effusion were found with diffuse pleura edema by video-assistanted thoracoscope, but with no pleural nodule,it was diagnosed as liver-related pleural effusion considering the patient history. 3 cases of malignant pleural effusion by remedial thoracoscope were confirmed by pathological examination after thoracentesis.

7 patients of malignant pleural effusion and 1 patient of liver-related pleural effusion in VATS group were given pleurodesis induced by talc under local anesthesia. In 2 patients who had recurrent pneumothorax, one had pneumoconiosis complicated with pneumothorax,another had simple lung bullae. Their bullarectomy were dissected by disposable slit and stitching instrument, and received pleurodesis induced by talc.

In non-thoracotomy group, the patients with thoracic tuberculosis achieved the same effects as general anesthesia operation, with no surgery-related complications. The inward depressed shadow was found in the chest X-ray film of those the patients had localized encapsulated pleural effusion, however, the patients felt all right like chest distress, the shadow fade away after operation. All the patients in this group got out of bed on the 1st day postoperatively, and recovered quickly compared with the patients treated with trachea-cathetered general anesthesia. In 10 patients, one case of rib benign tumor complained the pain, but finished the course of operation. During the operation, blood pressure, pulse and saturation of blood oxygen of patients in both groups were all at normal range, one patient was administered anesthetic sedative, others were administered with antiphlogistic and analgesic to relieve pain after operation. No complication and death was seen in perioperative period. No long-term complications were found following up in one to six months.

4 Discussion

In our study, thoracic operation in artificial pneumothorax (open and closed pneumothorax) under local anesthesia can be performed for completing the diagnosis and treatment of pleural-pulmonary diseases if the stability of mediastinm being kept. Because the lung keeps blood oxygen saturation at normal range through its functional self-regulation of hypoxic pulmonary vasoconstriction, the safety coefficient increases patient's operation in open pneumothorax and closed pneumothorax. No significant influence on heart, lung and mediastinum when patients closed pneumothorax without pleural thickening. Same condition can be seen in patients open pneumothorax with pleural thickening specially with partial pleural thickening. Moreover, using VATS to remove peripheral pulmonary nodules is also an alternate method in clinical practice with advantages in comparison with routine thoracotomy[1–5]. The medical cost for treating with wedge resection of lung by VATS is about one fifth less than general anesthesia.

In 1997, Nezu[8] completed 34 cases of pulmonary bulla marginal resection for spontaneous pneumothorax with special apparatus of VATS by straight slit and stitching instrument under local anesthesia and sedative were reported in Japan. Hemodynamics was stable in operation and post operation. Blood-gas analysis revealed normal. Three cases of them had slight complication of air leak, the cure rate was 91%. Also, less complications, shorter hospitalization time compared with general anesthesia were reported.

In 1998, Mukaida[9] treated 4 patients who had high-risk complicated spontaneous pneumothorax under local anesthesia and epidural anesthesia. The ages of these 4 patients were 67, 72, 76 and 77 years old respectively, blood oxygen saturation before operation were 64.3 mmHg, 74.6 mmHg, 52.0 mmHg and 47.5 mmHg respectively, and the preoperative diagnosis of them were bullous emphysema and bilateral bullae of lung respectively. No significant change of PaO2 was found after operation, which suggested that it was feasible to do thoracotomy under local anesthesia[6,7].

Keeping the mediastinum stabilizing in surgery is necessitated in our study. The minithoracotomy thoracic surgery was performed on the patients who had diffused pulmonary diseases and incrassated pleural disease. No mediastinal oscillation during thoracotomy was found. But for biopsy of the patients with localized pleural thickening and diffuse pulmonary diseases, mediastinal oscillation in the condition of open pneumothorax was observed. Our method is to interruptedly open and close thoracic cavity in surgery, let patients gradually adapted, then rapidly cutting pleura and lung lesions, close thoracic cavity at the time of lung inflation through mask ventilation. In diagnostic and remedial thoracoscope, we adopted to put colatus gas into thoracic cavity slowly, seal incision and prevent gas out, forming closed pneumothorax to operate in a stable mediastinal state. Under the illumination of video-assisted thoracoscope in closed pneumothorax, those canous nodus protruded to the surface of pleuras have high diagnostic positive ratio. Accurate location before surgery is more important for localized pleural biopsy in open pneumothorax. Traditional B ultrasound localization has some advantages and can visually prove the coverage of pleural lesions

and provide marks even more accurate than CT localization, especially in those patient with localized pleural thickening. 15 patients out of 16 with thickening pleural disease and diffuse pulmonary diseases got the definite diagnosis, the accurate rate was 94%, if the full-thickness pleural lesions could be obtained in one misdiagnosed case, the accurate rate reached 100%. In comparison with open lung biopsy under general anesthesia, the accurate ratio is much higher. According to our statistical analysis in 2004, 500 patients received percutaneous puncture biopsy of lung, 30 patients received biopsy of pleura, the positive ratio were 90% and 85% respectively, which were far less than pleural biopsy under local anesthesia (94%). For diffused pulmonary diseases, percutaneous puncture biopsy of lung has higher risk and complication, lower positive ratio. Our experience is that those thickening pleural disease and diffuse pulmonary diseases having no positive results with percutaneous puncture biopsy of lung and pleura are the better indications for thoracotomy under local anesthesia.

No report on the removal and biopsy of local wraped pleura diseases such as localized encapsulated effusion and tuberculosis under local anesthesia without thoracotomy can be found so far. Actually, the surgery we made was kind of localized extrapleural modified thoracic surgery, which was under local anesthesia. The patients who had tuberculous pleuritis or tuberculoma of pleura received in 1 year regular treatment were always found effusion by ultrasonography exploration and then, need to undergp punture and administration of corticosteriods and urokinase repeatedly. However, drugs could not be absorbed easily and increased the mental burden of patients. The common operation weakened patients, so it' s necessary to treat the disease of pleura like pleural endotheliomas removing the foci at more safe and microinvasive surgery. In our study, such surgery was performed on 10 patients, the effects of which were found similar as routine surgery but with lower cost (80RMB for local anesthesia, 1000RMB for general anesthesia according to the health care charge standards in Henan province). Therefore, the surgery was welcomed by our patients and was consisted with ecnomic condition of our country. In short, the biopsy of lung and pleura under local anesthesia is economic and microinvasive, having low anesthesia requirement but high positive rate, therefore can be wildly applied in clinic.

References

1. Fang WT, Xu MY, Chen G, *et al*. Minimally invasive approaches for histological diagnosis of anterior mediastinal masses. Chin Med J (Engl) 2007; 20; 120(8): 675 – 9.
2. Lee P, Yap WS, Pek WY, *et al*. An Audit of medical thoracoscopy and talc poudrage for pneumothorax prevention in advanced COPD. Chest 2004; 125(4): 1190 – 2.
3. Migliore M, Giuliano R, Aziz T, *et al*. Four-step local anesthesia and sedation for thoracoscopic diagnosis and management of pleural diseases. Chest 2002; 121(6): 2032 – 5.
4. Sakuraba M, Masuda K, Hebisawa A, *et al*. Diagnostic value of thoracoscopic pleural biopsy for pleurisy under local anaesthesia. ANZ J Surg 2006; 76(8): 722 – 4.
5. Alrawi SJ, Raju R, Acinapura AJ, *et al*. Primary thoracoscopic evaluation of pleural effusion with local anesthesia: an alternative approach. JSLS 2002; 6(2): 143 – 7.
6. Katlic MR.Video-assisted thoracic surgery utilizing local anesthesia and sedation. Eur J Cardiothorac Surg 2006; 30(3): 529 – 32.
7. Migliore M. Efficacy and safety of single-trocar technique for minimally invasive surgery of the chest in the treatment of noncomplex pleural disease. J Thorac Cardiovasc Surg 2003; 126(5): 1618 – 23.
8. Nezu K, Kushibe K, Tojo T, *et al*.Thoracoscopicwedge resection of blebs under local anesthesia with sedation for treatment of a spontaneous pneumothorax. Chest 1997; 111: 230 – 5.
9. Mukaida T, Andou A, Date H, *et al*. Thoracoscopic operation for secondary pneumothorac under local and epidural anesthesia in high-risk patientl. Ann Thoracsurg 1998; 65: 297 – 306.

The design of home care assistant system by the ZigBee technology

Chienyuan Liu*

Computer Science and Information Engineering Department, *Chengshiu University*, *Niausong Township*, *Kaohsiung County*, *Taiwan* 833, *ROC*, *China*

Received March 20, 2009

Abstract

Along with a tendency towards the combination of wireless network and digital life, there has never been a better time to develop the application of wireless sensor network based on ZigBee. This paper would demonstrate the design of ZigBee application for a home care assistant system. ZigBee technology is based on the IEEE 802.15.4 standard and is extended with a network layer and an application layer to constitute a wireless network enabling architecture. During the formation of ZigBee application system, a system designer can build from a lower protocol stack, then a complex operating system, to a higher application program. In contrast with the brick-and-mud mode, it is more efficient to utilize an application framework for developing a particular application system. The work of this paper is to design a feasible home care assistant system with the application framework published by the Texas Instrument. With wireless features and automation capability built in ZigBee, the designated home care assistant system is not too hard to code during the design phase, is convenient to deploy the sensing devices, provides with operation security and low requirement for maintenance. It also relieves the burden of home care nurse and enhances the quality of caring. [Life Science Journal. 2009; 6(2): 88 – 93] (ISSN: 1097 – 8135).

Keywords: home care; IEEE 802.15.4; wireless sensor network; ZigBee; TI Z-Stacke

1 Introduction

Recently, because of the rapid development of the technology of micro sensor and micro electro-mechanical systems, the advancement of wireless communications, and the integration with computers, it is the exact chance for industry and academic to invest in wireless sensor network (WSN).

WSN can apply to the application domain of home care, home control, security, and position tracking[1–4]. The features of WSN[5] are low cost, low power consumption, low volume, easy deployment, programmable, dynamic construct, and low maintenance after installation in great scale[6].

ZigBee technology[7,8] is one of the best solutions for WSN. ZigBee is based on IEEE 802.15.4 and is extended with network and application upper layers for simplifying the design effort of a WSN application. With proper integration of sensors, actuators, and ZigBee, it would be efficient to develop and build a wireless real-time monitor and control system.

The work of this paper attempts to utilize ZigBee integrated with bio-medical sensors to develop a home care assistant system (HCAS). Next section introduced the IEEE 802.15.4 standard which is used as the lower layers of ZigBee. ZigBee specification was presented in section 3, including the upper layers of application layer (APL), application support sub-layer (APS), and network layer (NWK), ZigBee device profile (ZDP) and application profile. TI Z-Stack, containing operating system abstraction layer application programming interface (OSAL API), ZigBee device object (ZDO) API, ZDP API, application framework (AF) API, APS API, NWK API, and hardware abstraction layer (HAL) API, was described in section 4. Section 5 explained the functions and application design of HCAS. Conclusions and future enhancement were given in section 6.

*Corresponding author. Email: cyliu@csu.edu.tw

2 EEE 802.15.4 standard

The IEEE 802.15.4 standard is specified for a personal area network (PAN)[9]. It contains physical layer (PHY) and media access control layer (MAC).

2.1 PHY

The PHY of IEEE 802.15.4 defines three industrial, sciential, and medical (ISM) bands located at 868 MHz, 902 MHz, and 2405 MHz, respectively. Where, the ISM band at 868 MHz provides one channel with 20 kbps bandwidth. The ISM band at 902 MHz contains 10 channels each with 40 kbps bandwidth. The ISM band at 2405 MHz consists of 16 channels each with 250 kbps bandwidth. The ISM bands at 868 MHz and 902 MHz are locally suitable in Europe and northern America. Whereas, the ISM band at 2405 MHz is globally applicable. Therefore, it is the common selection of PHY at 2405 MHz. Figure 1 is the ISM bands and channels of IEEE 802.15.4 PHY.

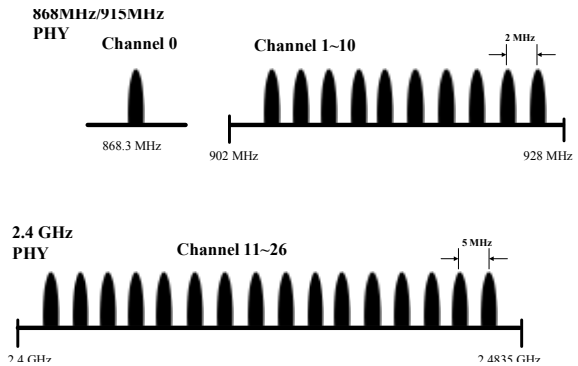

Figure 1. Bands and channels of IEEE 802.15.4 PHY.

The functions of PHY specify radio transceiver opening and closing, channel selection, clear channel assessment (CCA) evaluation, LQI inspection, channel energy detection, and frame signals transmission and reception, etc. The frame of PHY is named PHY protocol data unit (PPDU). There are 4 types of PPDU, including beacon frame, data frame, acknowledgement frame, and MAC command frame.

In Figure 2, the PPDU is composed of synchronous header (SHR), PHY header (PHR), and PSDU. SHR is consisted of preamble bits and start of frame delimiter (SFD). The length of preamble is 32 bits and the contents of it are all zero. The length of SFD is 8 bits and the contents of it are fixed as 11100101. The length of PHR is 8 bits. The first bit of PHR is 0 and the remainder 7 bits denote the length of the PSDU. PSDU contains the MAC data frame. The length of PSDU is limited within 127 bytes.

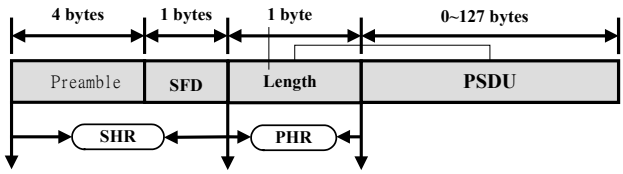

Figure 2. PPDU frame format.

2.2 MAC

The MAC Layer is divided into two sub-layers: logic link control (LLC) and MAC sub-layers. LLC is commonly adopted in all series of the IEEE 802 standards. Whereas MAC is vary for different PHY. The MAC of IEEE 802.15.4 provides data service and management service to the upper layer. It is in charge of beacon management, channel access control, guaranteed time slot (GTS) management, frame inspection, frame transmission and response, and device association and de-association. Since the functions of MAC are not too complex to choose a high speed CPU, thus a low-power consumption and low-cost micro-controller can be adopted for the realization of the MAC protocol.

Figure 3 depicts MAC frame format. It is composed of MAC header (MHR), MAC service data unit (MSDU), and MAC footer (MFR). MHR is consisted of 2 bytes control field, 1 byte sequence number, and at most 20 bytes address information. Control field denotes the frame type, the format of address information field, and the acknowledge mode for the frame transmission. The data sequence number is used as the frame identifier during frame communications. The replied frame should contain the same sequence number to indicate its acknowledgement to the previously transmitted frame. Thus, a reliable transmission could be achieved. The address field could contain a 64 bits IEEE address or a 16 bits network address. MFR is the frame check sequence (FCS) for inspecting whether the reception is successful or not. The MAC of IEEE 802.15.4 utilizes the carrier sense multiple access/collision avoidance (CSMA/CA) mechanism to control the access to wireless channel to solve the contention problem.

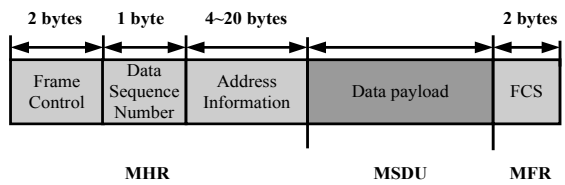

Figure 3. MAC frame format.

3 ZigBee specification

The draft of ZigBee specification was initiated by Honeywell, Invensys, Mitsubishi Electric, Motorola, and Philips in 2003[11]. The latest specification was released on December 2006. ZigBee adopts IEEE 802.15.4 as its MAC and PHY. In addition, NWK, APS, APL, ZDO, and security service are added over the MAC and PHY. Therefore, ZigBee has already become a complete network protocol for wireless application. The protocol stack of ZigBee is illustrated in Figure 4.

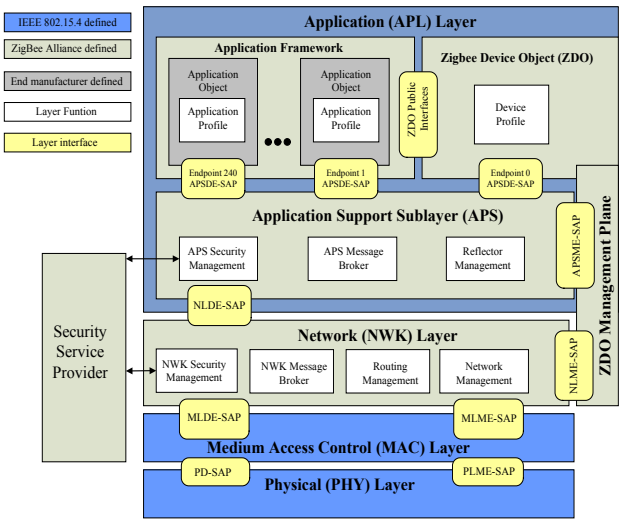

Figure 4. ZigBee stack.

Each layer in ZigBee stack is consisted of two entities: data entity (DE) and management entity (ME). DE provides data services, i.e. data packet transmission and reception. ME provides management services. Normally, the lower layer is the service provider and provides its services through the interface of service assess point (SAP) for the upper layer. Each SAP would implement a certain functionality to support its particular service.

The kernel of ZigBee Stack is NWK. NWK takes care of joining into or leaving network, finding route, and data packet transmission or reception for a ZigBee device.

The major functions of APS in APL include the ZigBee network formation and binding, data transmission management, and network security. The function of application object (APO) in APL is to implement the processing logic for the ZigBee application. In the other words, APO is the basic unit of application program. APO can communication with a remote APO through ZigBee network to realize specific application, e.g. to turn on a remote switch for lighting. Each APO should allocate only one endpoint (EP). An EP is identified by an EP ID ranged from 1 – 240. EP ID 0 denotes ZDO. EP ID 241 – 255 is reserved.

ZDP describes the behavior and properties of a ZigBee device and is mandatorily defined by the ZigBee Alliance. ZigBee application profile describes the functions and parameters for a particular application and is mandatorily defined by the ZigBee Alliance, too. Each ZigBee application profile has a unique Profile ID. Manufacturers should obey the ZDP and ZigBee application profile to design their ZigBee products. This is to assert the interoperability between different vendors. User can define a private application profile to be used in users' private application domain if the interoperation is not required. In ZigBee specification, each APO implements only one application profile. A unique EP ID should be allocated to an APO.

There are two types of ZigBee devices: full function device (FFD) and reduced function device (RFD). FFD can act as a coordinator or router, can communicate with all types of devices, and can support any type of network topologies. RFD can act only end device and can communicate only with a coordinator. There is only one coordinator in a ZigBee network, but it allows multiple routers and end devices.

ZigBee network specifies two network topologies: central controlled star network and peer-to-peer mesh network. Start topology was shown in Figure 5(A). In star network, there are multiple devices surround a central coordinator. The central coordinator responses for the network formation and maintenance, time slot planning and allocation, channel access control, GTS management, etc. The surrounding devices follow the policy, obtained from broadcasting beacon transferred by the coordinator, to access the channel. Figure 5(B) depicts a peer-t-peer mesh network. In the network, devices are not necessary to communicate with the coordinator. But RFD is only able to communicate via FFD.

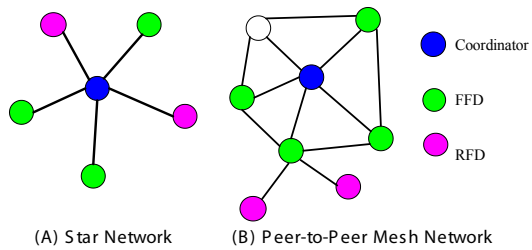

Figure 5. ZigBee Network Topology.

The operation manners of ZigBee network are classified into beacon-enabled network and non beacon-enabled network. In beacon-enable network, the beacon

is transmitted from a coordinator. The purpose of the beacon is to inform all devices the time synchronization information, PAN ID for devices to join, and super-frame structure. Super-frame with GTS and without GTS was shown in Figure 6 and 7, respectively. Within GTS, all time slots could only be used by certain preserved devices. The duration between beacon and GTS is named CAP and is accessed with CSMA/CA arbitration mechanism. In non beacon-enabled network, all devices merely access the channel with CSMA/CA arbitration mechanism in asynchronous way.

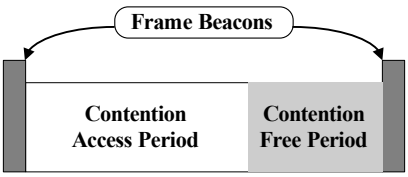

Figure 6. Super-frame with GTS.

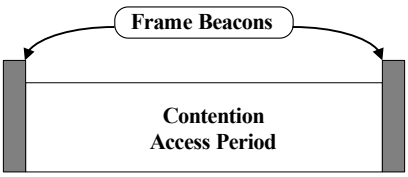

Figure 7. Super-frame without GTS.

4 TI Z-stack

First of all to develop a ZigBee application system is to implement the ZigBee protocol stack. This is a great challenge to a developing team. Currently, some companies have developed their own ZigBee Stack as a package, e.g. Texas Instrument Z-stack[12]. The project developing time could be obviously shortened by using TI Z-Stack to develop a ZigBee application system[13].

There are some categories of API in the TI Z-Stack, including OSAL API, ZDO API, ZDP API, AF API, APS API, NWK API, and HAL API. An application program can call these API to accomplish its communication and control requirements.

4.1 OSAL API

Through calling OSAL API[14], the program coding of APO can be independent with operating system, kernel modules, and system main control loop or hardware interrupts. This is because OSAL provides the following functions in hardware independent manner.

1) Task registration, initialization, and startup; 2) Messages delivery between tasks; 3) Synchronous mechanism between tasks; 4) Interrupt handling mechanism; 5) Timers control; 6) Dynamic memory management.

4.2 ZDO API

ZDO provides the management functions to a ZigBee device. An APO/EP can manage a coordinator, router, or end device through calling ZDO API[12]. The management functions contain network formation, device discovery, joining network, binding to other APO/EP, and security management.

ZDP defines the functionalities a ZigBee device should implement. ZDP specifies a device descriptor for the device and defines separate cluster by a cluster ID and a pair of EP ID and a command message. Through the command message, ZDP provides the following functions to ZDO and APO/EP.

1) Start device network; 2) Device discovery; 3) Binding end devices, device association and disassociation; 4) Network management.

The binding table is only stored at a coordinator. Therefore, only a coordinator can receive the binding request command and normally acts as a reflector to forward the messages between the binding end devices.

4.3 AF API

AF is the interface between AP and APS. APO/EP calls AF API[12] to perform wireless communication through APS and NWK. AF is also a receiving multiplexer for multiple APO/EP. AF provides the following functions to application.

1) APO/EP management; 2) Data packet transmission and reception.

4.4 APS API

APS API[12] provides the following management functions to the upper application program.

1) Management for binding table; 2) Management for group table; 3) Quick address search.

Besides the above mentioned functions, APS also provides data packet services. However, an application program could only use these data services via the interface of AF.

The binding table of APS is created in the static RAM. The capacity of binding table (maximum entry numbers and maximum cluster numbers per entry) can be specified by device configuration properties. Cluster denotes the relationship of a particular application for all related APO on various devices in ZigBee network. Each cluster has 8 bits cluster ID. When a message transferred with a particular cluster ID but not a destination network ad-

dress, it denotes to send this message to all APO on related devices. The cluster message is sending through a coordinator (reflector). Reflector forwards the message in uni-cast format to each APO on related devices by looking at the entries of its binding table.

4.5 NWK API

NWK API[12] provides the following functions to the upper layers.

1) Network management; 2) Address management; 3) Network status and utility functions.

In addition to the management function, NWK also provides data services. However, an application layer could not directly access data service in NWK. Instead, an application layer should call the function of AF to send data message.

4.6 HAL API

Application program can access hardware resources through HAL API[15]. These resources include timer, GPIO, UART, and ADC register. Basically, HAL API is classified into three types.

1) Initialization function calls: these functions are called to initiate certain services or to set some parameters related to hardware platform. Normally, these functions are called during initialization phase after power on; 2) Service access function Calls: they are also named as service functions. These functions can access directly to the content of hardware register (such as ADC register)[16,17] or can control the action of a hardware component (such as LED on/off); 3) Callback function calls: they are also named as event handler. The content of these functions should be implemented by the application programmer. These functions will be called and the status and message will be passed back to upper application task when a related hardware event occurred (such as interrupt, counting event, time-out event, or message packet arrival, etc.). Note that CPU-intensive computation or critical section should be avoided in the implementation of these functions to maintain the handling efficiency and response speed.

Generally, HAL driver provides timer, GPIO, LED, key, USRT, and ADC services to upper application. However, not all platforms provide all services to an application. Besides, devices can configure different hardware service features during the startup phase.

5 HCAS design

The configuration of the HCAS is consisted of a personal computer, a ZigBee coordinator, and multiple ZigBee end devices.

Figure 8 showed the man-machine interface performed in the main control PC. In Figure 8, PC is connected to a coordinator through USB cable. Via the coordinator, PC transmits a sensor's data request to end devices, saves the received data into database, and displays the sensor's data by graphic user interface. Then, it sends control instructions to end devices according to pre-defined rules.

The sensing data measured by HCAS include body temperature, heart beat rate, and the temperature of environment. These sensors were installed on separate end devices. Firstly, PC sends a data request command to end devices to collect sensor's data. Then, the collected data are written into database. If the body temperature and the heart beat rate are over a preset threshold, HCAS would generate an alarm to a caring nurse and would send a control instruction to the corresponding end devices to turn on the ventilation equipment. After suitable treatment by the caring nurse and the cared person becomes normal, HCAS will sends a control instruction to turn off the ventilation equipment. To maintain a comfortable environment, the indoor temperature is monitored by HCAS. HCAS operates and reacts to the indoor temperature in similar manner of body temperature except to inform the caring nurse by an alarm.

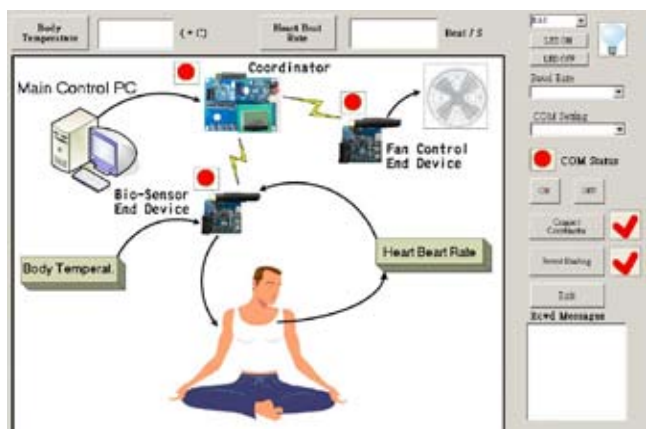

Figure 8. HCAS Man-machine Interface.

The TI Z-Stack was adopted in the design of HCAS. To use TI Z-Stack, one must follow its application design framework. When an application program executed in operating system, it is an application task of OSAL. The design procedure of HCAS is explained as follows.

OSAL_HCAS_App.c module is the startup module of HCAS. In OSAL_HCAS_App.c, the application should call osalTaskAdd() function to add and register system tasks and application task into operating system. The system tasks include Hal_Init() to start and initiate

HAL driver task, macTaskInit() to start and initiate IEEE 802.15.4 protocol stack, nwk_init() to start and initiate ZigBee stack, APS_Init() to start and initiate APS service and mamagement task, ZDApp_Init() to start and initiate ZDO task. Finally, the application should call osalTaskAdd() to add and register HCAS_App_Init() to start and initiate application object with application profile and application specific functions.

Basically, the former system tasks are declared within TI Z-Stack. Application programmer is not required to modify theses functions. As for the last step to add HCAS_App_Init(), it is related to the specific application and is needed to be implemented by the application designer. HCAS_App.c is the main application module of HCAS. Within this module, some functions need to be instantiated, including the HCAS_App_Init() to initiate the device, and HCAS_App_ProcessEvent() to handle system event for the application.

HCAS_App_Init() setups and startups the device and network with pre-defined system and device configuration properties. Next, it registers APO to the operating system. Then it registers application task events to the operating system. HCAS_App_ProcessEvent() is the main event processing function of the application. Within this function, many previously registered events passed back from system will be inspected and distributed to the corresponding handling functions, such as the receiving event from other devices would call the callback function HCAS_App_MsgCB() to handle the required response, or the interrupt event from hardware keys or switch would call the callback function HCAS_App_HandleKeys() to handle the required action, or the time-out event from timer would call the function HCAS_App_HandleTmr() to handle the necessary procedure and then setups the timer by calling osal_start_timerEx() for the next periodic event.

In event handling functions, if the device needs to send a data message to other device, it should call the AF_DataRequest() function in AF API for that sending request. If the device wants to read the sensor's data on other device, it should call the HalAdcRead() function in HAL API. If the device needs to send data via RS232 to PC or other device, it should call the HalUARTWrite() function in HAL API. If the device wants to turn its LED on, it should call the HalLedSet() function in HAL API. Other action requirements can refer to[12–15,18].

6 Conclusion

First challenge during the phase of the design and implementation for the HCAS is to study all related specifications, and the definitions and calling methods of all related API. This paper described our experience about the application framework of TI Z-Stack which was adopted for the development of HCAS.

The purpose of the pilot project of HCAS is to survey a feasible development platform based on ZigBee and to implement the pilot system to build up the required experiences upon the platform. Thus, the function of pilot HCAS is designed with ordinary scenario and uncomplicated system configuration.

Next stage, HCAS will be enhanced with practical scenario and advanced control facilities. For instance, the ventilation equipment could be replaced with air conditioner driven by continuous-speed inverter. In this case, not only the temperature can be controlled, but also the humility. The monitored bio-medical signals could be added by oxi-meter, breath-meter, blood-pressure meter, glucose meter, position tracking, and tilt-plus-gyro meter to detect fall down status. In addition, HCAS MMI could be redesigned from PC GUI to web-based GUI. Thus, medical experts can diagnose the cared person remotely, or the relatives can understand the healthy situation of the cared person.

References

1. Helal S, Mann W, El-Zabadani H, King J, Kaddoura Y, Jansen E. The gator tech smart house: a programmable pervasive space. IEEE Computer 2005; 38(3): 50 – 60.
2. Park H, Srivastava MB, Burke J. Design and implementation of a wireless sensor network for intelligent light control. In Proc. of Int' l Symposium on Information Processing in Sensor Networks (IPSN). 2007; 370 – 9.
3. Ross PE. Managing Care through the Air. IEEE Spectrum 2004; 26 – 31.
4. Sunny C, Peter R, Bill S, Sara B. Technology for care networks of elders. IEEE Pervasive Computing 2004; 3(2): 22 – 9.
5. Akyildiz I, Su W, Sankarasubramaniam Y, Cayirci E. A Survey on Sensor Networks. IEEE Communications Magazine 2002; 102 – 14.
6. Lee YF. Design and Implementation of a ZigBee-based Over-the-air Programming Platform. Proceedings of CCL Technical Journal 2007; 29 – 35.
7. Tsai HM, Tonguz OK, Saraydar C, Talty T, Ames M, Macdonald A. ZigBee-based intra-car wireless sensor networks: a case study. IEEE Wireless Communications Magazine 2007; 3965 – 71.
8. Li WK, Chou CH, Lin ZF. Design and Implementation of a Zigbee-based Communication Substrate for Wireless Sensor Networks. Proceedings of NCS, Oct 2006.
9. IEEE Standard 802.15.4a™-2007.
10. IEEE Standard 802.15.4™-2006.
11. ZigBee Specification, December 1, 2006.
12. Z-Stack API _F8W-2006-0021.pdf
13. Z-Stack Sample Applications, F8W-2006-0023.pdf
14. OSAL API_F8W-2003-0002.pdf
15. HAL Driver API _F8W-2005-1504_.pdf
16. cc2430.pdf (http://focus.ti.com/docs/prod/folders/print/cc2430.html)
17. cc2431.pdf (http://focus.ti.com/docs/prod/folders/print/cc2431.html)
18. Simple API for Z-Stack _F8W-2007-0021.pdf.

Author Index

Subject Index